# DEVELOPMENT OF DESIGN BASIS FOR HYDRODYNAMIC VORTEX SEPARATORS

**BY YUNJIE LI**

**A dissertation submitted to the**

**Graduate school-New Brunswick**

**Rutgers, The State University of New Jersey**

**in partial fulfillment of the requirements**

**for the degree of**

**Doctor of Philosophy**

**Graduate Program in Civil and Environmental Engineering**

**Written under the direction of**

**Professor Qizhong Guo**

**and approved by**

_____

_____

_____

_____

**New Brunswick, New Jersey**

**January, 2009**

## ABSTRACT OF THE DISSERTATION

**Development of Design Basis for Hydrodynamic Vortex Separators**

**by YUNJIE LI**

**Dissertation Director:**
**Professor Qizhong Guo**

Though many prototypes of hydrodynamic separators have been developed to remove solids from wastewater and stormwater, to date, not much fundamental development on unit performance evaluation exists due to the complexity of the problem. Design specifications of commercial separators are derived from empirical or semi-empirical equations that are unique and proprietary to each manufacturer. In this research, experimental and theoretical investigations were conducted to examine the mechanisms of solid-liquid separation for a general vortex separator, thereby providing a fundamental approach for unit performance evaluation. The main achievements and findings obtained through the experimental investigation and theoretical study are as follows.

Experimental investigation with four physical vortex models, three with varying inlet pipe elevations and one with a lower chamber height, reveal that the impact of a changing inlet pipe elevation on particle removal efficiency is insignificant; while the effect of a changing chamber height on removal efficiency is significant and measurable.

In the theoretical development, three topics, namely, flow pattern, particle trajectory, and unit performance evaluation, were researched. Based on the Rankine combined vortex model, the law of conservation of momentum, and the boundary conditions for a confined vortex chamber, a simple formula for angular velocity was

derived. By applying the Navier-Stokes governing equation coupled with the angular velocity derived in this study, a vortex flow pattern model was developed.

Based on the balance of forces acting on a particle, a new particle settling formula for natural sediment particles was proposed. Additionally, using the particle settling velocity and the flow pattern derived for the confined vortex chamber, the particle trajectory equations were derived in this study.

A new sizing equation for the confined vortex chamber was developed from the newly-derived particle trajectory. The new sizing equation was validated by laboratory measured particle removal efficiencies. The results generated from this dissertation research will help design, performance evaluation, as well as improvement of the hydrodynamic separators.

## ACKNOWLEDGEMENTS

First I would like to express my sincere gratitude to the members of my committee. I deeply appreciate my major advisor, Professor Qizhong Guo, who provided the fundamental ideas from the development of this work, supervised my dissertation and guided me in my studies throughout the program, as well as provided me with support and encouragement. I have benefited greatly from his experience and hope to continue collaboration with him in the future.

My sincere appreciations go to Professor Perumalsamy N. Balagura, Professor Steven Medlar and Professor Prosenjit Bagchi for their valuable suggestions and critical review of the work. Their consistent advices and encouragement are of great help throughout this study.

I would like to extend my appreciations to authors whose research works have provided the basis for this study. Appreciations are also extended to the faculty and staff of the Department of Civil and Environmental Engineering of Rutgers University, for their kind help throughout the years of my study. I would also like to thank Ms. Ellen Speace who helped to polish my English writing for this dissertation.

The author is also indebted to the Department of Civil and Environmental Engineering, Libraries and Computer labs of Rutgers University, for its facilities.

Finally, special thanks to my wife (Katherine), son (Tiger), and daughter (Angelina), for their constant love and support throughout these years.

## TABLE OF CONTENTS


| | | |
|---|---|---|
| **Abstract** | | ii |
| **Acknowledgements** | | iv |
| **List of Tables** | | viii |
| **List of Figures** | | ix |
| **Chapter 1** | **Introduction** | **1** |
| 1.1 | Impact of Land Use Behavior on Runoff Yield | 1 |
| 1.2 | Impact of Land Use on Water Quality | 3 |
| 1.3 | Management of Water Quality | 4 |
| 1.4 | Types of Hydrodynamic Vortex Devices | 6 |
| 1.5 | Objectives of Current Study | 6 |
| 1.6 | Organization of the Dissertation | 7 |
| **Chapter 2** | **Review of Literature** | **10** |
| 2.1 | The Key Developmental Stages of Hydrodynamic Separators | 10 |
| 2.2 | Reported Performance of Hydrodynamic Devices | 11 |
| 2.3 | Review of Sizing Approaches | 13 |
| 2.4 | Review of Particle Settling Velocities | 20 |
| 2.5 | Review of Types of Developed Vortex Models | 27 |
| 2.6 | Gaps in This Area | 34 |
| **Chapter 3** | **Experimental Study on the Particle Removal Efficiencies in Confined Vortex Chamber** | **35** |
| 3.1 | Introduction | 35 |

| | | |
|---|---|---|
| 3.2 | Experimental Setup and Procedure | 37 |
| 3.3 | Results and Discussions | 42 |
| 3.4 | Conclusions | 54 |
| **Chapter 4** | **Determination of Angular Velocity for Turbulent Vortex Chamber Flow** | **55** |
| 4.1 | Introduction | 55 |
| 4.2 | Physical Model and Assumptions | 56 |
| 4.3 | Determination of Driving Toque and Resistance Torque | 59 |
| 4.4 | Determination of Angular Velocity Formula | 67 |
| 4.5 | Nominal Angular Velocity | 83 |
| 4.6 | Conclusions | 84 |
| **Chapter 5** | **Determination of Flow Pattern in a Confined Vortex Chamber** | **86** |
| 5.1 | Introduction | 86 |
| 5.2 | Vortex Chamber Physical Model | 87 |
| 5.3 | Vortex Chamber Mathematical Model | 87 |
| 5.4 | Solutions to Governing Equations | 94 |
| 5.5 | Case Analysis and Discussions | 99 |
| 5.6 | Conclusions | 103 |
| **Chapter 6** | **Dynamic Analysis of Particle Motion in a One – Dimensional Upward Uniform Steady Flowfield** | **104** |
| 6.1 | General Equation of Particle Motion | 104 |
| 6.2 | Governing Equation of Particle Motion in a One – Dimensional | |

| | | |
|---|---|---|
| | Upward Uniform Steady Flowfield | 116 |
| 6.3 | Solutions to Governing Equation | 119 |
| 6.4 | Result Analysis and Discussions | 129 |
| 6.5 | Conclusions | 151 |
| **Chapter 7** | **Particle Trajectories in a Vortex Chamber Flow** | **152** |
| 7.1 | Problem Description and Assumptions | 152 |
| 7.2 | Physical Model | 153 |
| 7.3 | Particle Trajectories | 155 |
| 7.4 | Case Analysis and Discussions | 167 |
| 7.5 | Conclusions | 171 |
| **Chapter 8** | **Investigation of Unit Sizing Formula** | **172** |
| 8.1 | Introduction | 172 |
| 8.2 | Vortex Chamber Physical Model | 173 |
| 8.3 | Determination of Sizing Formula | 175 |
| 8.4 | Comparison of Predicted Results with Experimental Results | 182 |
| 8.5 | Sizing Example | 184 |
| 8.6 | Conclusions | 189 |
| **Chapter 9** | **Summary and Conclusions** | **190** |
| **References** | | **194** |
| **Vita** | | **204** |

## LIST OF TABLES


| | | |
|---|---|---|
| 3.1 | Sieve analysis results for manufactured materials | 39 |
| 3.2 | Data and results measured based on $D_1$ = 127 mm, $D_{in}$ = 12.7 mm, $H_o$ = 175 mm, and $H_{in}$ = 23 mm. | 44 |
| 3.3 | Data and results measured based on $D_1$ = 127 mm, $D_{in}$ = 12.7 mm, $H_o$ = 175 mm, and $H_{in}$ = 77 mm. | 44 |
| 3.4 | Data and results measured based on $D_1$ = 127 mm, $D_{in}$ = 12.7 mm, $H_o$ = 175 mm, and $H_{in}$ = 121 mm. | 45 |
| 3.5 | Data and results measured based on $D_1$ = 127 mm, $Di_n$ = 12.7 mm, $H_o$ = 120 mm, and $H_{in}$ = 23 mm. | 45 |
| 4.1 | Calculated angular velocities with Eq.(4.35) | 81 |
| 4.2 | Comparison of the calculated angular velocities with Eq. (4.35), Eq.(4.37), Eq.(4.39), and Eq.(4.41) | 81 |
| 4.3 | Comparison of calculated angular velocity with Eq.(4.35) to the calculated nominal angular velocity with Eq.(4.45) | 84 |
| 5.1 | Calculated angular velocities for various inflow rates | 101 |
| 6.1 | Fitting values of $K_1$, $K_2$ and $K_3$ for drag coefficient | 110 |
| 6.2 | Upper limit of spherical sand particles for $R_{ep} \leq 1.0$ | 133 |
| 6.3 | Upper limit of spherical sand particles for $1.0 < R_{ep} \leq 10.0$ | 133 |
| 6.4 | Upper limit of spherical sand particles for $10.0 < R_{ep} \leq 100.0$ | 133 |
| 6.5 | Upper limit of spherical sand particles for $100.0 \prec R_{ep} \leq 1000.0$ | 133 |

## LIST OF FIGURES


| | | |
|---|---|---|
| 2.1 | Schematic Illustration of the Rankine Combined Vortex Model | 31 |
| 3.1 | Schematic outline of experimental apparatus | 38 |
| 3.2 | Schematic illustration of the vortex chamber | 38 |
| 3.3 | Particle size distribution of manufactured blend material | 40 |
| 3.4 | Measured removal efficiency based on $D_1$ = 127 mm, $H_o$ = 175 mm, and $H_{in}$ = 23 mm. | 46 |
| 3.5 | Measured removal efficiency based on $D_1$ = 127 mm, $H_o$ = 175 mm, and $H_{in}$ = 77 mm. | 46 |
| 3.6 | Measured removal efficiency based on $D_1$ = 127 mm, $H_o$ = 175 mm, and $H_{in}$ = 121 mm. | 47 |
| 3.7 | Measured removal efficiency based on $D_1$ = 127 mm, $H_o$ = 120 mm, and $H_{in}$ = 23 mm. | 47 |
| 3.8 | Effect of inlet pipe elevation on removal efficiency based on $H_o$ = 175 mm and $D_{in}$ = 12.7 mm | 49 |
| 3.9 | Effect of inlet pipe elevation on removal efficiency based on $D_1$ = 127 mm and $H_{IN}$ = 23 mm | 49 |
| 3.10 | Comparison of experimental results with predicted results derived from Eq.(3.6) | 53 |
| 4.1 | Schematic illustration of the vortex chamber | 57 |
| 4.2 | Tangential velocity distribution of the Rankine combined vortex | 58 |
| 4.3 | Schematic illustration of integration area at the chamber bottom | 66 |

| | | |
|---|---|---|
| 5.1 | Schematic illustration of the vortex chamber model | 88 |
| 5.2 | Predicted tangential velocity distribution for various inflow rates Q | 102 |
| 5.3 | Vertical velocity distribution for various flow rates | 102 |
| 6.1 | Forces acting on a particle | 117 |
| 6.2 | Predicted limits of spherical sand particle in an upward uniform steady fluid flow (water) | 135 |
| 6.3a | Comparison of predicted results derived from Stokes' formula and Cheng's formula for spherical sand particles in the Stokes flow | 139 |
| 6.3b | Comparison of predicted results derived from Stokes' Modified formula and Cheng's formula for natural sand particles in the Stokes flow | 139 |
| 6.3c | Comparison of predicted results derived from Eq.(6.50a) with Cheng's formula for natural sand particles in the Stokes flow | 140 |
| 6.4 | Comparison of predicted results for natural sediment particles ranging from 100 to 300 micron. | 142 |
| 6.5 | Comparison of predicted results for natural sediment particles with diameter larger than 300 micron. | 142 |
| 6.6a | Particle velocity in an upward uniform steady fluid flow with $U_f$ = 5 mm/sec based on Rep < 1.0 | 147 |
| 6.6b | particle trajectory in an upward uniform steady fluid flow with $U_f$ = 5 mm/sec based on Rep < 1.0 | 147 |
| 6.7a | Particle velocity in an upward uniform steady fluid flow with $U_f$ = 10 mm/sec based on 1.0<Rep < 10.0 | 150 |
| 6.7b | particle trajectory in an upward uniform steady fluid flow with | |

$U_f$ = 10 mm/sec based on 1.0<Rep < 10.0 150

7.1 Schematic illustration of particle trajectory in a vortex chamber 154

7.2 Particle trajectories in the (z,r) plane based on Q = 46.49 ml/sec for particles injected from ro = $R_1$/100, $R_1$/10, $R_1$/5, $R_1$/4, $R_1$/3, and $R_1$/2, respectively. 169

7.3 Particle trajectories in the (z,r) plane based on Q = 84.67 ml/sec for particles injected from ro = $R_1$/100, $R_1$/10, $R_1$/5, $R_1$/4, $R_1$/3, and $R_1$/2, respectively. 169

7.4 Particle trajectories in the (z,r) plane based on Q = 105.55 ml/sec for particles injected from ro = $R_1$/100, $R_1$/10, $R_1$/5, $R_1$/4, $R_1$/3, and $R_1$/2, respectively. 170

7.5 Particle trajectories in the (z,r) plane based on Q = 130.62 ml/sec for particles injected from ro = $R_1$/100, $R_1$/10, $R_1$/5, $R_1$/4, $R_1$/3, and $R_1$/2, respectively. 170

8.1 Schematic illustration of the vortex chamber model 174

8.2 Relationship between particle injection locations ($r_o/R_1$) and chamber Reynolds number ($R_e$) 181

8.3 Comparison of predicted removal efficiency with experimental data based on chamber height Ho = 175 mm 183

8.4 Comparison of predicted removal efficiency with experimental data based on chamber height Ho = 120 mm 183

# Chapter 1

# Introduction

Water is one of the most valuable substances on earth. Stormwater runoff from human activity is the major source of water pollution. Water quality management is concerned with the control of this pollution from human activity; its main goal is to stop the degradation before it is no longer suitable for intended uses (Peavy, et al, 1985). However, with the growth of population, more and more rural areas are experiencing increased commercial, industrial, and residential development. This change in land-use has negatively impact on earth's hydrological cycle by increasing the area of impermeable surfaces (such as parking lots, paved roads, roofs, driveway, and sidewalks, etc.), and thereby increasing the loading of pollutants. Pollutants and other threats are becoming increasing prevalent nowadays. Therefore, stormwater runoff must be treated under sticker policy before entering the receiving water system so that it can better serve our society. Water quality management is one of most important issues of the 21$^{st}$ century.

## 1.1 Impacts of Land Use Behavior on Runoff Yield

Field monitoring and theoretical studies have shown that land use behavior, particularly urbanization, has significant impact on hydrological response (Bhaduri, et al, 2001; Roesner, et al, 2001; Sharma, et al., 2001; Stork, et al., 1998; and Wong and Li, 1997 & 1999). Urbanization can significantly impact hydrology and increase runoff volume and peak discharge. It can also reduce the time of concentration, and thereby

increase the flooding frequency, compared to an undeveloped area. In general, for a given rainstorm event, a developed area will yield significantly more runoff volume than prior to development; the increase in peak discharge can range from 2 to 10 times more (Roesner, et al., 2001). To assess the effect of urbanization on annual average runoff, Bhaduri, et al. (2001) developed a Long-term Hydrological Assessment model to predict the annual runoff volume, which was tested against the well known U.S. Storm Water Management Model (SWMM). By applying Bhaduri's model to two small watersheds near O'Hare International Airport, it was found that for a 10% increase in impervious area, the predicted average increase in annual runoff volume was between 6.6% and 7.3%. In a second study, Wong and Li (1997 & 1999) examined the effect of urbanization on the maximum peak discharge for an overland plane. The research showed that for a fully urbanized impermeable basin, the increase in flood peak ranged from 4 to 34 times than prior to development. The above two studies indicated that the urban land-use could significantly increase runoff volume and peak discharge.

Further, Stork, et al. (1998) examined the impacts of forest harvest and forest roads on peak stream flows in the Pacific Northwest. Stork's research showed that the peak runoff rate could increase up to 30% due to complete forest harvesting that reduces the time of concentration. However, the average increase in peak flow was 17.41% owing to forest road networks only. On the other hand, Sharma, et al (2001) conducted research to prioritize watersheds on the basis of runoff yield due to existing land condition in India. The impact of soil and water conservation measures on runoff was evaluated. This research showed that the runoff yield after conservation with planting decreased 42% of the value at pre-conservation. These two studies indicated that the

cultivated activities would decrease runoff, whereas the removing timber would increase the runoff. However, the studies by Bhaduri, et al. (2001) and Wong and Li (19997 & 1999) showed that the urban land-use would increase runoff volume and peak discharge. These four studies indicated that the land-use behavior has significant impact on hydrological response.

## 1.2 Impacts of Land Use on Water Quality

Research has shown that the land-use, especially urbanization, has significant impact on water quality (Avco, 1970; Roesner et al., 2001). Sources of pollution can be grouped into two categories: point source pollution, and non-point source (NPS) pollution. Point source pollution comes from an identifiable location and can be measured as discharge from industrial activities into a river through a pipe of ditch. In practice, this type of pollution can be easily controlled at the identifiable source locations before it is discharged into receiving waters. No-point source pollution occurs when stormwater runs over impermeable surfaces (such as roads and parking lots) or permeable surface (such as lawns), picking up oil, grease, heavy metals, airborne fallout, assorted chemicals, nutrients, and fertilizers, pesticides, bacteria, sediments, debris, and other contaminants. The later results are the pollution of natural resources such as receiving water that is no longer suitable for aquatic life or intended uses

To evaluate if the quality of water is good for the intended purpose such as drinking, recreation, or aquatic life, the water quality parameters are used to describe the quality of the water. Water quality parameters can provide useful information about the health of a water body. Water quality parameters of concern in storm water runoff

include total suspended solids (TSSs), Biochemical Oxygen Demand (BOD), Chemical Oxygen Demand (COD), heavy metals (Cu, Pb, and Zn), nutrients (P and N), and fecal bacteria (E. coli) (EPA, 1983; Roesner et al., 2001; NJDEP, 2004). Land surface characteristics not only influence the drainage of a watershed, but also affect the amount of pollution produced per unit area. Field investigations of pollution loads from storm water runoff in urban areas indicated that there is a strong relationship among the land surface characteristics, the degree of development, and storm water pollutant concentrations (Avco, 1970; EPA, 1983; Osborne, et al, 1998; and NACRF & FWQA, 1970). Avco (1970) conducted an investigation of the pollution concentrations and loads from storm water runoff in an urban area in Tulsa, Oklahoma. An assessment of pollution parameters measured on 15 urban watersheds by Avco (1970) indicated that the magnitudes of total suspended solids, Biochemical Oxygen Demand, Chemical Oxygen Demand, heavy metals (Cu, Pb, and Zn), nutrients (P and N), and fecal bacteria (E. coli), etc. are much higher than the common values found in stormwater runoff (NJDEP, 2004). Therefore the urban, commercial and industrial land-use has a great impact on stormwater quality. As this change in land-use increases, so does the threat of potential problems that could be caused by this activity.

## 1.3 Management of Water Quality

In the last few decades, the United States Environmental Protection Agency (EPA) has taken measures to curb water contamination. Great effort has been made to improve the overall water quality in lakes, rivers and streams by the control of point source and non-point sources pollutants before entering a waterway. However, among

these crucial water quality parameters in storm water runoff, the removal of total suspended solids (TSS) is one of the most important concerns for storm water treatment. To achieve the goal of TSS removal, many stormwater structural Best Management Practices (BMPs) have been designed and installed to remove pollutants from stormwater runoff before entering receiving water systems. A structural BMP is a physical device that is designed and constructed to trap pollutants from runoff. BMPs are techniques used to control stormwater runoff, sediment control, and soil stabilization; they also consist of management decisions to reduce non-point source pollution. The EPA defines a BMP as a "technique, measure or structural control that is used for a given set of conditions to manage the quantity and improve the quality of stormwater runoff in the most cost-effective manner." The major types of structural BMPs, which are recommended by New Jersey Stormwater Best Management Practices Manual (2004), are:

- Bioretention Systems
- Constructed Stormwater Wetlands
- Dry Well
- Extended Detention Basins
- Infiltration Structure
- Wet Pond
- Manufactured Treatment Devices
- Pervious Paving System
- Sand Filter
- Vegetative Filter

In general, the Manufactured Treatment Devices (MTDs) can be classified into two categories: hydrodynamic devices and filtration devices (NJDEP, 2004). As MTDs may

provide the desired performance for solid removal in less space and therefore in less cost compared to the traditional wet or dry basins, and furthermore, the mosquito control may be less of an issue than with traditional wet basins, the MTDs have been widely installed for storm water runoff treatment.

## 1.4 Types of Hydrodynamic Vortex Devices

The concept of hydrodynamic vortex separation was first developed and tested by Bernard Smisson at Bristol in the U.K. to treat combined sewer overflows (CSOs) in the early 1960s. Based on Smisson's pioneering work, a series of prototypes of hydrodynamic vortex separators, such as Swirl Concentrator, Storm King® Overflow, Downstream Defender®, and Vortechs™ Stormwater Treatment System, etc., have been developed, tested, and installed for wastewater and stormwater treatment over the last 40 years.

## 1.5 Objectives of the Current Study

Many prototypes of hydrodynamics separators have been developed for wastewater and stormwater treatment. Additionally, multiple laboratory studies and field tests have been performed. However, with these advances, so far not much fundamental development has been found in the current literature search due to the complexity of the problem. Design specifications of commercial separators are derived from empirical equations that unique and proprietary to each manufacturer. For a given design flow rate and the desired particle removal efficiency, the equations that could provide a direct determination of removal efficiency as a function of design flow rate, fluid and solid

properties and unit dimensions are what we are looking for. The overall objective of the study is to theoretically establish some design basis for a selected type of vortex separator. The specific goals of this investigation are:

- To experimentally investigate the effects of the chamber height and the inlet pipe elevation on the particle removal efficiency of selected vortex chambers.
- To theoretically determine the angular velocity for turbulent vortex chamber flow.
- To theoretically determine the flow pattern in the confined vortex chamber.
- To investigate the dynamic response of a single particle in an upward uniform steady flowfield.
- To determine the particle trajectories in a confined vortex chamber flow.
- To develop a general formula, based on the selected vortex separator, for unit performance evaluation and sizing.

## 1.6 Organization of the Dissertation

In this chapter, the impacts of land use behavior on runoff yield and stormwater quality are briefly discussed. Some of the major types of structural stormwater best management practices (BMPs) for stormwater treatment are presented.

Chapter 2 provides an overview about the development and evolution of hydrodynamic devices over the past 40 years. The developed unit sizing approaches by previous investigators for these devices are summarized and discussed based on current literature review. Equations characterizing particle settling velocity are also reviewed

and discussed in this chapter. Finally, based on the literature review, the gaps in the selected study area are identified.

In Chapter 3, an experimental study on the particle removal efficiency in the confined vortex chamber has been conducted. The impacts of chamber height and the elevation of the tangential inlet pipe on the removal efficiencies were examined by changing the chamber height and the inlet pipe elevation, respectively.

In Chapter 4, based on the law of conservation of angular momentum and the boundary conditions, a simple formula has been derived to determine the angular velocity for turbulent vortex chamber flows. It is possible to predict the angular velocity for the confined turbulent vortex chamber flows.

In Chapter 5, a vortex model, based on Navier-Stokes governing equations and boundary conditions, for simulating the flow pattern in a confined vortex chamber with the tangential inflow has been developed.

In Chapter 6, the characteristics of particle motion in a one-dimensional upward uniform steady fluid flow are investigated. The analytical solutions for particle motion in a one-dimensional upward uniform steady fluid flow are obtained. The derived formulas were compared with previous studies such as Cheng's formula and a good agreement was observed.

In Chapter 7, the characteristics of particle motion in a confined vortex chamber were investigated. The analytical solutions of particle trajectories in the confined vortex chamber, based on the vortex models developed in Chapters 6 and the governing equation of particle motion, have been derived.

In Chapter 8, a unit sizing formula, based on the particle trajectory equation derived in Chapter 7, has been developed. The predicted results for particle removal efficiency with this formula were compared with the experimental results and a good agreement was obtained.

In Chapter 9, a summary of main achievements and findings obtained through this study is presented. The recommendations for future work are also provided.

# Chapter 2

# Review of Literature

Vortex separators are manufactured solid-liquid separation devices that use the vortex principles to remove suspended pollutants from stormwater runoff in highly developed areas where the available land space is limited. These devices were primarily designed to remove suspended particles from stormwater runoff, but some of them were also designed with the features to remove floatable pollutants (Andon & Smisson, 1994; Fenner and Tyack, 1998). The following literature review provides an overview about the development and evolution of hydrodynamic devices, the reported performances, and the development of sizing approaches.

## 2.1 The Key Developmental Stages of Hydrodynamic Separators

The history of dynamic separation can be dated back to the early of 1960s, when Mr. Bernard Smisson developed the first full-size cylindrical vortex chamber to treat the combined sewer overflow (CSO) at Bristol in the U.K. (Smission, 1967; Andoh & Smission, 1994). Measured results indicated that this first generation vortex separator could effectively remove about 70% of the pollutant loadings (Smisson, 1967). Since then, a family of hydrodynamic vortex separators has evolved from Smisson's original model.

In the 1970s, based on Smisson's initial work and with his help as a consultant, a second generation of hydrodynamic vortex separator (HDVS) – USEPA Swirl Concentrator and Swirl Primary Separator were developed to remove the settleable solids

from combined sewer overflows by the American Public Works Associations and EPA (Field, 1972; Sullivan, et. al., 1978; Andoh & Smission, 1994). Based on his initiative, Mr. Smisson received "an APWA award of merit in recognition of the excellence of his work, ingenuity, resourcefulness, and grasp of hydraulic engineering principles" (Andoh and Smisson, 1994).

In 1980s, further research work continued in the United Kingdom. In order to overcome some disadvantages of the EPA Swirl Concentrator, such as "shoaling of solids on the base, reduction of head loss at high flows and to further improve the performance" (Andoh and Saul, 2003), a much improved third generation of HDVS – Storm King® Overflow with specially designed internal components and high separation efficiencies was developed and subsequently commercialized in the UK.

During the 1990s and early of 2000s, the swirl concentrator was further advanced in the USA. This led to the development of fourth generation HDVS – Downstream Defender® and Vortechs$^{TM}$ Stormwater Treatment System for stormwater treatment. These new developed devices in configuration differ from the CSO treatment devices. Unlike the CSO operations, solids removed from stormwater are trapped in the bottom of the chamber that could be stored for several months before periodical removal (H.I.L. Technology, 2005; Vortechnics$^{TM}$ **,** 2004).

## 2.2 Reported Performance of Hydrodynamic Devices

The solids removal performance of hydrodynamic vortex separators depends on the settling characteristics of the suspended solids, operating conditions, evaluation (lab and field) techniques, and the fraction of dissolved solids in the wastewater or stormwater

(Andoh and Smisson, 1994 and 1996; Field and O'Connor, 1996; Guo, 2005). Reported test results show that removal efficiencies decrease with decreasing particle size in hydrodynamic separators (Sullivan et al., 1972; Deamer et. al., 1994; Brueske, 2000; H.I.L Technology, 2005). The vortex separation technology could not remove non-settleable solids. In general, non-settleable solids are defined as those that remain in suspension after a specified settling period of 1 hour (APHA, 1987). According to this definition, these non-settleable solids are generally less than 10 $\mu m$ in diameter (Andoh & Smisson, 1994). The limit of suspended particles that may be removed in a vortex separator is with a settling velocity of 0.1 – 0.14 cm/sec; while particles tested at a settling velocity lower than this range may not be effectively removed in a hydrodynamic separator (Field and O'connor, 1996; Brueske, 2000). According to Stokes particle settling law, this limit of settling velocity is associated with a spherical particle diameter of approximate 68 $\mu m$ based on a specific gravity of 2.65 at $20^{o}$C

Sullivan, et al. (1972) stated that the swirl concentrator is very efficient in separating both grit and settleable solids in their middle (>0.2 mm) and larger grain size ranges, while for the smaller grain sizes the separation was less efficient. Based on a large pilot testing, Sullivan et al. (1978) reported that a 12-ft diameter swirl concentrator achieved 60% and 42% removal efficiencies of settleable solids for the hydraulic application rate (HAR) of 1.8 gpm/ft$^2$ and 2.8 gpm/ft$^2$ for untreated sewage in Toronto, Canada.

Laboratory test results from a Vortecs$^{TM}$ unit and a Downstream defender$^{TM}$ unit indicated that solids removal efficiency decreases with decreasing particle size and increasing flow rate. Based on the test results, the Downstream defender$^{TM}$ performance

could achieve a 70% solids mass removal efficiency, sized at a hydraulic loading rate of 20 $gpm/ft^2$ for F-95 sand with an average influent concentration of 240 mg/l, an average $d_{50}$ particles size of 120 $\mu m$ (H.I.L Technology, 2005). The laboratory test results for Vortechnics$^{TM}$ unit, with particle size ranging from 38 $\mu m$ to 500 $\mu m$, showed that for particles greater than 63 $\mu m$, removal efficiencies were greater than 80% when the hydraulic loading rates were less than 10 - 20 $gpm/ft^2$ of grit chamber area (Vortechnics, 2004; Winkler and Guswa, 2002).

## 2.3 Review of Sizing Approaches

Since Mr. Bernard Smisson first built and tested a full-scale cylindrical vortex unit to treat the combined sewer overflow (CSO) at Bristol in the U.K., different types of vortex technologies have been developed to treat wastewater and stormwater during the last forty years. At the same time, many researchers have been investigating the sizing approaches for these hydrodynamic devices. Some studies have attempted to investigate the relationship between the performances of model and prototype separators with semi-empirical equations, or using the scaling laws such as Froude scale and Hazen scale (Sullivan et al, 1972 & 1978; Deamer, et al, 1994; Andoh and Smisson, 1994; Fenner and Track, 1997 &1998; Luyckx and Berlamont, 2004). However, not much published work, which could provide a straightforward method to size the device units, was found in the current literature search. A brief review of the sizing approaches in the current practice is summarized in the following paragraphs.

### 2.3.1. EPA Swirl Concentrator / Swirl Primary Separator

Based on Smisson's original work, a device, called a swirl concentrator was developed by the American Public Works Association Research Foundation (Sullivan, et al, 1972). To further investigate its application as a combined sewer overflow regulator and as a grit chamber, a series of intensive studies were performed by USEPA to determine the configurations of the swirl concentrator, flow patterns, and settleable solid removal efficiency by means of the hydraulic test models and mathematical models in 1970s and 1980s (Sullivan, et al., 1974; Sullivan, et al., 1978; Sullivan, et al., 1982; and Pisano, et al., 1984). The comparison of their numerical solutions from the mathematical model against the laboratory results indicated that the velocity profile from the mathematical model basically match with the physical model (Sullivan, et al, 1972, and Sullivan, et al., 1978). The mathematical model correctly predicted the trends of removal efficiency due to the variations in flow rate, size, settling velocity, and geometric changes. Sullivan's analysis also showed that the predicted separation efficiencies are very close to the measured values for very slow and very fast settling particles, while for the intermediate settling rates and higher flows the mathematical model will over-predict the concentrator performance.

Based on the study of the hydraulic models, and the mathematical model that was developed to predict the performance of the swirl concentrator with variable design criteria, Sullivan, et al (1972 and 1978) recommended that scaling for the liquid flow pattern and particle flow pattern for a swirl concentrator of size $S_1$ (model), could be

scaled to represent the liquid and particle flows in a geometrically similar concentrator of size $S_2$ (prototype) using Froude number ($F_r$) scaling factor:

$$F_r = \frac{V}{\sqrt{gS}} \tag{2.1}$$

where S is the reference length, V is the reference velocity (e.g. flow velocities and particle settling velocities), and g is the acceleration due to gravity.

Sullivan et al. (1972) also stated that the performance of prototype scale device could be accurately predicted from the laboratory tests. By maintaining the same Froude number between the model and the prototype, the flow velocities, particle settling velocities, and design flow rate from the model for a swirl concentrator of size $S_{model}$ can be scaled to represent the flow in a geometrically similar concentrator of size $S_{prototype.}$ The relationships for flow velocities, particles settling velocities, and flow rates between these two concentrators can be written as:

$$\frac{V_{prototype}}{V_{model}} = \sqrt{\frac{S_{prototype}}{S_{model}}} \tag{2.2}$$

$$\frac{Q_{prototype}}{Q_{model}} = \left( \frac{S_{prototype}}{S_{model}} \right)^{5/2} \tag{2.3}$$

More recently, Luyckx and Berlamont (2004) conducted research to investigate the removal efficiency of vortex separators with a simple vortex test model made of a

steel plate in the hydraulic laboratory of the University of Ghent in Belgium. The steel model was constructed with an overflow crest and a base flow pipe at the center of the bottom (same as the combined sewer over flows). The diameter of the overflow chamber was 1.2 m, and the inlet pipe had changeable sizes of 25 cm, 30 cm and 35 cm located at the bottom of the chamber. This device works when the inflow enters the chamber tangentially. Based on 462 experimental results obtained from the literature search, and their own model test results, as well as with the help of regression analysis, a removal efficiency formula was derived:

$$\eta = 1 - \left(1 - \frac{q}{Q}\right).\exp\left[-K \cdot f_1\left(\frac{v_s}{v_i}\right) \cdot f_2\left(\frac{h}{D}\right) \cdot f_3\left(\frac{D}{d}\right) \cdot f_4\left(R_e\right)\right] \tag{2.4}$$

in which

$$k = 30 \tag{2.4a}$$

$$f_1 = \max\left[\frac{v_s}{v_i}\left(1 - 2.5 \cdot \exp\left[-250\frac{v_s}{v_i}\right]\right), 0\right] \tag{2.4b}$$

$$f_2 = 1 - \exp\left(1.4\frac{h}{D}\right) \tag{2.4c}$$

$$f_3 = \max\left[1, 0.05\left(\frac{D}{d}\right)^2\right] \tag{2.4d}$$

$$f_4 = \begin{cases} 1, & for\ R_e \le 20000 \\ 1 - \exp\left(-\dfrac{22000}{R_e - 20000}\right), & for\ R_e \succ 20000 \end{cases} \tag{2.4e}$$

where $\eta$ is removal efficiency, q is base flow rate ($m^3/s$), Q is inflow ($m^3/s$), $v_s$ is settling velocity of the sediments (m/s), $v_i$ is mean velocity in the inlet pipe (m/s), h is height of the overflow crest (m), D is diameter of the overflow chamber (m), d is diameter of the inlet pipe (m), and Re is Reynolds number in the inlet pipe.

This equation indicates that the removal efficiency is a function of the 5 dimensionless numbers of $\frac{q}{Q}, \frac{v_s}{v_i}, \frac{h}{D}, \frac{D}{d}, and\ R_e$. Though this is a reliable equation for device sizing, the derivation of this equation is based on different particle size distributions and different unit internal components. The predicted results from this equation greatly deviate from the experimental data collected. For a given separator, the removal efficiency generally varies with different particle size distributions. Therefore the validation of this equation for different particle size needs to be further investigated.

### 2.3.2 Storm King™ Overflow

The Storm King™ Overflow units, which are a precursor to H.I.L Technology's Downstream Defender™, are hydrodynamic separators operating with underflows. Andoh and Smisson (1994) developed a semi-empirical mathematical equation for the Storm King™ device. The general form of the equation is as follows:

$$\frac{D^2 S_v}{Q} = K_a^{K_b} \sqrt{\frac{N}{R}\left(\frac{1-P}{P}\right)} \qquad (2.5)$$

where D is the diameter of separator; $S_v$ is the settling velocity of particle in fluid; Q is the flow rate, N is the ratio between solids concentration in the underflow to that in the overflow; R is the ratio of overflow to underflow; P is underflow proportion; $K_a$ and $K_b$ are empirical coefficients, which were derived from several tank arrangements and geometries based on the calibration of separator units (Andoh and Smisson, 1994). This design equation can be applied to predict the removal efficiency for the separators with underflow at differing settling velocities.

Moreover, based on the analysis of laboratory results of removal efficiencies from a series of geometrically similar hydrodynamic separators operating without baseflow, Fenner and Tyack (1997) concluded that the use of single dimensionless groups such as Froude number or Hazen number has limited applicability to predict the full-scale separator performance. By scaling the flow rates for a series of geometrically similar models to a 1,600-mm diameter prototype separator with different scaling protocols, Fenner and Tyack found that Froude scaling of the model flows produces the best fit to the observed performance of the prototype over the high flows; while for the low flow ranges, a better fit to the observed prototype data were obtained with Hazen scaling law (which is defined as the ratio of the chamber flow rate to the particle settling velocity). Fenner and Tyack (1997) pointed out that Froude scaling law is applicable to systems with a significant free surface where the gravitational forces dominate. Fenner and Tyack found that the use of a hybrid protocol incorporating the more dominant Hazen scaling over the low flow ranges could successfully predict the efficiency of solids removal from full-scale hydrodynamic separators over a wide range of flow conditions. Based on the

data from the 300-mm model and associated prototype tests, Fenner and Track (1997) proposed a hybrid equation:

$$Q_{prototype} = Q_{model}\left[\left(\eta_m L_r^2\right) + \left(1-\eta_m\right)L_r^{2.5} + \frac{B}{3}\left(1-\eta_m\right)L_r^{2.5}\right] \tag{2.6}$$

where $\eta_m$ is the model efficiency (%)/100 at corresponding $Q_{model}$ flow; $Q_{prototype}$ is the inflow to prototype separator (L/s); $L_r$ is the length ratio for geometric similarity (usually inlet pipe or chamber diameters); and B is the average particle diameter (mm).

Furthermore, by comparing the performances of a 300-mm diameter model with a full-scale prototype separator with an underflow condition, Fenner and Tyack (1998) extended their earlier study to examine whether the developed hybrid equation could be applied to this kind of device. Based on the model studies using Hazen and Froude scaling, Fenner and Tyack (1998) concluded that no single dimensionless group could be used for scaling over the whole flow range for separators operating with an underflow. This conclusion is consistent with that obtained by Fenner and Tyack (1997) for separators without underflow. Their analysis showed that Eq.(2.6) could not predict the observed efficiency of the 1,600-mm diameter prototype when operating with an underflow. Based on the results from the 300-mm diameter model and the 1,600-mm diameter prototype, a simplified hybrid equation for separators operating with an underflow was proposed by Fenner and Tyack (1998):

$$Q_{prototype} = Q_{model}\left[\left(\eta_m L_r^2\right) + 0.75\left(1-\eta_m\right)L_r^{2.5}\right] \tag{2.7}$$

This study showed that this equation provides a good fit to all the observed data of prototype separator with an underflow. However, Fenner and Tyack's early study (1997) showed that scaling for devices without underflow conditions partially depended upon particle size, while the modified but similar hybrid equation indicated that scaling is independent of particle size for separators operating with an underflow. This may be due to the effect of the different flow pattern in the core zone of the chamber.

### 2.3.3 Downstream Defender® and Vortechs$^{TM}$ System

For the design of Downstream Defender and Vortechs$^{TM}$ system, though some numerical research has been conducted to simulate the flow patterns and estimate the solids removal efficiency (such as Faram and Harwood, 2003), so far there are no empirical or theoretical equations that could provide a straightforward determination of the efficiency as a function of unit configuration sizes and design flow rate. The unit sizing approach is still based on the scaling methods at the current practice.

## 2.4 Review of Particle Settling Velocity

### 2.4.1 Stokes' Law

The settling velocity of sediment particles is defined as the rate at which the sediment settles in fluids. When we talk about the settling velocity or terminal velocity of sediment particles, it is inevitable to recall George Gabriel Stokes and his Law. George Gabriel Stokes was an Irish-born mathematician who had spent much of his life to work with fluid properties. He is most famous due to his work describing the motion

of a sphere through viscous fluids. This leads to the development of his famous settling law, Stokes' Law, in 1851. By equating the drag resistance $3\pi\mu d V_s$ to the net weight of a spherical particle, the equation of particle settling velocity in the present notations is as follows:

$$V_s = \frac{(\rho_p - \rho_f)gd^2}{18\mu} \tag{2.8}$$

where $V_s$ is the terminal settling velocity of particle; d is the diameter of sphere; $\rho_p$ is the density of particle; $\rho_f$ density of fluid; g is the gravitational acceleration; and $\mu$ is the viscosity of fluid. This law indicates that for a given fluid and temperature, the particle settling velocity depends upon both of its size and density. Though Stoke's Law can provide a representative indication of orders of magnitude of terminal settling velocities, it cannot accurately predict the real life settling phenomena due to the combined effects of flocculation, adsorption, re-suspension, and turbulence (Simons & Senturk, 1992; Andoh & Smisson, 1994; Cheng, 1997; and Nikora, et al, 2004).

### 2.4.2 Limitations of Stokes' Law

**Flow Conditions**: Stokes' law pertains to the terminal settling velocity of a sphere in a fluid. It has been widely applied to water and wastewater treatment design since its development. However, this relationship only holds for laminar flow (i.e. the fluid moves around the object in an orderly, non-turbulent way), while for turbulent settler, this equation is not valid. Therefore, Stokes' law only holds for low Reynolds numbers

($R_e \leq 0.1$)), but, in practice, many investigators usually apply Stokes law to Reynolds number up to the limit of $R_e = 1.0$. Reynolds Number $R_e$ is used to describe whether flow conditions around a sphere are laminar, transition or turbulent:

$$R_e = \frac{\rho_f V_s d}{\mu} \tag{2.9}$$

Flow conditions are (Sincero & Sincero1996):

Laminar flow for $R_e \leq 1.0$

Transitional flow for $1.0 \prec R_e \prec 10^4$

Turbulent flow for $R_e \succ 10^4$

**Range of Particle Size**: Stokes' law cannot be applied to all the particles settling in a fluid. Research shows that to keep particles falling in a straight line, particles sizes must be greater than 0.5 micron in diameter (Carver, 1971). This is because Brownian movement of fluid molecules will affect the movement of very fine particles. In term of that Stokes' law being a function of Reynolds number, temperature, and the particles density, particles of quartz spheres should not be greater than the theoretically determined size of 50 micron in diameter ($R_e \approx 0.1$) (Oseen, 1913; Carver, 1971; Clif, et al, 1978; Sincero & Sincero, 1996). If particles are larger than this limit, the turbulence condition will occur during settling of particles. However, in practice, many investigators apply Stokes' Law to particles up to the size limit of sand 100 micron ($R_e \approx 1.0$). Rubey (1933) found that the observed settling velocity, for particles with sizes up to 140 micron,

differs little from the theoretically determined Stokes' values. This indicated that the settling velocities for clay and silt particles might be approximately estimated from Stokes' law, while for grains with diameters greater than 140 micron (such as sand, pebbles, and boulders), Stokes' law no longer holds.

**Shape of Particles**: The derivation of Stokes' law was based on the assumption that the particles are spheres in shape. But most particles of practical interest are irregular in shape. In nature, no particles are perfect spheres, and many naturally occurring solid particles possess an oblate or lenticular form. For natural particles, the shape effect on settling velocity for large particles is bigger than that for smaller particles (Van Rijin, 1993). The shape of particles can generally be defined by the Corey shape factor (Graf, 1971):

$$SF = \frac{c}{\sqrt{ab}} \tag{2.10}$$

where a is the length along longest axis perpendicular to other two axes, b is the length along intermediate axis perpendicular to other two axes, and c is the length along short axis perpendicular to other two axes. The average SF-factor is approximately 0.7 for natural sand (Graf, 1971; Van Rijin, 1993; Cheng, 1997; Jimenez and Madsen, 2003). The effect of particle shape on settling velocities was not considered in Stokes law.

### 2.4.3 Particles above the Range of Stokes' Law

As stated in the above, Stokes' law is restricted to $R_e \leq 1.0$ and spherical particles with an upper limit of 50 – 100 micron, to overcome this shortcoming, many equations,

which can be applied to a wider range of Reynolds numbers, have been proposed by numerous investigators from the early of the last century (Rubey, 1933; Albertson, 1953; Graf, 1971; Clift, et. Al., 1978; Hallermeier, 1981; Dietrich, 1982; Van Rijn, 1993; Cheng, 1997; Ahrens, 2000; Aimerez, et. Al., 2003; Jimenez and Madsen, 2003; Brown and Lawler, 2003; Nikora, et. Al., 2004); a few of them are summarized as follows.

#### 2.4.3.1 Rubey's Formula

By considering the viscous resistance and impact of the fluid, Rubey (1933) developed a general equation to estimate the settling velocities for sphere particles within the size range of Stokes' law as well as to coarser particles (such as sand and gravel):

$$V_s = \frac{\sqrt{\frac{4}{3} g \rho_f \left(\rho_p - \rho_f\right) r^3 + 9\mu^2} - 3\mu}{\rho_f \, r} \tag{2.11}$$

where particle settling velocity ($V_s$) and radii (r) are measured in centimeters. Rubey compared the predicted results from this general equation with the observed data for quartz grains and a good agreement was obtained. However, Rubey's formula can not be directly applied to the natural sediment particles as it does not consider the shape effect of particles in the formula.

#### 2.4.3.2 Van Rijn's Formula

Van Rijin (1993) pointed out that "the shape effect is largest for relatively large particles (>300 $\mu m$) which deviate more from a sphere than a small particle". The

equations derived for spherical particles could not be directly applied to the natural sediment particles due to the differences in shape. Therefore, to solve this problem, Van Rijn (1993), based on his study, proposed the following equations to determine the terminal fall velocity of non-spherical particles:

$$V_s = \frac{(s-1)gd^2}{18\nu} \qquad for \quad 1 \prec d \le 100\ \mu m \qquad (2.12a)$$

$$V_s = \frac{10\nu}{d}\left[\left(1+\frac{0.01(S-1)gd^3}{\nu^2}\right)^{0.5} - 1\right] \quad for \ \ 100 \prec d \prec 1000\ \mu m \qquad (2.12b)$$

$$V_s = 1.1[(s-1)gd]^{0.5} \qquad for \quad d \ge 1000\ \mu m \qquad (2.12c)$$

where d is the sieve diameter, which is defined as the diameter of a sphere equal to the length of the side of a square sieve opening through which the given particle will just pass, S is the specific gravity ( $\rho_p / \rho_f$ ), and $\nu$ is the kinematic viscosity coefficient.

### 2.4.3.3 Cheng's Formula

Cheng (1997) proposed a simple formula to predict the settling velocities for the natural sediment particles in the present notation:

$$\frac{V_s d}{\nu} = \left(\sqrt{25 + 1.2d_*^2} - 5\right)^{1.5} \qquad (2.13)$$

where $V_s$ is the settling velocity, $\nu$ is the kinematic viscosity coefficient, and $d_*$ is the dimensionless particle parameter which is defined as:

$$d_* = \left[\frac{(s-1)g}{\nu^2}\right]^{1/3} d \tag{2.13a}$$

in which S is the specific gravity of the sediment given by $\rho_p / \rho_f$ , and g is the gravitational acceleration. This equation can be applied to a wide range of Reynolds number ranging from the Stokes flow to the turbulent flow. However, this equation does not explicitly account for shape of particle.

**2.4.3.4 Jimenez and Madsen' s Formula**

More recently, and based on the previous work of Dietrich and the assumption that the sediment shape factor and roundness are known, Jimenez and Madsen (2003) presented another formula to estimate the terminal settling velocity of natural sediment particles in a quiescent fluid for grain sizes between 63 $\mu m$ and 1000 $\mu m$:

$$\frac{1}{V_*} = A + \frac{B}{S_*} \tag{2.14a}$$

$$V_* = \frac{V_s}{\sqrt{(s-1)gd}} = \sqrt{\frac{4}{3C_D}} \tag{2.14b}$$

$$S_* = \frac{d}{4\nu}\sqrt{(s-1)gd} \tag{2.14c}$$

where $V_*$ is the dimensionless settling velocity; $S_*$ is the fluid-sediment parameter; s is the specific gravity; g is the gravitational acceleration; $\nu$ is the kinematic viscosity coefficient; d is the sediment diameter, $C_D$ is the drag coefficient, A and B are constants to be determined by fitting equation (2.16a) to the experimental data.

## 2.5 Review of Types of Developed Vortex Models

Historically, the study of vortex phenomena can be traced to the 1930s when Rosenhead evaluated the two-dimensional flow with a point vortex method (See Lamb, 1945; Lugt, 1983; Ying and Zhang, 1997; Cottet and Koumoutsakos, 2000). However, the development of vortex methods was limited due to the lack of computational tools until 1970s (see Ying and Zhang, 1997). After that, the vortex method was rapidly developed with the increasing power of computational tools. A lot of numerical calculations were performed to simulate the vortex phenomena (Chorin, 1973, 1978, 1980, 1990 and 1993; Leonard 1975, 1980, and 1985). At the same time, many mathematicians (such as Batchelor, 1967; Greenspan, 1980; Saffman, 1992; Ying and Zhang, 1997; Cottet and Koumoutsakos, 2000; etc.) were attracted by these numerical works, and joined this research field. Thereafter the principles of vortex methods have also been applied to many fields such as the design of vortex nuclear reactors, and centrifugal settlers or cyclones as well as the simulation of meteorology (Lugt, 1983; Ogawa, 1992). The vortex method has become one of the most important methods to simulate the incompressible flows.

In general, there are two types of vortex. One is called the free (irrotational) vortex, and the other is the forced (rotational) vortex. The rotational flow regimes are

generally described as irrotational (free vortex) or rotational (forced vortex) flow that possesses vorticity, which is defined as the circulation per unit area at a point in the flow field. When the external force applied to the fluid is only the gravitational force and the fluid is rotating around a common axis, the free vortex is created. However, when we consider the motion of a viscous fluid, since the viscosity gives the resistance force (frictional force) to the motion of fluid, the forced (rotational) vortex is formed. The vortex flows are normally turbulent flows. Subsequently, due to its practical applications in technology and nature, several vortex models, such as the Rankine combined vortex, the Burgers vortex, and the Sullivan vortex models, etc., have been developed to simulate the practical problems such as tornado, hurricanes, ocean circulations, tidal vortices, etc. Several of the typical vortex models are described as follows.

### 2.5.1 Free Vortex (Irrotational Vortex)

For free vortex, the tangential velocity ($U_\theta$ ) along any streamline is inversely proportional to the radius (r) of the streamline (Lamb, 1945; Shapiro, 1959; Lugt, 1983; Ogawa, 1993):

$$U_\theta = \frac{\Gamma}{2\pi r} \tag{2.15}$$

where $\Gamma$ is the circulation for any closed circuit enclosing the origin. It is defined as the line integral of the velocity around any closed curve (C):

$$\Gamma \equiv \oint_C U \cos\alpha \, dl \equiv \oint_C \vec{U} \cdot d\vec{r} \tag{2.16}$$

where $\vec{U}$ denotes the vector velocity and $\vec{r}$ the vector radius from any fixed origin. The vorticity of the free vortex is zero everywhere, except for a singularity at the center-line. The circulation of any closed circuit enclosing the origin has the same value for each closed circuit. The free vortex demands that the tangential velocity at the axis of rotation to be infinite. This kind of flow patterns does not occur in real fluids. In real fluids, the existence of viscosity will result in the velocity gradients and vorticity to occur. Moreover, the boundary layer effects will cause the creation of a secondary flow superimposed on the primary flow (Greenspan, 1980; Andoh and Smisson, 1994).

### 2.5.2 Forced Vortex (Rotational Vortex)

The forced vortex flow regime corresponds to a solid body type of angular motion about an axis. Since in this case, the individual fluid particles maintain their relative positions as in the case of a rigid solid, the tangential velocity along a streamline can be expressed as (Lamb, 1945; Shapiro, 1959; Greenspan, 1980; Ogawa, 1993):

$$U_\theta = \omega \, r \tag{2.17}$$

where $\omega$ is the angular velocity; and r is the radius.

### 2.5.3 Rankine Combined Vortex Model

Fluid motion consisted of a potential vortex (free vortex) and a solid-body rotation (forced vortex) is called a Rankine Vortex (Lugt, 1983). For a rational flow that is composed of a forced vortex in the core, and a free vortex in the outer, the Rankine Vortex model may best describe this phenomenon (see Figure 2.1).

The Rankine combined vortex is a simple model that has two separate flow fields only with the tangential velocities. The tangential velocity in the interior flow field (core) that rotates like a solid body increases linearly with the radius from zero along the central axis to a maximum value at a radius (a). The exterior flow field (tail) is also tangential with a maximum velocity at radius (a). The velocity decreases inversely with radius from this point outward. The mathematical model for the tangential velocity in Rankine combined vortex model can be expressed as (Lugt, 1983; Saffman, 1992; and Ogawa, 1993):

$$U_\theta = \begin{cases} \omega r & r \le a \\ \dfrac{\Gamma}{2\pi r} & r \succ a \end{cases} \tag{2.18}$$

where $\omega$ is the angular velocity; a is the radius of the vortex core; r is the radial coordinate; and $\Gamma$ is the circulation for any closed circuit enclosing the origin. The Rankine combined vortex model is useful to define the diameter of a vortex. This vortex model is occasionally used to predict the wind distribution in hurricanes and tornadoes.

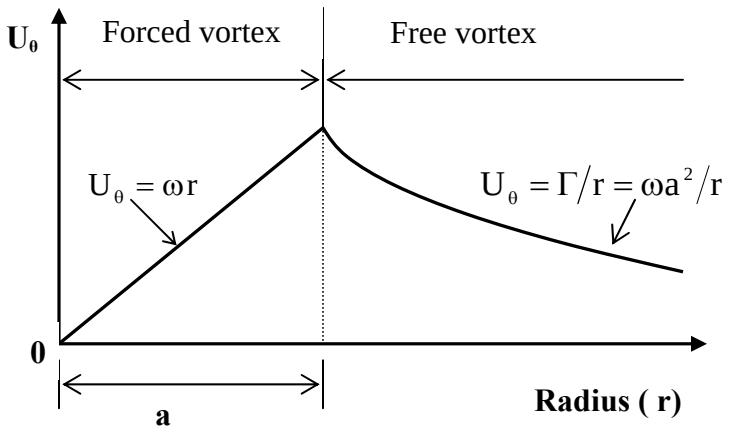


**Figure 2.1 Schematic Illustration of the Rankine Combined Vortex Model**

### 2.5.4 Burgers Vortex Model

Burgers vortex model is an exact solution of the Navier-Stokes equation for three-dimensional vortex flow (Burgers, 1948). The assumptions for Burgers vortex model are that the fluid flow is the steady state; the fluid flow is axis-symmetry; the axial gradient (d/dz) of the physical quantities is small; the radial velocity only depends on the radius r, the axial velocity is a linear function of z. Mathematic expressions for the tangential, radial, and axial velocity components as well as the vorticity components in the present notations are as follows:

$$U_\theta = \frac{\Gamma}{2\pi r}\left(1 - e^{-\frac{a r^2}{2\nu}}\right), \quad a \succ 0 \tag{2.19a}$$

$$U_r = -a\,r \tag{2.19b}$$

$$U_z = 2\,a\,z \tag{2.19c}$$

$$\Omega_z = \frac{\Gamma a}{2\pi\nu} e^{-\frac{a r^2}{2\nu}} \tag{2.20a}$$

$$\Omega_r = \Omega_t = 0 \tag{2.20b}$$

where the parameter a is a measure of the radial influx. $U_\theta$ is independent of z, but depends on the influx parameter a. At the center r = 0, $\Omega_z$ has the maximum value of $\Gamma a/2\pi\nu$, which is twice the angular velocity of the solid-body rotation of the core:

$$U_\theta = \frac{\Gamma a}{4\pi\nu} \quad or \quad \Omega = \frac{\Gamma a}{4\pi\nu} \quad for \quad \frac{a r^2}{2\nu} \le 1 \tag{2.20c}$$

The pressure field is given by the following equations:

$$p(r,z) = p(0,0) + \rho\frac{\Gamma^2 a}{16\pi^2\nu}\int_0^{\frac{ar^2}{2\nu}}\left(\frac{1-e^{-x}}{x}\right)^2 dx - \frac{\rho}{2}a^2\left(r^2+4z^2\right) \tag{2.20d}$$

Burgers vortex model is also occasionally used to predict the wind distribution in hurricanes.

### 2.5.5 Sullivan Vortex Model

The Sullivan vortex is a closed solution to Navier-Stokes Equation (Ogawa, 1993). For a stead two-celled vortex, which is characterized by a reversal axial flow near the axis compared to the outer flow, Sullivan derived the following solution in the present notions (Lugt, 1983; and Ogawa, 1993):

$$U_\theta = \frac{\Gamma}{2\pi r}\frac{H\left(ar^2/2\nu\right)}{H(\infty)} \tag{2.21a}$$

$$U_r = -ar + \frac{6\nu}{r}\left(1-e^{-\frac{ar^2}{2\nu}}\right) \tag{2.21b}$$

$$U_z = 2az\left(1-3e^{-\frac{ar^2}{2\nu}}\right) \tag{2.21c}$$

where

$$H\left(\frac{ar^2}{2\nu}\right) = \int_0^{ar^2/2\nu}\exp\left[-x+3\int_0^x\left(1-e^{-s}\right)s^{-1}ds\right]dx \tag{3.22a}$$

$$H(\infty) = 37.905 \tag{3.22b}$$

The distribution of the static pressure can be written as:

$$P(r,z) = P(0,z) - \frac{\rho}{2}\left\{4a^2z^2 + a^2r^2 + \frac{36\nu^2}{r^2}\left[1 - e^{-ar^2/2\nu}\right]^2\right\} + \rho\int_0^r \frac{V_\theta^2}{r}dr \tag{3.23}$$

Sullivan vortex model is also occasionally used to predict the wind distribution in tornadoes. All of the vortex models that are solutions of the Navier-Stokes equation are steady state. That is, any term involving $\partial/\partial t$ is not present in the equation.

## 2.6 Gaps in This Area

Though many types of hydrodynamic separators have been developed for wastewater and stormwater treatment, to date minimal fundamental study exists on this topic. Design specifications of commercial devices are based on the semi-empirical equations that are suitable only for the specific manufacturer. No unifying scenarios exist. The fundamental investigation about the mechanisms of solid-liquid separation in a confined vortex chamber is necessary for the achievement of the optimum design.

# Chapter 3

# Experimental Study on Particle Removal Efficiencies in Confined Vortex Chamber

In this chapter, the particle removal efficiencies in the confined vortex chambers operating with a tangential inlet pipe and without underflow were experimentally examined. The effects of the chamber heights and the inlet pipe elevations on the particle removal efficiencies were investigated by changing the heights of the chamber and the inlet pipe, respectively. Four physical test models were considered: three with different inlet pipe elevations and one with a lower chamber height. The measured results indicate that for a given chamber height and chamber diameter the changing of inlet pipe height has no significant impact on the particle removal efficiency. However for a given chamber diameter and a given inlet pipe height the particle removal efficiency has a significant increase with increasing the chamber height.

## 3.1 INTRODUCTION

A vortex is defined as the rotational motion of fluid around a common center (Lugt, 1883). Vortex separators are manufactured hydrodynamic devices that utilize the vortex principle to remove suspended solids from inflow. Unlike the conventional treatment technology that rely only on gravity settling, solids in a confined vortex separator are removed by both gravity settling and secondary flows which transport settling solids to the center of vortex chamber to settle (Andoh and Smisson, 1994;

Wong, 1997; Minton, 2005). This is the primary mechanism for heavy solids removal in the swirl/vortex separators.

Since Smisson (1967) developed the very first full-scale cylindrical vortex separator to treat the combined sewer overflow at Bristol., this treatment technology has been unmatched in treating wastewater and/or stormwater in the past 40 years. A family of hydrodynamic vortex separators, such as USEPA Swirl Concentrator, Storm King, etc., has been evolved from Smisson's original design model. At the same time, many scientists are investigating the sizing approaches for these hydrodynamic devices. Some studies have attempted to investigate the relationship between the performances of test models and prototype separators with semi-empirical equations, or using the scaling laws such as Froude scale and Hazen scale (Sullivan et al, 1972 & 1978; Deamer, et al, 1994; Andoh and Smisson, 1994; Weiβ and Michelbach, 1996; Weiβ, 1997; Fenner and Track, 1997 & 1998; Luyckx and Berlamont, 2004).

The accurate prediction of particle removal efficiency in a swirl/vortex separator is of considerable concern for the purpose of design and improved operation. Multiple factors may affect the motion of particles in the rotational fluid flow, and thereby in some cases prevent any reasonable theoretical approach. Therefore, the overall objective of the study was to experimentally investigate the particle removal efficiencies in confined vortex chambers, and thereby contributing some experimental data for the theoretical study in the future. The effects of the chamber height and the relative position of inlet pipe on particle removal efficiencies were examined by changing the height of the chamber and inlet pipe, respectively.

## 3.2 EXPERIMENTAL SETUP AND PROCEDURE

### 3.2.1 Experimental Apparatus

The experimental apparatus used for this study is schematically illustrated in Fig. 3.1. The system consists of an inflow pipe which is connected to a drinkable tap water supply (the inflow for the system), an overflow tank which provides a constant water pressure head for the system, an inlet pipe which is connected to the overflow tank and the vortex chamber, a sand feed funnel which is connected to the inlet pipe with a transparency pipe, a scale which is used to measure the hydrostatic pressure head, a vortex chamber without underflow exit, and two drain tanks. The rotational flow field in the chamber is generated by the momentum transfer from the tangential inflow. The outflow flows out along the top edge of the chamber.

The vortex chambers were made of wood with a tangential PVC inlet pipe as shown in Fig.3.2. The diameter and height of the chamber are D1 ($= 2R_1$) and $H_o$ respectively; while the inlet pipe diameter is $D_{IN}$ ($= 2R_{IN}$). In this study four vortex chamber models were tested: three of them have a fixed chamber height of $H_o$ = 175mm and a fixed inlet pipe diameter of $D_{IN}$ = 12.7mm, but with varied inlet pipe elevations of $H_{IN}$ = 23mm, 77mm, and 121mm (the inlet pipe elevation $H_{IN}$ is measured from the chamber bottom to the inlet pipe invert level), respectively. One of chambers is fixed with a chamber diameter of $D_1$ = 127mm and inlet pipe diameter $D_{IN}$ = 12.7mm, but with a reduced chamber height $H_o$ = 120mm.

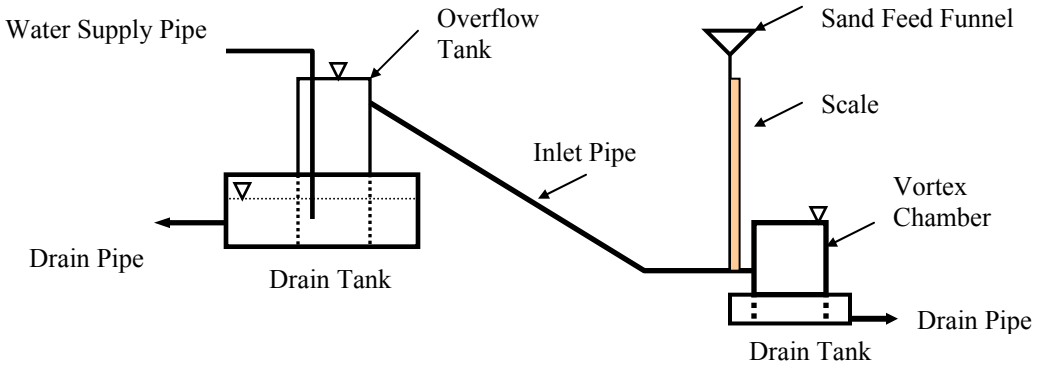


**Fig. 3.1 Schematic Outline of Experimental Apparatus**

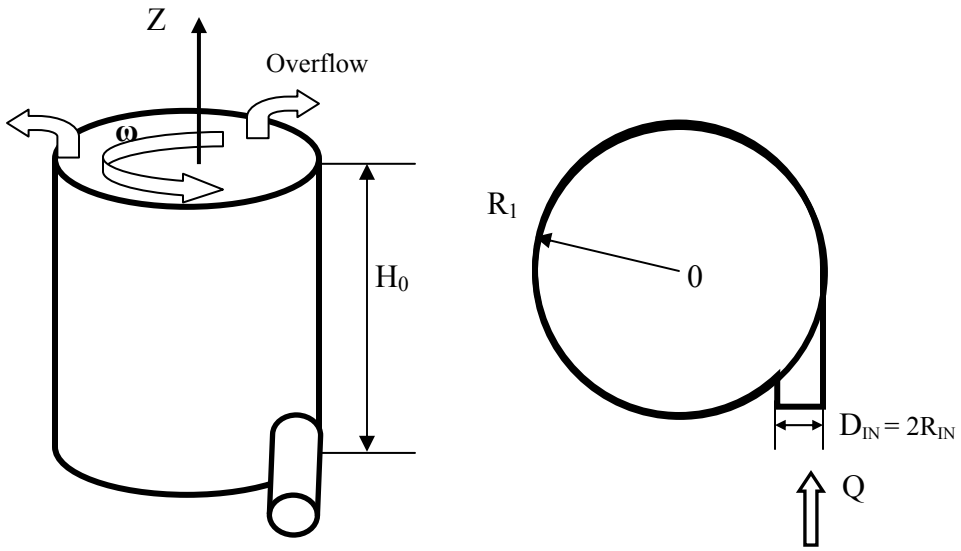


**Fig. 3.2 Schematic Illustration of the Vortex chamber**

### 3.2.2 Experimental Materials

The solid particles used in this study were manufactured by Power Technology, Inc. (PTI), Burnsville, Minnesota. The substance was made of quartz with a density of 2650 $kg/m^3$. The particle size ranged from 0 to 1000 microns. The particle size distribution of the manufactured solid particles was determined by the sieve method (Guo, 2006). The sieve analysis results, based on three samples (each sample was 100 grams) are reproduced in Table 3.1. The particle size distribution curve is shown in Fig. 3.3 that was based on the percent coarser by weight.

**Table 3.1 Sieve Analysis Results for Manufactured Material**

| Screen | | On Screen Material | | | | |
|---|---|---|---|---|---|---|
| Mesh | Micron | Weight (grams) | | | | % |
| | | (1) | (2) | (3) | Ave | |
| 18 | 1000 | 0.0 | 0.0 | 0.0 | 0.0 | 0.0 |
| 35 | 500 | 5.5 | 5.3 | 5.6 | 5.5 | 5.5 |
| 60 | 250 | 5.4 | 5.6 | 5.1 | 5.4 | 5.4 |
| 140 | 106 | 30.2 | 30.1 | 30.4 | 30.2 | 30.2 |
| 270 | 53 | 21.9 | 22.2 | 21.7 | 21.9 | 21.9 |
| Pan | -53 | 37.0 | 36.8 | 37.2 | 37.0 | 37.0 |

**(Source: Guo, 2006)**

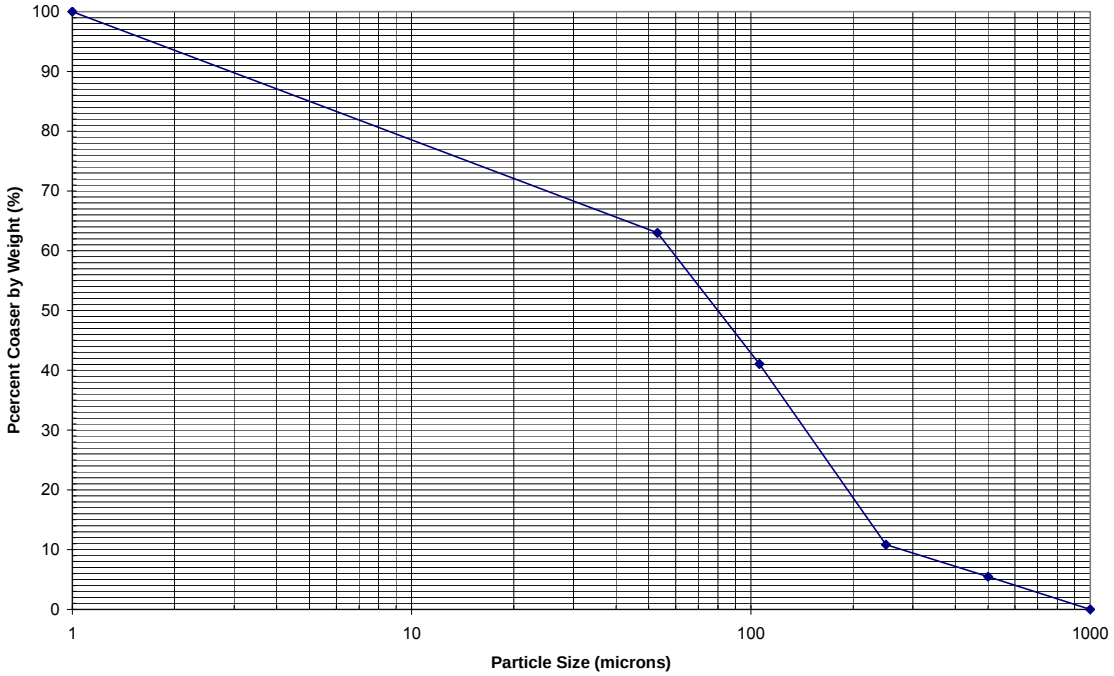


**Fig. 3.3 Particle Size Distribution of Manufactured Blend Material (0 to 1000 microns)**

### 3.2.3 Experimental Procedures

In this study the drinkable water is used as the fluid medium. Experiments were conducted with water temperature around T = $9^{o}C$. For a typical trial, the following operational procedures were followed.

First, the apparatus was connected and leveled as shown in Fig.3.1. The water from drinking tap water is discharged into the overflow tank, then into the vortex chamber through the inlet pipe, and finally flows out along the top edge of the chamber and into the drain tank underneath the vortex chamber. When the overflow tank is full, the overflow occurs, and a constant water pressure head for the system is maintained. Waiting for a while, a steady fluid flow is obtained.

After that, the measurements of the flow rate (Q) with a graduated cylinder and a stopwatch, water levels at the sand feed pipe that represents the hydrostatic pressure head in front of the vortex chamber, and the fluid temperature are performed and recorded.

Next, a certain quantity of sand material is measured with a precise balance ($\pm 0.01$ g). The quantity of sand material used in this experiment ranged from 50 to 100 grams for each sample. The sand materials were slowly fed into the vortex chamber (with an average influence concentration of about 700 mg/l) through the sand feed funnel located in front of the vortex chamber as shown in Fig.3.1.

Then, the drinkable tap water was turned off after about 10 residence times. The maximum residence time was about 85 seconds. The whole liquid with solids captured in the chamber was poured into a big container. The chamber was washed several times with drinking water to ensure that all of the captured solids were collected for each sample. Finally, the collected sample was heated in an oven to promote evaporation with

particle retention. The mass of the dried sand particles captured in the chamber was measured with a precise balance and recorded.

## 3.3 RESULTS AND DISCUSSIONS

### 3.3.1 Definition of Removal Efficiency

The performance of any commercial solid-liquid separators can be characterized by the separation efficiency. For solid-liquid separator if M is the total fed mass; $M_c$ is the mass separated from the feed; and $M_e$ is the mass escaped from the separator; the total mass of the feed must be equal to the sum of the total masses of the products, i.e.:

$$M = M_c + M_e \tag{3.1}$$

In general the total efficiency of separation $E_T$ is simply defined as the ratio of mass $M_c$ of all particles separated from the mass M of all solids fed into the unit:

$$E_T = \frac{M_c}{M} \tag{3.2}$$

or it can be written as:

$$E_T = 1 - \frac{M_e}{M} \tag{3.3}$$

### 3.3.2 Experimental Results

The experimental data and measured results based on the four vortex chamber models are summarized in Tables 3.2, 3.3, 3.4 and 3.5. The first row in the tables is the measured inflow rate Q; the second row is the measured hydrostatic pressure head above the top of the chamber; the third and forth rows are the added sand material mass and the captured sand material mass by the vortex chamber; and the last row is the calculated removal efficiency based on each inflow rate.

Figures 3.4, 3.5, 3.6, and 3.7 show the relationship between the measured removal efficiencies and the measured inflow rates obtained from the four test models. The horizontal axis represents the measured inflow rates; while the vertical axis represents the measured removal efficiencies. These figures indicate that for a given vortex chamber the removal efficiency decreases with an increasing flow rate. In practice, to achieve the goal of the high removal efficiency, a low design inflow rate is desirable. The correlation analysis indicates that for a given unit configuration the removal efficiency is almost completely interrelated with the inflow rate, and it can be approximately expressed by the quadratic polynomial of the flow rate.

### 3.3.3 Effect of Inlet Pipe Height on Removal Efficiency

Fig. 3.8 shows the comparison of measured removal efficiencies based on three vortex test models with a fixed chamber diameter ($D_1$ = 127mm), chamber height ($H_o$ = 175mm), and inlet pipe diameter ($D_{IN}$ = 12.7mm), but with the varied inlet pipe elevation of $H_{IN}$ = 23mm, 77mm and 121mm, respectively. The values for $H_{IN}$ are measured from the chamber floor to the invert level of the inlet pipe.

**Table 3.2 Data and Results Measured Based on $D_1$ = 127 mm, $D_{IN}$ = 12.7 mm, Ho = 175 mm, and $H_{IN}$ = 23 mm (water temperature T=$9^oC$ )**

| Inflow Rate Q ( ml/sec ) | 46.5 | 56.6 | 84.7 | 90.8 | 105.6 | 130.6 | 196.8 |
|---|---|---|---|---|---|---|---|
| Pressure Head ΔH (mm) | 11 | 12 | 14 | 19 | 23 | 29 | 54 |
| Mass Added M ( g ) | 62.85 | 55.65 | 64.17 | 79.82 | 83.83 | 106.56 | 87.87 |
| Mass Captured Mc (g) | 34.53 | 29.24 | 27.52 | 32.75 | 31.47 | 33.09 | 17.17 |
| Removal Efficiency (%) | 54.94 | 52.54 | 42.89 | 41.03 | 37.54 | 31.05 | 19.54 |

**Table 3.3 Data and Results Measured Based on $D_1$ = 127 mm, $D_{IN}$ = 12.7 mm, Ho = 175 mm, and $H_{IN}$ = 77 mm (water temperature T=$9^oC$ )**

| Inflow Rate Q ( ml/sec ) | 26.1 | 41.9 | 86.5 | 101.9 | 115.3 | 211.9 |
|---|---|---|---|---|---|---|
| Pressure Head ΔH (mm) | 4 | 0.9 | 18 | 23 | 26 | 62 |
| Mass Added M ( g ) | 53.92 | 52.32 | 86.48 | 65.13 | 69.84 | 103.39 |
| Mass Captured Mc (g) | 35.44 | 30.01 | 24.78 | 25.94 | 26.47 | 23.32 |
| Removal Efficiency (%) | 65.73 | 56.98 | 44.81 | 39.83 | 37.90 | 22.56 |

**Table 3.4 Data and Results Based on $D_1$ = 127 mm, $D_{IN}$ = 12.7 mm, Ho = 175 mm, and $H_{IN}$ = 121 mm (water temperature T=$9^oC$ )**

| | | | | | | |
|---|---|---|---|---|---|---|
| Inflow Rate Q ( ml/sec ) | 43.6 | 64.5 | 81.3 | 96.5 | 122.1 | 131.3 |
| Pressure Head ΔH (mm) | 7 | 11 | 13 | 17 | 26 | 32 |
| Mass Added M ( g ) | 49.13 | 58.99 | 56.89 | 53.43 | 55.93 | 57.27 |
| Mass Captured Mc (g) | 27.50 | 28.32 | 24.77 | 21.92 | 19.87 | 18.86 |
| Removal Efficiency (%) | 55.97 | 48.01 | 43.54 | 41.03 | 35.53 | 32.93 |

**Table 3.5 Data and Results Measured Based on $D_1$ = 127 mm, $D_{IN}$ = 12.7 mm, Ho = 120 mm, and $H_{IN}$ = 23 mm (water temperature T=$9^oC$ )**

| | | | | | |
|---|---|---|---|---|---|
| Inflow Rate Q ( ml/sec ) | 42.5 | 82.7 | 95.2 | 122.5 | 129.5 |
| Pressure Head ΔH (mm) | 6 | 13 | 18 | 27 | 29 |
| Mass Added M ( g ) | 52.63 | 53.8 | 60.24 | 63.47 | 84.07 |
| Mass Captured Mc (g) | 29.29 | 21.29 | 21.79 | 19.44 | 24.98 |
| Removal Efficiency (%) | 55.65 | 39.57 | 36.17 | 30.62 | 29.71 |

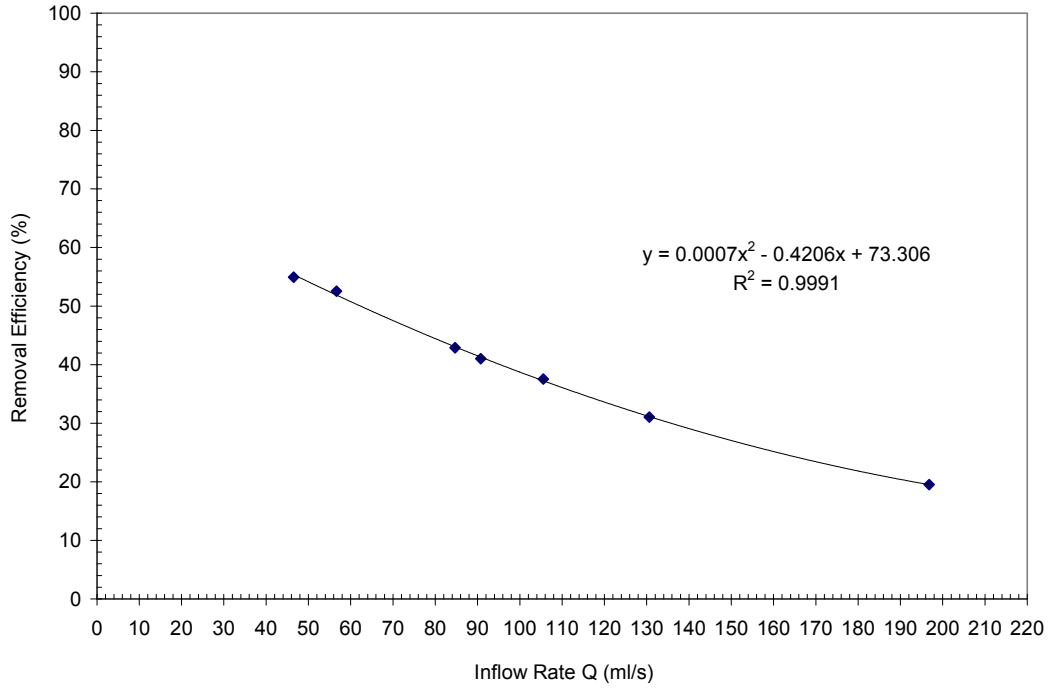


Fig.3.4 Measured Removal Efficiency Based on $D_1$ = 127 mm, Ho = 175 mm and $H_{IN}$ = 23 mm

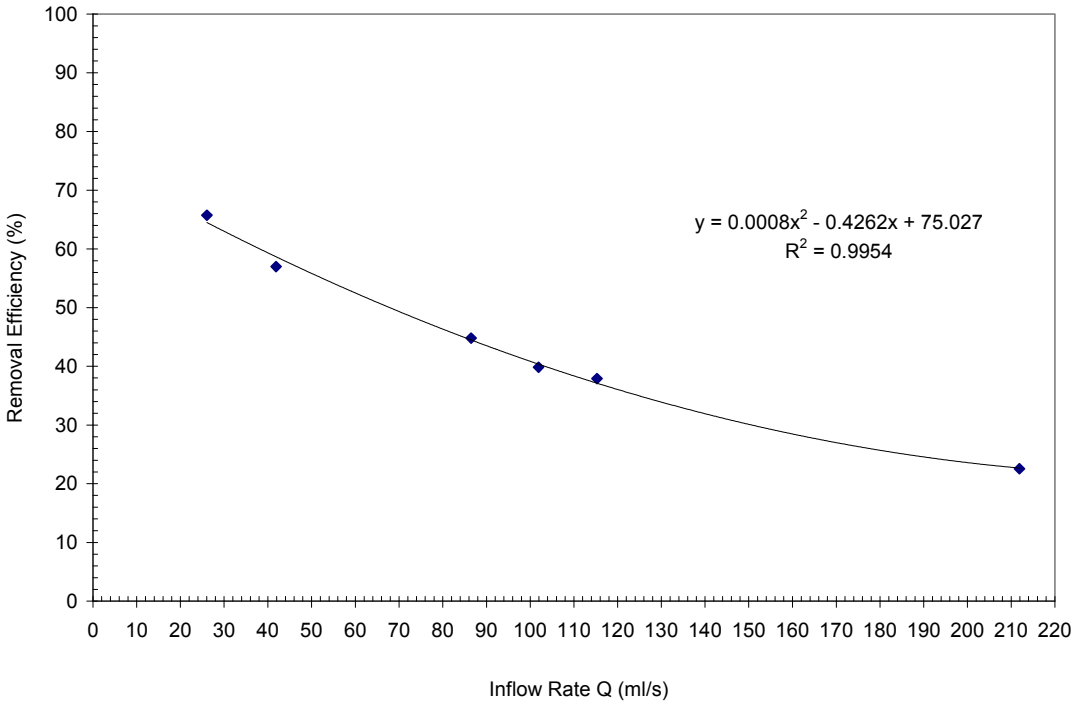


Fig. 3.5 Measured Removal Efficiency Based on $D_1$ = 127 mm, Ho = 175 mm and $H_{IN}$ =77 mm

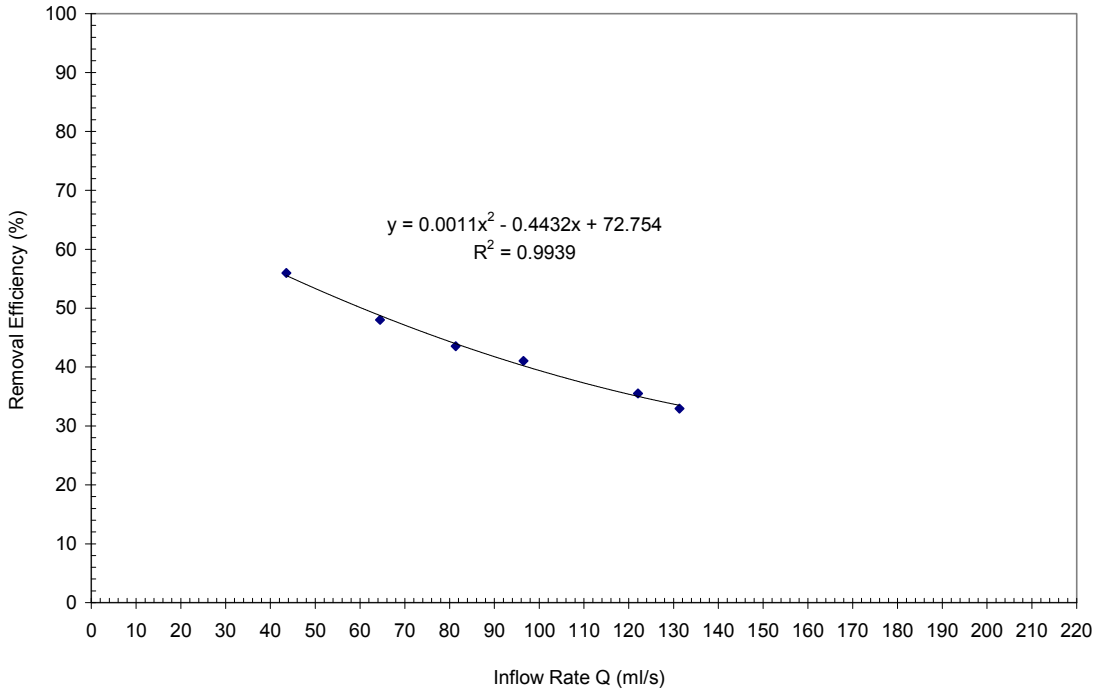


Fig. 3.6 Measured Removal Efficiency Based on $D_1$ = 127 mm, Ho = 175 mm and $H_{IN}$ = 121 mm

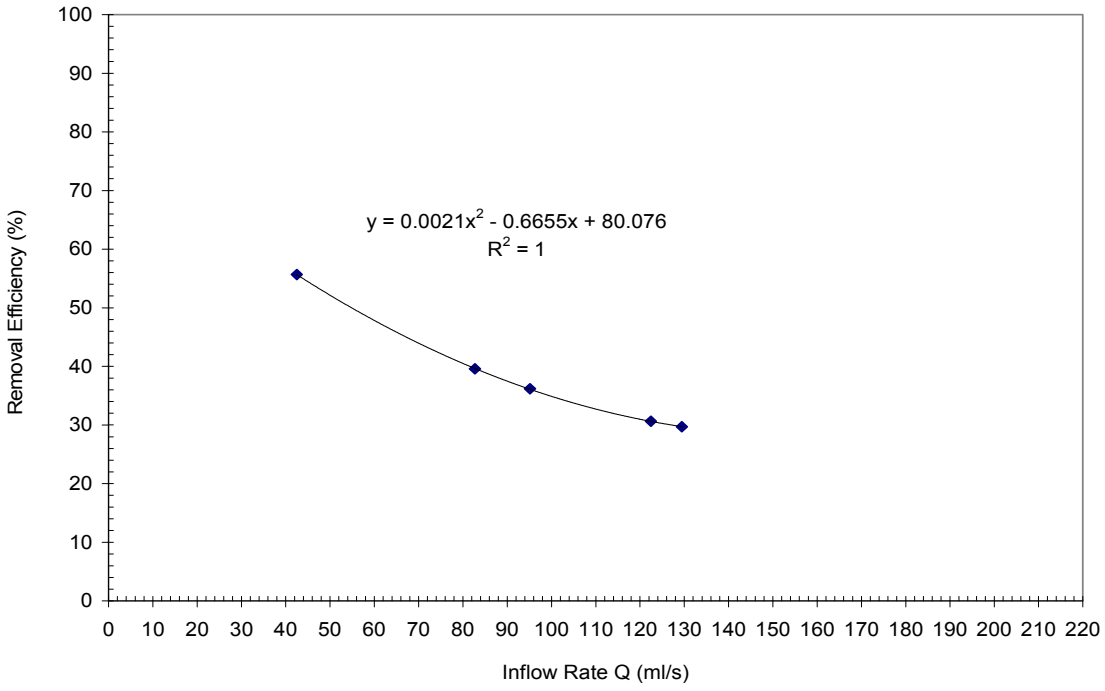


Fig.3.7 Measured Removal Efficiency Based on $D_1$ = 127 mm, Ho = 120 mm and $H_{IN}$ = 23 mm

This figure shows that by increasing the heights of the inlet pipe from $H_{IN}$ = 23 mm to $H_{IN}$ = 121 mm, the measured points from these three test models distributed with the same trend and closed together. The average difference of the measured removal efficiencies among these three test models is about 2%. This means that the removal efficiency can not be improved by changing the inlet pipe locations. Therefore it can be concluded that the effect of inlet pipe elevation on particle removal efficiency is insignificant.

### 3.3.4 Effect of Chamber Height on Removal Efficiency

Fig. 3.9 shows the comparison of measured removal efficiencies from two vortex test models with the fixed chamber diameter ($D_1$ = 127 mm), inlet pipe diameter ($D_{IN}$ = 12.7 mm), and inlet pipe height ($H_{IN}$ = 23 mm), but with different chamber heights of $H_o$ = 120 mm and Ho = 175 mm, respectively.

Fig.3.9 indicates that the measured points from the chamber with height of Ho = 175 mm are overall above the measured points from that with chamber height of Ho = 120mm. This means that for a given inflow rate the removal efficiency increases with increasing height of the chamber. For flow rates within the range from Q = 80 ml/sec to 110 ml/sec (which is equivalent to the chamber overflow rate of $U_{OR} = Q/\pi R_1^2$ = 2.0 mm/s to 2.8 mm/s), the removal efficiencies increases about 10% when the chamber height increases 45.8%. The change of chamber height could cause a significant change in removal efficiency, because removal efficiency is sensitive to the chamber height; it could be improved by increasing the chamber height.

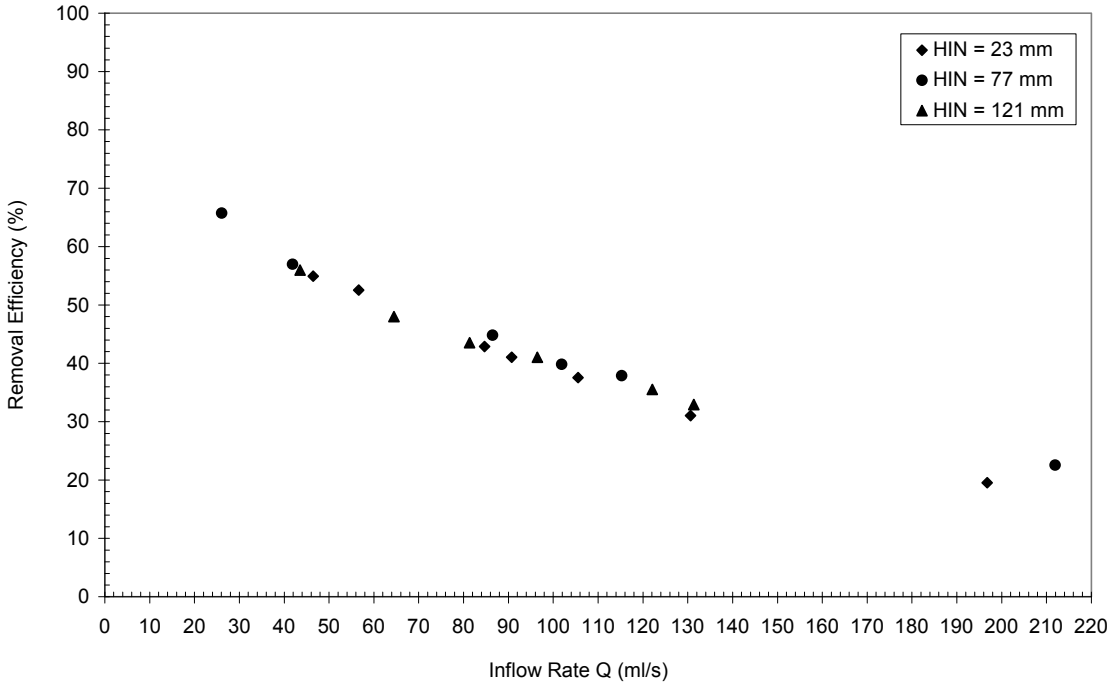


Fig. 3.8 Effect of Inlet Pipe Elevation on Removal Efficency Based on Ho = 175 and $D_{IN}$ = 12.7 mm

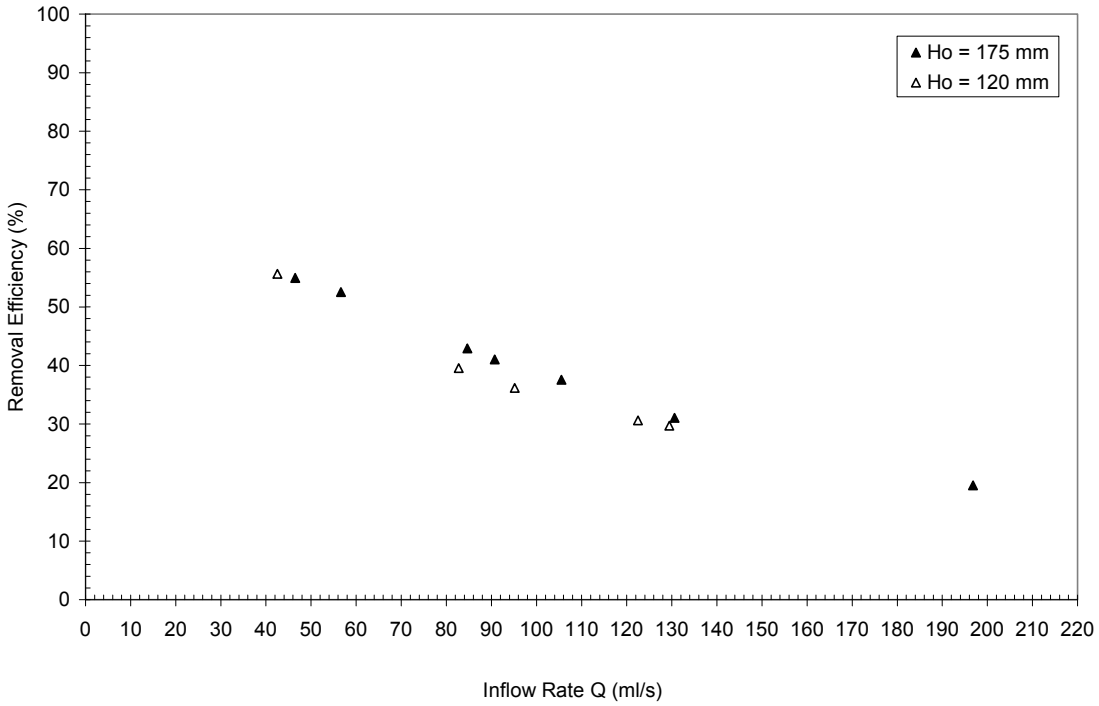


Fig. 3.9 Effect of Chamber Heigt on Removal Efficiency Based on $D_1$ = 127 mm and $H_{IN}$ = 23 mm

However, within the range of low flows, for example, referring to the first point in Fig. 3.9, the measured removal efficiency from a chamber with $H_o$ = 120 mm is very close to that from a chamber with $H_o$ = 175 mm. This is probably due to the fact that at low flow rates the centrifugal effect is small and the gravitational separation dominates. Under this condition, the particle trajectory is almost along the tangential and vertical directions (i.e., along a cylindrical plane) in the chamber. This motion is similar to that a particle moves in a one-dimensional upward fluid flow. Therefore, the removal efficiency would not increase significantly with increasing water depth (chamber height). However, at high flow rates the centrifugal effect is larger, and the particles will move simultaneously forward (tangential), outward (radial), and upward or downward (vertical) in the chamber. The taller the chamber, the more particles could be captured by the chamber due to the centrifugal effect. The separation is the combined contribution of centrifugal effect and gravitational effect.

### 3.3.5 Comparison of Predicted Results with Experimental Results

In this section, the gravitational settling method is employed to predict the particle removal efficiency in a confined vortex chamber. In general, sedimentation analysis is done to determine the settling velocities of particles with different size, shape, and density. The particle settling velocities are normally expressed in terms of the order of diameters of quartz particles that settle in a fluid. For a given overflow rate of $U_{OR}$ in a vortex chamber, particles with settling velocities, $U_s$, greater than the overflow rate will settle to the bottom of the chamber; while particles with settling velocities less than the overflow rate will escape from the chamber. Therefore, the critical particle settling

diameter (dc) can be determined with equating the particle settling velocity ( $U_s$ ) to the chamber overflow rate ( $U_{OR}$ ). The chamber overflow rate can be written as:

$$U_{OR} = \frac{Q}{\pi R_1^2} = \frac{4Q}{\pi D_1^2} \tag{3.4}$$

Cheng (1997) proposed a general formula to predict the terminal settling velocity of natural sediment particles in the present notation as follows:

$$U_s = \frac{\nu}{d}\left\{\sqrt{25 + 1.2\left[\left(\frac{\rho_p}{\rho_f} - 1\right)\frac{g}{\nu^2}\right]^{2/3} d^2} - 5\right\}^{1.5} \tag{3.5}$$

where $U_s$ is the particle settling velocity, d is particle diameter, $\nu$ is the kinematic viscosity of the fluid, g is gravitational acceleration, $\rho_p$ and $\rho_f$ are particle density and fluid density, respectively. Equating Eq.(3.4) to Eq.(3.5) and rearranging yields:

$$d_c = \frac{\left(\frac{4Q}{\pi D_1^2}\right)^{1/2}\left\{\left(\frac{4Q}{\pi D_1^2}\right) + \sqrt{\left(\frac{4Q}{\pi D_1^2}\right)^2 + 48\left[\left(\frac{\rho_p}{\rho_f} - 1\right)\nu g\right]^{2/3}}\right\}^{3/2}}{3.718\left[\left(\frac{\rho_p}{\rho_f} - 1\right)g\right]} \tag{3.6}$$

where dc is the critical particle diameter. For a given design flow rate Q and the chamber Diameter D1, the critical particle settling size (dc) can be determined with Eq.(3.6).

Referring to the Particle Size Distribution (PSD) curve, the percent coarser particles (i.e., the particle removal efficiency) can be estimated.

Figure 3.10 shows the comparison of experimental results with predicted results derived from Eq.(3.6) coupled with the PSD curve (Fig.3.3). This figure indicates that the predicted results (dashed line) are overall below the experimental results for both chamber heights of $H_o$ = 175 mm and $H_o$ = 120 mm. This means that Eq.(3.6) could be used to predict the lower limit of removal efficiency for a vortex separator.

However, the experimental results with a chamber height of $H_o$ = 120 mm are very close to the predicted results with Eq.(3.6), except within the low flow range. This is due to the fact that the particle size distribution curve was derived from sieve analysis that was based on the screen mesh from 18 to 270 (1000 to 53 micron) (see Table 3.1). Particle size distribution for particles with a diameter less than 53 micron was not analyzed. Thus, the particle size distribution with this range could not accurately predict the percent coarser by weight.

### 3.3.6 Sizing Formula

Based on the previous comparison made, it was found that the predicted results from Eq.(3.6) has a good agreement with the experimental data obtained from the chamber with a diameter of $D_1$ = 127 mm and height of $H_o$ = 120 mm. However, the ratio of chamber height to chamber diameter is about $H_o/D_1 \approx 1.0$. This means that for chambers with the ratio of $H_o/D_1 = 1.0$, Eq.(3.6) might be used for unit sizing. By rearranging Eq.(3.6), the following unit sizing formula is suggested:

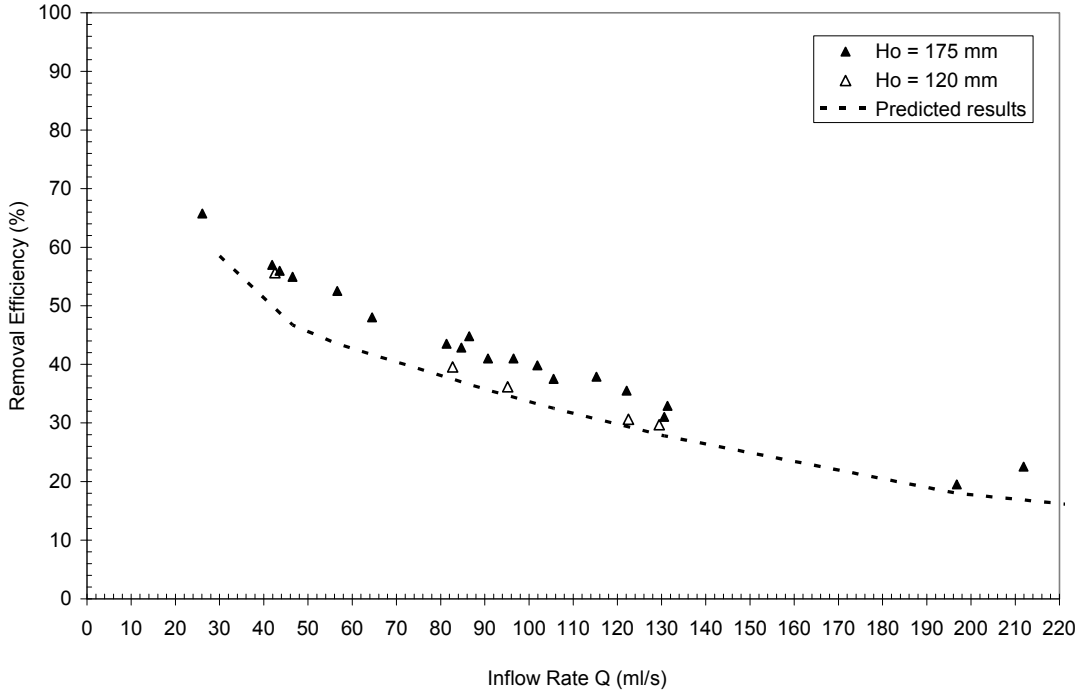


Fig.3.10 Comparison of Experimental Results with Predicted Results Derived from Eq.(3.6)

$$D_1 = \left(\frac{4Q d_c}{\pi \nu}\right)^{0.5} \left\{ \sqrt{25 + 1.2\left[\left(\frac{\rho_p}{\rho_f} - 1\right)\frac{g}{\nu^2}\right]^{2/3} d_c^2} - 5 \right\}^{-0.75} \tag{3.7}$$

## 3.4 Conclusions

In terms of this analysis, the following conclusions are made. The removal efficiency decreases with increasing inflow rate. The effect of inlet pipe elevation on particle removal efficiency is insignificant; while the chamber height has a significant impact on the particle removal efficiency.

The predicted results with gravitational separation only could yield a lower limit of particle removal efficiency. For chambers with a ratio of chamber height to chamber diameter of $H_o / D_1 = 1.0$, Eq.(3.7) coupled with the particle size distribution curve is applicable for unit sizing.

# Chapter 4
# Determination of Angular Velocity for Turbulent Vortex Chamber Flow

Understanding flow patterns in a confined vortex chamber is an important step when investigating the mechanisms of liquid-solid separation. However, the angular velocity of fluid motion around a common axis is an important parameter to theoretically determine flow patterns and particle trajectories in the rotational flowfields. In this chapter, a simple formula is derived, based on the law of conservation of angular momentum and the boundary conditions, to determine the angular velocity for turbulent vortex chamber flow. It can be applied to predict the angular velocity in a confined vortex chamber with a tangential inlet pipe.

## 4.1 Introduction

Since Smisson (1967) developed the very first full-scale cylindrical vortex separator to treat the combined sewer overflow at Bristol in the 1960s, a family of hydrodynamic vortex separators, such as USEPA Swirl Concentrator, Storm King, etc., has since evolved from Smisson's original design model for wastewater and stormwater treatment over the past 40 years (Sullivan, et. al., 1972; Sullivan, et al., 1982; Field & O'Connor, 1996; Luyckx & Berlamont, 2004). At the same time, many studies have been conducted to investigate the mechanisms of solid-liquid separation and the sizing approaches for these hydrodynamic devices (Sullivan et al, 1972; Sullivan et al, 1974; Sullivan et al 1978; Sullivan 1982; Fenner and Track, 1997 & 1998; Deamer, et al, 1994;

Andoh and Smisson, 1994; Luyckx and Berlamont, 2004). Some investigators have attempted to establish relationships between test models and prototype separators with scaling laws such as Froude scale and Hazen scale, or semi-empirical equations (Sullivan et al, 1972; Sullivan et al, 1974; Sullivan et al 1978; Fenner and Track, 1997 & 1998; Deamer, et al, 1994; Andoh and Smisson, 1994; Luyckx and Berlamont, 2004). However, there are too many factors (such as unit geometry and fluid flow parameters as well as particle properties) that might affect the motion of particles in the chamber, and thereby in some cases prevent scaling. The angular velocity of fluid motion around a common axis is an important parameter which governs the motion of the rotational fluid flow and particle trajectories in the chamber. The purpose of the chapter is to derive a formula, based on the law of conservation of momentum and boundary conditions, to estimate the angular velocity for vortex chamber flows.

## 4.2 Physical Model and Assumptions

In terms of the literature review conducted in Chapter 2, so far not much fundamental development exists for vortex separators with geometries similar to that of the Vortechs™ system and Downstream Defender®. Therefore, in this study a vortex chamber with a similar geometry of Vortechs™ main chamber is selected as the study model as shown in Fig.4.1. The dimensions of the chamber are also shown in Fig.4.1. The fluid flow enters tangent to the chamber and generates a rotational flowfield around the vertical axis. It then flows out along the top edge of the chamber. A Rankine-like tangential velocity profile is generated as shown in Fig.4.2 (Lugt, 1983; Ogawa, 1993; Escudier & Merkli, 1979; Vatistas et. al., 1986; Vatistas et. al., 1988). The velocity in the

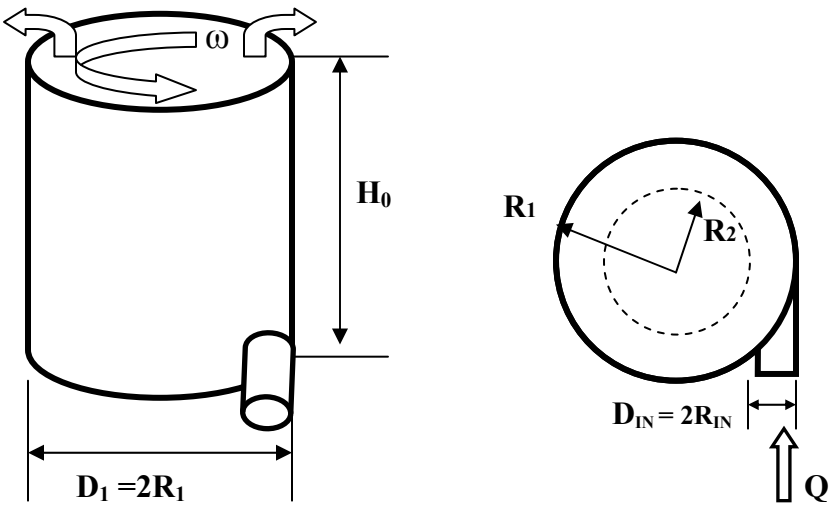


**(a) Perspective View** **(b) Top View**

**Fig. 4.1 Schematic Illustration of the Vortex Chamber**

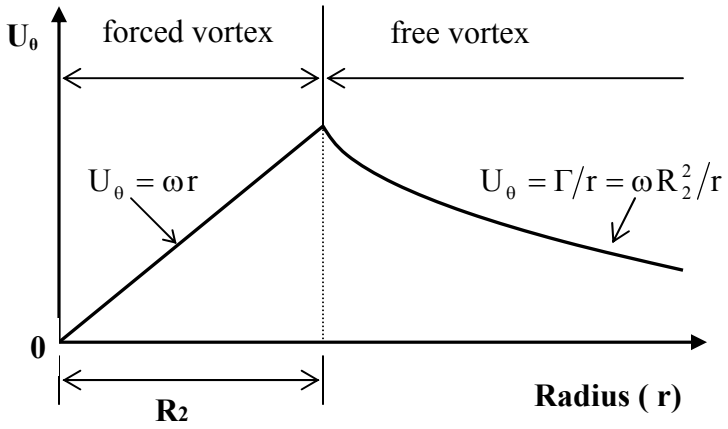


**Fig. 4.2 Tangential Velocity Distribution of the Rankine Combined Vortex**

chamber is conveniently resolved into three components: tangential ( $U_\theta$ ), axial ($U_z$), and radial ($U_r$). However, the radial velocity is small in comparison with the tangential and vertical velocity components, and thus negligible (Rudinger, 1980; Svarovsky, 1981; Ogawa, 1993).

It is well known from the Rankine combined vortex model (Fig.4.2) that the tangential velocity profile in a confined vortex chamber changes from a type of free vortex to a type of forced vortex when the flow approaches the central axis of rotation (Ogawa, 1984 and 1993; Vatistas et al, 1986; Vatistas et al, 1988). Previous cyclone experimental studies have shown that for a given inflow rate (Q) the tangential velocity does not vary significantly along the height of the chamber (Vatistas, et al., 1986; Vatistas, et al., 1988). It can be assumed that the forced vortex zone and the free vortex zone within the chamber are both constant along the height of the chamber. For a given inflow condition, the tangential velocity is a function of the radial coordinate ( r ), rather than vertical coordinate (z). Therefore, under the steady tangential inflow condition it can be assumed that the angular velocity is constant in the chamber. Further assumptions include: the flowfield is axi-symmetrical around the vertical axis, the fluid flow is incompressible and steady, and the distribution of the inflow is uniform.

## 4.3 Determination of Driving Torque and Resistance Torque

### 4.3.1 The Law of Conservation of Angular Momentum

The angular velocity can be determined by applying the law of conservation of angular momentum to the system. In a steady equilibrium system the angular momentum (L) is constant. The time derivative of angular momentum is called torque:

$$T = \frac{dL}{dt} = r \times \vec{F} \tag{4.1}$$

where $\vec{F}$ is the external force acting on the system. Therefore for a steady and equilibrium system the following relation is equivalent:

$$L_{system} = \text{Constant} \quad \Leftrightarrow \quad \sum T_{ext} = 0 \tag{4.2}$$

where $T_{ext}$ is the external torque acting on the system, which include the tangential pressure force from the inlet pipe flow and the frictional force from the chamber wall and bottom.

### 4.3.2 Determination of Average Boundary Shear Stress

The complexity of the boundary conditions in the vortex chamber makes it difficult to determine the shear forces between the chamber surface and the fluid (i.e. the force per unit area exerted by the boundary surface on the fluid, and vice versa). However, the fluid motion in the tangential direction in the chamber is similar to that in an open channel. To simplify the problem and get an analytical solution of the angular velocity formula, the constant boundary shear stress is assumed and the Chezy's Formula is employed to estimate the boundary shear stress along the boundary (Yang, 1996; Street, et al., 1996):

$$\tau_o = \frac{1}{8} f \rho_f U^2 \tag{4.3}$$

where $\tau_o$ is shear stress along the boundary; $\rho_f$ is fluid density; U is the average fluid velocity; and *f* is Darcy-Weisbach friction factor which is a function of the relative roughness (e/D) and the Reynolds number ( $R_e$ ):

$$\mathrm{f} = \mathrm{function}\left(\frac{\mathrm{e}}{\mathrm{D}}, \mathrm{R_e}\right) \tag{4.4}$$

where e is the average roughness height; D is characteristic diameter, and Reynolds number is defined as

$$R_e = \frac{UD}{\nu} \tag{4.5}$$

where U is characteristic average fluid velocity; and $\nu$ is the kinematic viscosity of the fluid. For turbulent rough flow the fiction factor depends only on the relative roughness. The friction factor can be approximated as constant (Street et al., 1996). In this study, only the turbulent vortex flow is considered.

In terms of Rankine Combined Vortex model (Fig.4.2), the tangential velocity distribution ( $\mathrm{U_\theta}$ ) in the forced vortex region (core region) and free vortex region (outer region) of the chamber can be expressed as:

$$U_\theta = \omega r \qquad (r = 0 \quad to \quad R_2) \tag{4.6}$$

and

$$U_\theta = \frac{\Gamma}{r} \qquad (r = R_2 \quad to \quad R_1) \tag{4.7}$$

where $\omega$ is the angular velocity of the core; $R_2$ is the radius of maximum tangential velocity; and $\Gamma$ is a constant. At the boundary of the free vortex and the forced vortex (i.e., $r = R_2$) the tangential velocity ($U_\theta$) has the same value for the forced vortex region and the free vortex region. Thus the following relationship can be obtained:

$$U_{\theta,R_2} = \omega R_2 = \frac{\Gamma}{R_2} \tag{4.8}$$

Therefore the constant $\Gamma$ can be expressed as:

$$\Gamma = \omega R_2^2 \tag{4.9}$$

Substituting Eq.(4.9) into Eq.(4.7), the tangential velocity in the free vortex region can be expressed as:

$$U_\theta = \frac{\omega R_2^2}{r} \tag{4.10}$$

The average tangential velocity U can be determined by

$$U = \frac{Q_\theta}{A} = \frac{Q_\theta}{R_1 H_0} = \frac{1}{R_1 H_0}\left[\int_0^{R_2} U_\theta H_0 dr + \int_{R_2}^{R_1} U_\theta H_0 dr\right]$$

where A is the cross-sectional area of the fluid flow in the tangential direction, and can be determined by multiplying the chamber height ($H_0$) by the chamber radius ($R_1$). $Q_\theta$ is the total flow rate passing through this cross-sectional area in the tangential direction. By substituting Eqs.(4.6) and (4.10) into the above equation and integrating, the average tangential velocity can be written as:

$$U = \left(\frac{1}{2} + \ln\frac{R_1}{R_2}\right)\frac{\omega R_2^2}{R_1} \tag{4.11}$$

Then by substituting Eq.(4.11) into Eq.(4.3) and rearranging, the average boundary shear stress can be expressed as:

$$\tau_o = \frac{1}{8} f \rho_f U^2 = \left(\frac{1}{2} + \ln\frac{R_1}{R_2}\right)^2 \frac{f\,\rho_f\,\omega^2 R_2^4}{8R_1^2} \tag{4.12}$$

### 4.3.3 Determination of the Driving Torque

The driving force pushing fluid to rotate in a confined vortex chamber is the hydrostatic pressure force from the tangential inlet pipe flow. The total inlet hydrostatic pressure force acting on the vortex chamber can be expressed as:

$$F_{total,inlet} = pA_{IN} = \left(\rho_f g\ \Delta H\right)\left(\pi R_{IN}^2\right) = \pi\rho_f g R_{IN}^2\ \Delta H \tag{4.13}$$

where $F_{total,\ inlet}$ is the total inlet hydrostatic pressure force exerted on the rotating flow system; p is the net hydrostatic pressure at the center of the inlet pipe; $A_{IN}$ is the cross-sectional area of inlet pipe; $\Delta H$ is the net hydrostatic pressure head above the top of the chamber (also called pressure head drop); $R_{IN}$ is the radius of inlet pipe. Then the total driving torque from the tangential inflow can be written as:

$$T_{total,inlet} = F_{total,inlet} R_{IC} = \pi\rho_f g\, R_{IN}^2 R_{IC}\, \Delta H = \pi\rho_f g\left(R_1 - R_{IN}\right) R_{IN}^2\, \Delta H \tag{4.14}$$

where $R_{IC}$ is the radius from the center of the chamber to the centerline of inlet pipe (i.e. $R_{IC} = R_1 - R_{IN}$ ).

### 4.3.4 Determination of the Resistance Torque

Primarily, the resistance torque comes from the boundary frictional force between the chamber surface and fluid. In this study, in order to simplify the derivation and obtain an analytical solution of the angular velocity formula, the average boundary shear stress, as expressed by Eq.(4.12), is employed to determine the boundary frictional force. The resistance torque from the chamber wall and the chamber bottom frictions is derived as follows.

#### 4.3.4.1 Resistance torque from chamber wall surface friction

The boundary shear force from the chamber wall surface can be expressed as:

$$F_{wall} = \tau_o A_{wall}$$

where $F_{wall}$ is the frictional force from chamber wall surface, and $A_{wall}$ is the surface area of the chamber wall. Substituting Eq.(4.12) into the above equation and rearranging yields:

$$F_{wall} = \frac{\pi f \rho_f \omega^2 R_2^4 H_0}{4R_1}\left(\frac{1}{2} + \ln\frac{R_1}{R_2}\right)^2 \tag{4.15}$$

Therefore, the resistance torque due to the wall friction resistance can be written as:

$$T_{wall} = F_{wall} R_1 = \frac{1}{4}\left(\frac{1}{2} + \ln\frac{R_1}{R_2}\right)^2 \left(\pi f \rho_f \omega^2 R_2^4 H_0\right) \tag{4.16}$$

#### 4.3.4.2 Resistance torque from chamber bottom surface friction

Let's consider an infinitesimal ring strip with width of dr within the bottom of the chamber as shown in Fig. 4.3. Similarly, the total resistance torque from the chamber bottom can be expressed as:

$$T_{bott.} = \int_0^{R_2} \tau_o 2\pi r^2 dr + \int_{R_2}^{R_1} \tau_o 2\pi r^2 dr \tag{4.17}$$

By substituting Eq.(4.12) into the above equation and integrating, the resistance torque due to the chamber bottom friction resistance can be written as:

$$T_{bott} = \frac{1}{12}\left(\frac{1}{2} + \ln\frac{R_1}{R_2}\right)^2 \left(\pi\ f\ \rho_f \omega^2 R_2^4 R_1\right) \tag{4.18}$$

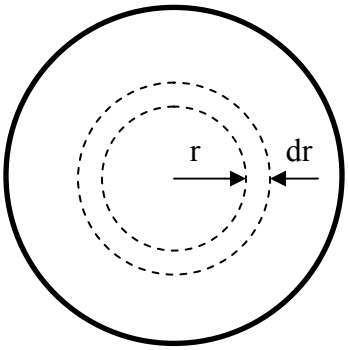


**Fig. 4.3 Schematic Illustration of Integration Area at the Chamber Bottom**

#### 4.3.4.3 Total resistance torque

The total resistance torque can be obtained by summing the resistance torque from the chamber wall friction resistance and the chamber bottom friction resistance:

$$T_{tot,shear} = T_{wall} + T_{bott} = \frac{1}{4}\left(\frac{1}{2} + \ln\frac{R_1}{R_2}\right)^2 \left(\pi\ f\ \rho_f \omega^2 R_2^4 H_0\right) + \frac{1}{12}\left(\frac{1}{2} + \ln\frac{R_1}{R_2}\right)^2 \left(\pi\ f\ \rho_f \omega^2 R_2^4 R_1\right)$$

Rearranging the above equation yields:

$$T_{tot,shear} = \frac{1}{4}\left(\frac{1}{2} + \ln\frac{R_1}{R_2}\right)^2 \left(H_0 + \frac{R_1}{3}\right)\left(\pi\, f\, \rho_f \omega^2 R_2^4\right) \tag{4.19}$$

## 4.4 Determination of Angular Velocity Formula

In terms of the law of conservation of momentum, the total external torque acting on the system must be zero, i.e., $T_{tot,inlet} = T_{tot,shear}$. Equating Eq.(4.14) to Eq.(4.19) gives:

$$\pi\rho_f g\left(R_1 - R_{IN}\right)R_{IN}^2\, \Delta H = \frac{1}{4}\left(\frac{1}{2} + \ln\frac{R_1}{R_2}\right)^2 \left(H_0 + \frac{R_1}{3}\right)\left(\pi\, f\, \rho_f \omega^2 R_2^4\right)$$

By dividing both sides of the above equation by $(\pi \rho_f)$ and rearranging, a simple formulae of angular velocity is obtained:

$$\omega = \left(\frac{K_2}{K_1}\right)^{1/2} \left(\Delta H\right)^{1/2} \tag{4.20}$$

in which

$$K_1 = \left(\frac{1}{2} + \ln\frac{R_1}{R_2}\right)^2 \left(H_0 + \frac{R_1}{3}\right) \tag{4.20a}$$

$$K_2 = \frac{4g\left(R_1 - R_{IN}\right)R_{IN}^2}{f\, R_2^4} \tag{4.20b}$$

### 4.4.1 Determination of Characteristic Diameter (D) and Friction Factor (f)

For turbulent rough flow the friction factor (*f*) is constant. It can be found from the Moody diagram if the relative roughness (e/D) and the characteristic diameter D are known (Street et al., 1996). The characteristic diameter D can be determined by considering the force balance in the system. Since fluid motion in the tangential direction is similar to that in an open channel, the resistance force and driving force, based on the assumption that the energy slope ($S_e$) in the tangential direction is constant, can be written as:

Resistance Force: $\tau_{wall} A_{wall} + \tau_{bott} A_{bott} = \tau_0 \left( A_{wall} + A_{bott} \right) = \left( 2\pi R_1 H_0 + \pi R_1^2 \right)$

Driving Force: $\left( \rho_f g \pi R_1^2 H_0 \right) S_e$

By equating the resistance force to the driving force, the following relationship is obtained:

$$\tau_0 \left( 2\pi R_1 H_0 + \pi R_1^2 \right) = \left( \rho_f g \pi R_1^2 H_0 \right) S_e \tag{4.21}$$

Rearranging Eq.(4.21) yields:

$$\tau_0 = \frac{\rho_f g \pi R_1^2 H_0 S_e}{2\pi R_1 H_0 + \pi R_1^2} \tag{4.22}$$

Then equating Eq.(4.3) to Eq.(4.24) gives.:

$$\tau_0 = \frac{1}{8} f \rho_f U^2 = \frac{\rho_f g \pi R_1^2 H_0 S_e}{2\pi R_1 H_0 + \pi R_1^2} \tag{4.23}$$

Rearranging the above equation yields:

$$S_e = \frac{h_f}{L} = f \frac{1}{4\left(\frac{R_1 H_0}{2H_0 + R_1}\right)} \frac{U^2}{2g} \tag{4.24}$$

where L is the average circumference and is defined as $L = \pi R_1$. By comparing Eq.(4.24) with Darcy-Weisbach formula, the following relationship is obtained:

$$D = 4R_h = 4\left(\frac{R_1 H_0}{2H_0 + R_1}\right) \tag{4.25}$$

where $R_h$ is the hydraulic radius. In terms of the relative roughness (e/D) and characteristic diameter (D) which is determined by Eq.(4.25), the frictional factor (f) can be determined from Moody diagram which can be found in various textbook or professional engineering handbooks.

### 4.4.2 Determination of Head Loss

In the vortex chamber system, major head loss comes from the frictional resistance of the chamber surface exerting on the fluid and the inlet pipe exit loss. The summation of them should be equal to the pressure drop between the chamber inlet and

chamber outlet. For a given unity geometry, the head loss is a function of inflow rate Q. For practical purpose, it is useful to represent the pressure head drop ( $\Delta H$ ) as a function of flow rate and unit geometry. It is derived as follows.

#### 4.4.2.1 Head loss in the vortex chamber

The motion of fluid in a vortex chamber can be classified into two components: vertical component and tangential component. In terms of Darcy-Weisbach equation, the frictional losses in the vertical direction of the chamber can be expressed as follows

$$h_{f_z} = f\frac{L}{D}\frac{U^2}{2g} = f_z\frac{H_o}{2R_1}\frac{\left(Q/\pi R_1^2\right)^2}{2g} = f_z\frac{H_o Q^2}{4g\pi^2 R_1^5} \tag{4.26}$$

where $h_{f_z}$ is the head loss in the vertical direction of the chamber; $f_z$ is the Darcy-Weisbach friction factor in the vertical direction. The friction loss in the tangential direction of the chamber can be written as:

$$h_{f_\theta} = f_\theta\frac{L_\theta}{4R_h}\frac{U_\theta^2}{2g} = f_\theta\frac{\pi\left(2H_o + R_1\right)R_2^4}{8gH_o R_1^2}\left(\frac{1}{2} + \ln\frac{R_1}{R_2}\right)^2\omega^2 \tag{4.27}$$

where $h_{f_\theta}$ is the head loss in the vertical direction of the chamber; $f_\theta$ is the Darcy-Weisbach friction factor in the tangential direction.

#### 4.4.2.2 Head Loss in the inlet pipe exit

The head loss for a sudden pipe expansion can be estimated with the following equation (Street, et al., 1996; Durance al., 2003):

$$h_{L_e} = K_L \left| \frac{U_{IN}^2 - U_\theta^2}{2g} \right| \tag{4.28}$$

where $U_{IN}$ is average inlet pipe velocity and is defined as $\pi / \pi R_{IN}^2$ ; $U_\theta$ is the average tangential velocity in the chamber which can be represented by Eq.(4.11); and $K_L$ is head loss coefficient which is a function of the inlet pipe velocity. For a sudden pipe expansion, the loss coefficient $K_L$ is about one.

Substituting $U_{IN}$ and $U_\theta$ into Eq.(4.28) and rearranging gives:

$$h_f = K_L \frac{Q^2}{2g\pi^2 R_{IN}^4} - K_L \frac{R_2^4}{2gR_1^2} \left( \frac{1}{2} + \ln \frac{R_1}{R_2} \right)^2 \omega^2 \tag{4.29}$$

#### 4.4.2.3 Total head loss:

Then the total head loss can be determined by summing the head losses from chamber and inlet pipe exit, i.e.:

$$\begin{aligned} h_l = {} & f_z \frac{H_o Q^2}{4g\pi^2 R_1^5} + f_\theta \frac{\pi(2H_o + R_1)R_2^4}{8gH_o R_1^2} \left( \frac{1}{2} + \ln \frac{R_1}{R_2} \right)^2 \omega^2 \\ & + K_L \frac{Q^2}{2g\pi^2 R_{IN}^4} - K_L \frac{R_2^4}{2gR_1^2} \left( \frac{1}{2} + \ln \frac{R_1}{R_2} \right)^2 \omega^2 \end{aligned} \tag{4.30}$$

In order to observe the contributions of the first term and the second term of Eq.(4.30) to the total head loss, two factors of $\alpha_z$ and $\alpha_\theta$ are added in the front of the first term and second term of Eq.(4.29), respectively. The values of $\alpha_z$ and $\alpha_\theta$ are equal to one or zero. If the term is considered, then the value of $\alpha_z$ or $\alpha_\theta$ is set to one, otherwise it is set to zero. Then the above equation is rewritten as:

$$h_l = \alpha_z f_z \frac{H_o Q^2}{4g\pi^2 R_1^5} + \alpha_\theta f_\theta \frac{\pi(2H_o + R_1)R_2^4}{8gH_o R_1^2}\left(\frac{1}{2} + \ln\frac{R_1}{R_2}\right)^2 \omega^2 + K_L \frac{Q^2}{2g\pi^2 R_{IN}^4} - K_L \frac{R_2^4}{2gR_1^2}\left(\frac{1}{2} + \ln\frac{R_1}{R_2}\right)^2 \omega^2 \tag{4.30a}$$

### 4.4.3 Determination of Angular Velocity ($\omega$) and Pressure Head Drop ($\Delta H$)

#### 4.4.3.1 General equations for angular velocity and pressure head drop

By rearranging Eq.(4.20), the pressure head drop($\Delta H$) can be expressed as:

$$\Delta H = f_\theta \frac{R_2^4(H_o + R_1/3)}{4g(R_1 - R_{IN})R_{IN}^2}\left(\frac{1}{2} + \ln\frac{R_1}{R_2}\right)^2 \omega^2 \tag{4.31}$$

By equating Eq.(4.30a) to Eq.(4.31) and rearranging, the angular velocity can be rewritten as follows:

$$\omega = \left(\frac{\lambda_2}{\lambda_1}\right)^{1/2} Q \tag{4.32}$$

in which

$$\lambda_1 = \frac{\left(H_o + R_1/3\right)R_1^2}{2\left(R_1 - R_{IN}\right)R_{IN}^2} - \alpha_\theta \frac{\pi\left(2H_o + R_1\right)}{4H_o} + \left(\frac{K_L}{f_\theta}\right) \tag{4.32a}$$

$$\lambda_2 = \frac{\alpha_z\left(\frac{f_z}{f_\theta}\right)\left(\frac{H_o}{R_1^3}\right) + \left(\frac{K_L}{f_\theta}\right)\frac{R_1^2}{R_{IN}^4}}{\pi^2 R_2^4\left(\frac{1}{2} + \ln\frac{R_1}{R_2}\right)^2} \tag{4.32b}$$

By substituting Eq.(4.32) into Eq.(4.31) and rearranging, the pressure head drop can be expressed as:

$$\Delta H = \left(\frac{\varphi_2}{\varphi_1}\right)Q^2 \tag{4.33}$$

in which

$$\varphi_1 = \frac{\left(H_o + R_1/3\right)R_1^2}{2\left(R_1 - R_{IN}\right)R_{IN}^2} - \alpha_\theta \frac{\pi\left(2H_o + R_1\right)}{4H_o} + \left(\frac{K_L}{f_\theta}\right) \tag{4.33a}$$

$$\varphi_2 = \frac{\left(H_o + R_1/3\right)}{4\pi^2 g\left(R_1 - R_{IN}\right)R_{IN}^2}\left[\alpha_z f_z\left(\frac{H_o}{R_1^3}\right) + K_L\left(\frac{R_1^2}{R_{IN}^4}\right)\right] \tag{4.33b}$$

In general, the flow in the tangential direction is turbulent rough flow and the friction factor $f_\theta$ is constant; while the flow in the vertical direction is laminar flow due to the

low overflow rate desired for solid separation, and the fraction factor $f_z$ can be determined in terms of the calculated Reynolds number. The Reynolds number in the vertical direction can be expressed as follows:

$$\mathrm{Re}_z = \frac{UD}{\nu} = \frac{2Q}{\pi R_1 \nu} \tag{4.34}$$

In terms of the calculated Reynolds number ($\mathrm{Re}_z$) and the relative roughness ($e/D$), the friction factor $f_z$ can be determined from Moody's diagram (Street et al., 1996).

#### 4.4.3.2 Effect of head loss terms on angular velocity

Moreover, in order to examine the significance of each term in Eq.(4.30a), the following cases, based on different combination of the terms in Eq.(4.30a), are considered:

**Case 1 $\alpha_\theta$ = 1.0 and $\alpha_z$ = 1.0**

If all of the terms in Eq.(4.30a) are included in the calculation of pressure head drop, (i.e.: the values of $\alpha_z$ and $\alpha_\theta$ are equal to one), then from Eq.(4.32) the general equation for angular velocity can be expressed as:

$$\omega = \left(\frac{\lambda_2}{\lambda_1}\right)^{1/2} Q \tag{4.35}$$

in which

$$\lambda_1 = \frac{\left(H_o + R_1/3\right)R_1^2}{2\left(R_1 - R_{IN}\right)R_{IN}^2} - \frac{\pi\left(2H_o + R_1\right)}{4H_o} + \left(\frac{K_L}{f_\theta}\right) \tag{4.35a}$$

$$\lambda_2 = \frac{\left(\frac{f_z}{f_\theta}\right)\left(\frac{H_o}{R_1^3}\right) + \left(\frac{K_L}{f_\theta}\right)\frac{R_1^2}{R_{IN}^4}}{\pi^2 R_2^4\left(\frac{1}{2} + \ln\frac{R_1}{R_2}\right)^2} \tag{4.35b}$$

and from Eq.(4.33) the general equation for pressure drop can be expressed as:

$$\Delta H = \left(\frac{\varphi_2}{\varphi_1}\right)Q^2 \tag{4.36}$$

in which

$$\varphi_1 = \frac{\left(H_o + R_1/3\right)R_1^2}{2\left(R_1 - R_{IN}\right)R_{IN}^2} - \frac{\pi\left(2H_o + R_1\right)}{4H_o} + \left(\frac{K_L}{f_\theta}\right) \tag{4.36a}$$

$$\varphi_2 = \frac{\left(H_o + R_1/3\right)}{4\pi^2 g\left(R_1 - R_{IN}\right)R_{IN}^2}\left[f_z\left(\frac{H_o}{R_1^3}\right) + K_L\left(\frac{R_1^2}{R_{IN}^4}\right)\right] \tag{4.36b}$$

**Case 2** $\alpha_\theta$ **= 1 and** $\alpha_z$ **= 0**

If the second term of Eq.(4.30a) is neglected (i.e.: $\alpha_z = 0$ but $\alpha_\theta = 1$), then from Eq.(4.32) the angular velocity can be rewritten as:

$$\omega = \left(\frac{\lambda_2}{\lambda_1}\right)^{1/2} Q \tag{4.37}$$

where

$$\lambda_1 = \frac{(H_o + R_1/3)R_1^2}{2(R_1 - R_{IN})R_{IN}^2} - \frac{\pi(2H_o + R_1)}{4H_o} + \left(\frac{K_L}{f_\theta}\right) \tag{4.37a}$$

$$\lambda_2 = \frac{1}{\pi^2}\left(\frac{K_L}{f_\theta}\right)\left(\frac{R_1^2}{R_{IN}^4 R_2^4}\right)\left(\frac{1}{2} + \ln\frac{R_1}{R_2}\right)^{-2} \tag{4.37b}$$

and from Eq.(4.33) the equation for pressure head drop can be written as

$$\Delta H = \left(\frac{\varphi_2}{\varphi_1}\right) Q^2 \tag{4.38}$$

in which

$$\varphi_1 = \frac{(H_o + R_1/3)R_1^2}{2(R_1 - R_{IN})R_{IN}^2} - \frac{\pi(2H_o + R_1)}{4H_o} + \left(\frac{K_L}{f_\theta}\right) \tag{4.38a}$$

$$\varphi_2 = \left(\frac{K_L}{4\pi^2 g}\right)\frac{(H_o + R_1/3)R_1^2}{(R_1 - R_{IN})R_{IN}^6} \tag{4.38b}$$

**Case 3** $\alpha_\theta = 0$ **and** $\alpha_z = 1$

If the first term of Eq.(4.30a) is neglected (i.e.: $\alpha_\theta$ = 0 but $\alpha_z$ = 1), then from Eq.(4.32) the angular velocity can be rewritten as:

$$\omega = \left(\frac{\lambda_2}{\lambda_1}\right)^{1/2} Q \tag{4.39}$$

in which

$$\lambda_1 = \frac{(H_o + R_1/3)R_1^2}{2(R_1 - R_{IN})R_{IN}^2} + \left(\frac{K_L}{f_\theta}\right) \tag{4.39a}$$

$$\lambda_2 = \frac{\left(\frac{f_z}{f_\theta}\right)\left(\frac{H_o}{R_1^3}\right) + \left(\frac{K_L}{f_\theta}\right)\frac{R_1^2}{R_{IN}^4}}{\pi^2 R_2^4 \left(\frac{1}{2} + \ln\frac{R_1}{R_2}\right)^2} \tag{4.39b}$$

and from Eq.(4.33) the pressure drop formula can be expressed as:

$$\Delta H = \left(\frac{\varphi_2}{\varphi_1}\right) Q^2 \tag{4.40}$$

in which

$$\varphi_1 = \frac{(H_o + R_1/3)R_1^2}{2(R_1 - R_{IN})R_{IN}^2} + \left(\frac{K_L}{f_\theta}\right) \tag{4.40a}$$

$$\varphi_2 = \frac{\left(H_o + R_1/3\right)}{4\pi^2 g\left(R_1 - R_{IN}\right)R_{IN}^2}\left[\alpha_z f_z\left(\frac{H_o}{R_1^3}\right) + K_L\left(\frac{R_1^2}{R_{IN}^4}\right)\right] \tag{4.40b}$$

**Case 4** $\alpha_\theta = 0$ **and** $\alpha_z = 0$

If the first and second terms of Eq.(4.30a) are neglected (i.e.: the values of $\alpha_z$ and $\alpha_\theta$ are equal to zero), then the angular velocity can be reduced to:

$$\omega = \left(\frac{\lambda_2}{\lambda_1}\right)^{1/2} Q \tag{4.41}$$

in which

$$\lambda_1 = \frac{\left(H_o + R_1/3\right)R_1^2}{2\left(R_1 - R_{IN}\right)R_{IN}^2} + \left(\frac{K_L}{f_\theta}\right) \tag{4.41a}$$

$$\lambda_2 = \frac{1}{\pi^2}\left(\frac{K_L}{f_\theta}\right)\left(\frac{R_1^2}{R_{IN}^4 R_2^4}\right)\left(\frac{1}{2} + \ln\frac{R_1}{R_2}\right)^{-2} \tag{4.41b}$$

and from Eq.(4.33) the pressure head drop equation can be reduced to:

$$\Delta H = \left(\frac{\varphi_2}{\varphi_1}\right)Q^2 \tag{4.42}$$

in which

$$\varphi_1 = \frac{(H_o + R_1/3)R_1^2}{2(R_1 - R_{IN})R_{IN}^2} + \left(\frac{K_L}{f_\theta}\right) \tag{4.42a}$$

$$\varphi_2 = \left(\frac{K_L}{4\pi^2 g}\right)\frac{(H_o + R_1/3)R_1^2}{(R_1 - R_{IN})R_{IN}^6} \tag{4.42b}$$

In order to conveniently compare the difference of the predicted results for angular velocity with Eq.(4.35), Eq.(4.37), Eq.(4.39), and Eq.(4.41) and thereby simplify the angular velocity formula by eliminating the insignificant terms in Eq.(4.35), a confined vortex chamber with $R_1$ = 63.5mm, $R_{IN}$ = 6.35mm, $R_2$ = 50.8mm, and $H_o$ = 175mm is selected as the case study.

Table 4.1 shows the calculated results with Eq.(4.35) for various measured inflow rates (Q) based on the selected chamber model. The first row is the measured inflow rates. The second row is the local loss coefficient. The third row is the characteristic diameter for fluid motion in the tangential direction. The fourth row is the relative roughness. The fifth row is the friction factor for fluid motion in the tangential direction, which is determined with Moody diagram (Street et al., 1996). The sixth row and seventh row are the Reynolds number and friction factor for fluid motion in the vertical direction, which are determined with Eq.(4.34) and Moody diagram. The eighth row is the calculated angular velocity with Eq.(4.35)

This table indicates that the calculated angular velocity (ω) increases with increasing the inflow rate (Q). The fluid flow in the vertical direction is laminar flow; while the Reynolds numbers in the tangential direction range about from 10,000 to 40,000 for inflow rates from 46.49 ml/s to 196.78 ml/s, which are estimated using

average tangential velocity (Eq.(4.11)) and the characteristic diameter D = 0.107 m. Thus the flow in the tangential direction is turbulent rough flow.

Table 4.2 shows the comparison of calculated angular velocities with Eq. (4.35), Eq.(4.37), Eq.(4.39) and Eq.(4.41), respectively. The first row represents the measured inflow rates from the inlet pipe. The rests of the rows are calculated angular velocities based on different combined contributions of head losses to the total head loss. The second row is calculated angular velocities that are considering all of the head losses. The third and forth rows are angular velocities that are obtained by neglecting the vertical frictional head loss and tangential frictional head loss, respectively; while the last row is the angular velocities that are calculated by neglecting the both of vertical and tangential head losses.

By comparing these calculated results, it was found that the differences among them are within the range of 0.5%. This means that the effect of the vertical and tangential frictional head losses on the angular velocity is insignificant, and thus this two terms can be eliminated in Eq.(4.35) for angular velocity and Eq.(4.36) for pressure head drop.

#### 4.4.3.3 Angular velocity and Pressure Head Drop

In terms of the above analysis, the angular velocity formula of Eq.(4.35) can be further reduced to:

$$\omega = \left( \frac{\lambda_2}{\lambda_1} \right)^{1/2} Q \tag{4.43}$$

**Table 4.1 Calculated Angular Velocity with Eq.(4.35)**

| Q (ml/sec) | 46.5 | 56.6 | 84.7 | 90.8 | 105.6 | 130.6 | 196.8 |
|---|---|---|---|---|---|---|---|
| $K_L$ | 1.00 | 1.00 | 1.00 | 1.00 | 1.00 | 1.00 | 1.00 |
| $D = 4R_h$ (m) | 0.107 | 0.107 | 0.107 | 0.107 | 0.107 | 0.107 | 0.107 |
| $e/D$ | 0.09 | 0.09 | 0.09 | 0.09 | 0.09 | 0.09 | 0.09 |
| $f_\theta$ | 0.037 | 0.037 | 0.037 | 0.037 | 0.037 | 0.037 | 0.037 |
| $\mathrm{Re}_z$ | 349.40 | 425.67 | 636.33 | 682.02 | 793.25 | 981.66 | 1478.88 |
| $f_z$ | 0.183 | 0.150 | 0.101 | 0.094 | 0.081 | 0.065 | 0.043 |
| ω (1/sec) | 4.63 | 5.64 | 8.43 | 9.03 | 10.51 | 12.95 | 19.22 |

**Table 4.2 Comparison of the Calculated Angular Velocities with Eq.(4.35), Eq.(4.37), Eq.(4.39), and Eq.(4.41)**

| Q(ml/sec) | 46.5 | 56.6 | 84.7 | 90.8 | 105.6 | 130.6 | 196.8 |
|---|---|---|---|---|---|---|---|
| $\alpha_\theta = 1$ $\alpha_z = 1$ | 4.63 | 5.64 | 8.43 | 9.03 | 10.51 | 12.95 | 19.22 |
| $\alpha_\theta = 1$ $\alpha_z = 0$ | 4.63 | 5.64 | 8.43 | 9.03 | 10.51 | 12.95 | 19.22 |
| $\alpha_\theta = 0$ $\alpha_z = 1$ | 4.61 | 5.61 | 8.39 | 8.99 | 10.46 | 12.89 | 19.12 |
| $\alpha_\theta = 0$ $\alpha_z = 0$ | 4.61 | 5.61 | 8.39 | 8.99 | 10.46 | 12.89 | 19.12 |

in which

$$\lambda_1 = \frac{(H_o + R_1/3)R_1^2}{2(R_1 - R_{IN})R_{IN}^2} + \left(\frac{K_L}{f_\theta}\right) \tag{4.43a}$$

$$\lambda_2 = \frac{1}{\pi^2}\left(\frac{K_L}{f_\theta}\right)\left(\frac{R_1^2}{R_{IN}^4 R_2^4}\right)\left(\frac{1}{2} + \ln\frac{R_1}{R_2}\right)^{-2} \tag{4.43b}$$

and the pressure head drop formula of Eq.(4.36) can be further simplified to:

$$\Delta H = \left(\frac{\varphi_2}{\varphi_1}\right)Q^2 \tag{4.44}$$

in which

$$\varphi_1 = \frac{(H_o + R_1/3)R_1^2}{2(R_1 - R_{IN})R_{IN}^2} + \left(\frac{K_L}{f_\theta}\right) \tag{4.44a}$$

$$\varphi_2 = \left(\frac{K_L}{4\pi^2 g}\right)\frac{(H_o + R_1/3)R_1^2}{(R_1 - R_{IN})R_{IN}^6} \tag{4.44b}$$

The above two equations, Eq.(4.43) and Eq.(4.44), are the equations that are suggested in this study for angular velocity estimation and pressure drop estimation, respectively. Unfortunately, there is no published formula on angular velocity for turbulent vortex chamber flows or measured data for the similar unit geometry that could be used to compare against this study. However, the visual observation with an object in the

chamber found that the times for the object to rotate one revolution are about 0.5 to 1.0 seconds (i.e., $\omega = 2\pi/t = 6.24$ to 12.8) for the various inflows which are basically close the range of the predicted angular velocities as shown in Table 4.2.

## 4.5 Nominal Angular Velocity ($\omega_n$)

Furthermore, if the inlet pipe average velocity ($\overline{U}_{IN} = Q/\pi R_{IN}^2$) is used to estimate the "angular velocity", here known as the "nominal angular velocity ($\omega_n$)" to distinguish it with the real angular velocity ($\omega$), at the radius of $r = R_1 - R_{IN}$, then the "nominal angular velocity" can be written as:

$$\omega_n = \frac{\overline{U}_{IN}}{R_1 - R_{IN}} = \frac{Q}{\pi R_{IN}^2 (R_1 - R_{IN})} \tag{4.45}$$

In general, this nominal angular velocity should be greater than the real angular velocity determined by Eq.(4.43) as it is directly calculated by the inlet pipe average velocity without considering the frictional losses in the vortex chamber system. The ratio of the real angular velocity ($\omega$) to the nominal angular velocity ($\omega_n$) is known as the angular velocity decay factor ($\delta$):

$$\delta = \frac{\omega}{\omega_n} \tag{4.46}$$

Table 4.3 shows the comparison of the calculated angular velocity of Eq.(3.35) to the calculated nominal angular velocity of Eq.(3.45) based on the above selected study case. This table indicates that for a given vortex chamber the angular velocity decay factor ( $\delta$ ) does not change significantly with the changing inflow rates Q, and it is close to a constant of 0.70.

**Table 4.3 Comparison of the Calculated Angular Velocity (ω) with Eq.(4.35) to the Calculated Nominal Angular Velocity ($\omega_n$) with Eq.(4.45)**

| Q (ml/sec) | 46.5 | 56.6 | 84.7 | 90.8 | 105.6 | 130.6 | 196.8 |
|---|---|---|---|---|---|---|---|
| ω (1/sec) | 4.63 | 5.64 | 8.43 | 9.03 | 10.51 | 12.95 | 19.22 |
| $\omega_n$ (1/sec) | 6.42 | 7.82 | 11.70 | 12.54 | 14.58 | 18.04 | 27.18 |
| $\delta = \omega/\omega_n$ | 0.72 | 0.71 | 0.70 | 0.70 | 0.70 | 0.69 | 0.69 |

## 4.6 Conclusions

For turbulent vortex chamber flow, based on the law of conservation of momentum and the boundary conditions, a formula of angular velocity for turbulent vortex chamber flows has been derived (Eq.(4.20)). For practical purpose, this equation was further developed by establishing the relationship between the pressure head drop ( $\Delta H$ ) and inflow rate (Q). Based on the case analysis, a simple angular velocity formula for turbulent vortex chamber flows was proposed (Eq.(4.43)). The case analysis indicates that the angular velocity increases with increasing the inflow rate.

Unfortunately there is not a published formula for angular velocity or experimental data from a similar unit configuration to compare with this study. However, by visual observation, it was found that the observed results were similar to the predicted results. This equation (Eq.(4.43)) can be applied to predict the angular velocity in a confined vortex chamber with a tangential inlet pipe, but without underflow exit.

# Chapter 5
# Determination of Flow Pattern in a Confined Vortex Flow

The determination of flow patterns in a confined vortex chamber is an important step to investigate the mechanisms of solid-liquid separation. In this chapter, based on the Navier-Stokes governing equations coupled with the boundary conditions in a vortex chamber as well as the angular velocity derived in Chapter 4, a mathematical model has been developed to describe the flow patterns in a confined vortex chamber operating with tangential inflow, but without underflow exit.

## 5.1 Introduction

Vortex separators are manufactured solid-liquid separation devices that use the vortex principle to remove suspended pollutants from wastewater or stormwater in highly developed areas where the available space is limited (Fenner and Tyack, 1998). The main difference between wastewater treatment units and stormwater treatment units is that the stormwater treatment unit exists without underflow exit underneath the chambers.

Prior knowledge of the patterns of fluid and particle motion in a confined vortex chamber is critical for understanding the mechanisms of the solid-liquid separation, thereby developing some deign basis. Additionally, an understanding of the flow pattern in a vortex chamber is an important step to achieve these goals. Unfortunately, it is very difficult to get the exact analytical solutions of the flow patterns due to the complexity of the flow patterns within a chamber unit. For practical design purpose, one often has to be

with the help of computer programming (such as CFD) to simulate the flow fields, and thus reduce the lab works (Wong, 1997). The purpose of this chapter, based on the Navier-Stokes governing equations and some assumptions, is to develop a mathematical model to simulate the flow patterns for the selected vortex chamber model.

## 5.2 Vortex Chamber Physical Model

In this study, the selected vortex chamber model is shown in Fig.5.1. In this system, the flow tangentially enters the unit to generate the rotational flow fields and then flows out over the top edge of the chamber. The dimensions of the unit configuration are also shown in Fig. 5.1. The fluid velocity in the chamber is resolved into three components: tangential ($U_\theta$), axial ($U_z$) and radial ($U_r$). The radial velocity component is small in comparison to both the tangential and vertical components (Rudinger, 1980; Svarovsky, 1981; Ogawa, 1992). For simplification, the radial velocity is neglected in this study.

## 5.3 Vortex Chamber Mathematical Model

### 5.3.1 Assumptions

In order to simplify the problem at hand and deduce an analytical solution of the flow patterns, the following assumptions must be considered:

- The fluid is incompressible and steady
- The flow field is axi-symmetrical around the z-axis
- A Rankine-like tangential velocity profile is assumed
- The angular velocity is constant along the height of the chamber

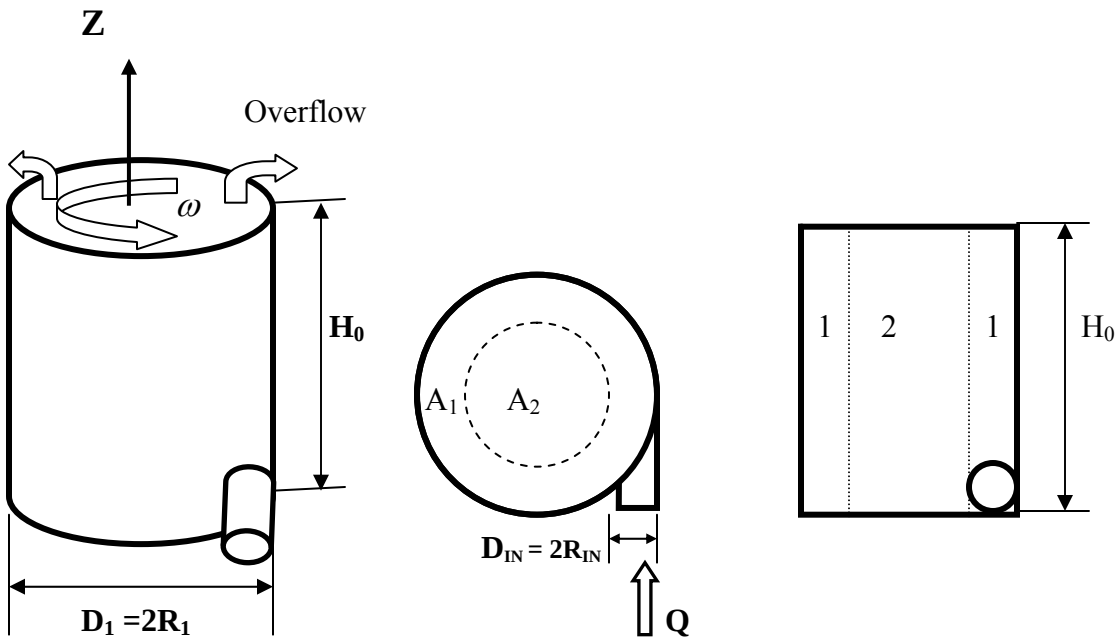


**(a) Perspective View** **(b) Top View** **(c) Elevation View**

**Fig. 5.1 Schematic Illustration of the Vortex Chamber Model**

- The radial velocity $U_r$ is small and neglected compared with tangential and axial velocities
- Neglecting the effects of vibration of vortex flow

Furthermore, in terms of the Rankine-combined vortex model, the rotational flowfield in a vortex chamber is divided into two zones: a free vortex region (outer region) and a forced vortex region (core region), as shown in Fig.4.2. The total inflow rate is divided into two portions $Q_1$ and $Q_2$: $Q_1$ is the portion passing through the outer upward helical vortex region 1; and $Q_2$ is the portion passing through the inner upward helical vortex region 2 ($Q = Q_1 + Q_2$).

### 5.3.2 Governing Equations for Vortex Chamber Flow

Through the last century, vortex flows have been considered one of the most important subjects of fluid motion by many scientists. To investigate the mechanisms of vortex motion and mathematically simulate its flow pattern, numerous experimental and theoretical studies have been conducted (Taylor, 1921; Rosenhead, 1932; Lin, 1943; Lamb, 1945; Shapiro, 1953; Rouse, 1959; Batchelor, 1967; Greenspan, 1980; Khader and Ayad, 1980; Escudier, et al, 1980; Shakespeare and Levy, 1980, Ogawa, 1992; Saffman, 1992). In terms of previously conducted studies, the general governing equations for vortex flows, based on cylindrical coordinates, are described as follows.

#### 5.3.2.1 Equations of continuity

The continuity equations can be written as (see Rouse, 1959; Whitaker, 1981; Schling & Gerten, 2000; Ogawa, 1992):

$$\frac{\partial(\rho_f U_r r)}{r\partial r} + \frac{\partial(\rho_f U_\theta)}{r\partial\theta} + \frac{\partial(\rho_f U_z)}{\partial z} = -\frac{\partial(\rho_f)}{\partial t} \tag{5.1}$$

For an incompressible fluid, the above equation reduces to:

$$\frac{\partial(U_r r)}{r\partial r} + \frac{\partial(U_\theta)}{r\partial\theta} + \frac{\partial(U_z)}{\partial z} = 0 \tag{5.1a}$$

where $\rho_f$ is the density of fluid; $U_r$, $U_\theta$ and $U_z$ are radial, tangential and axial velocities, respectively. For axi-symmetrical flow around the z-axis, Eq.(5.1a) can be further reduced to:

$$\frac{\partial(U_r r)}{r\partial r} + \frac{\partial(U_z)}{\partial z} = 0 \tag{5.1b}$$

For a confined vortex chamber flow, the radial velocity ($U_r$) is small in comparison to the tangential velocity ($U_\theta$) and the vertical velocity ($U_z$); and thus $U_r$ is negligible (Rudinger, 1980; Svarovsky, 1981; Ogawa, 1992). Eq.(5.1b) is further reduced to:

$$\frac{\partial U_z}{\partial z} = 0 \tag{5.1c}$$

Eq.(5.1c) indicates that the fluid motion in the vertical direction of the chamber is similar to that of the one-dimensional fluid flow. The vertical velocity component ($U_z$) is constant at the location of radius of r.

#### 5.3.2.2 Navier-Stokes governing equation

The Navier-Stokes governing equations can be written in vector notation (Batchelor, 1967; Ogawa, 1993):

$$\rho_f \frac{D\vec{U}}{Dt} = \rho_f \left[ \frac{\partial \vec{U}}{\partial t} + \left(\vec{U} \cdot \nabla\right)\vec{U} \right] = -\nabla p + \vec{F} + \mu \nabla^2 \vec{U} \tag{5.2}$$

where $\vec{F}$ is body force per unit volume; p is pressure; $\vec{U}$ is velocity vector; D/Dt is material derivative; $\rho_f$ is the density of fluid; and $\mu$ is viscosity. If the vector equation of Navier-Stokes is decomposed into three directions for cylindrical coordinates, the following equations are obtained:

$$\begin{aligned} &\rho_f \left( \frac{\partial U_r}{\partial t} + U_r \frac{\partial U_r}{\partial r} + U_\theta \frac{\partial U_r}{r \partial \theta} + U_z \frac{\partial U_r}{\partial z} - \frac{U_\theta^2}{r} \right) \\ &= F_r - \frac{\partial P}{\partial r} + \mu \left( \frac{\partial^2 U_r}{\partial r^2} + \frac{1}{r}\frac{\partial U_r}{\partial r} + \frac{1}{r^2}\frac{\partial^2 U_r}{\partial \theta^2} + \frac{\partial^2 U_r}{\partial z^2} - \frac{U_r}{r^2} - \frac{2}{r^2}\frac{\partial U_\theta}{\partial \theta} \right) \end{aligned} \tag{5.3a}$$

$$\begin{aligned} &\rho_f \left( \frac{\partial U_\theta}{\partial t} + U_r \frac{\partial U_\theta}{\partial r} + U_\theta \frac{\partial U_\theta}{r \partial \theta} + U_z \frac{\partial U_\theta}{\partial z} + \frac{U_r U_\theta}{r} \right) \\ &= F_\theta - \frac{1}{r}\frac{\partial P}{\partial \theta} + \mu \left( \frac{\partial^2 U_\theta}{\partial r^2} + \frac{1}{r}\frac{\partial U_\theta}{\partial r} + \frac{1}{r^2}\frac{\partial^2 U_\theta}{\partial \theta^2} + \frac{\partial^2 U_\theta}{\partial z^2} - \frac{U_\theta}{r^2} + \frac{2}{r^2}\frac{\partial U_r}{\partial \theta} \right) \end{aligned} \tag{5.3b}$$

$$\rho_f\left(\frac{\partial U_z}{\partial t}+U_r\frac{\partial U_z}{\partial r}+V_\theta\frac{\partial U_z}{r\partial\theta}+V_z\frac{\partial U_z}{\partial z}\right)$$
$$=F_z-\frac{\partial P}{\partial z}+\mu\left(\frac{\partial^2 U_z}{\partial r^2}+\frac{1}{r}\frac{\partial U_z}{\partial r}+\frac{1}{r^2}\frac{\partial^2 U_z}{\partial\theta^2}+\frac{\partial^2 U_z}{\partial z^2}\right) \quad (5.3c)$$

where $F_r, F_\theta, and\ F_z$ denote the body forces per unit volume respectively; and $U_r$, $U_\theta$, and $U_z$ are the velocity components in the radial, tangential and vertical directions, respectively.

These equations were originally derived by Navier, Cauchy, and Poisson in the early of last century (see, Rouse, 1959; Yih, 1977; Ogawa, 1993). The current expression of the above equations is from mid-century analyses by Saint-Venant and by Stokes. The nonlinear character of these equations, coupled with the complex boundary conditions, make it very difficult to obtain the exact analytical solutions of the fluid flows.

Furthermore, when fluid has a viscosity of $\mu=0$ (i.e.: the fluid is invicid), the above governing equations are reduced to the Euler Equations:

$$\frac{\partial U_r}{\partial t}+U_r\frac{\partial U_r}{\partial r}+U_\theta\frac{\partial U_r}{r\partial\theta}+U_z\frac{\partial U_r}{\partial z}-\frac{U_\theta^2}{r}=F_r-\frac{1}{\rho_f}\frac{\partial P}{\partial r} \quad (5.4a)$$

$$\frac{\partial U_\theta}{\partial t}+U_r\frac{\partial U_\theta}{\partial r}+U_\theta\frac{\partial U_\theta}{r\partial\theta}+U_z\frac{\partial U_\theta}{\partial z}+\frac{U_rU_\theta}{r}=F_\theta-\frac{1}{\rho_f}\frac{\partial P}{r\partial\theta} \quad (5.4b)$$

$$\frac{\partial U_z}{\partial t}+U_r\frac{\partial U_z}{\partial r}+U_\theta\frac{\partial U_z}{r\partial\theta}+U_z\frac{\partial U_z}{\partial z}=F_z-\frac{1}{\rho_f}\frac{\partial P}{\partial z} \quad (5.4c)$$

Euler's equations are only valid for inviscid flows. For a real fluid, the viscosity causes the presence of shear forces (or shear stresses) addition to the pressure force (or normal stress). For steady fluid flow, Navier-Stokes equations reduce to:

$$\rho_f\left(U_r\frac{\partial U_r}{\partial r}+U_\theta\frac{\partial U_r}{r\partial\theta}+U_z\frac{\partial U_r}{\partial z}-\frac{U_\theta^2}{r}\right)$$
$$=F_r-\frac{\partial P}{\partial r}+\mu\left(\frac{\partial^2 U_r}{\partial r^2}+\frac{1}{r}\frac{\partial U_r}{\partial r}+\frac{1}{r^2}\frac{\partial^2 U_r}{\partial\theta^2}+\frac{\partial^2 U_r}{\partial z^2}-\frac{U_r}{r^2}-\frac{2}{r^2}\frac{\partial U_\theta}{\partial\theta}\right) \quad (5.5a)$$

$$\rho_f\left(U_r\frac{\partial U_\theta}{\partial r}+U_\theta\frac{\partial U_\theta}{r\partial\theta}+U_z\frac{\partial U_\theta}{\partial z}+\frac{U_rU_\theta}{r}\right)$$
$$=F_\theta-\frac{1}{r}\frac{\partial P}{\partial\theta}+\mu\left(\frac{\partial^2 U_\theta}{\partial r^2}+\frac{1}{r}\frac{\partial U_\theta}{\partial r}+\frac{1}{r^2}\frac{\partial^2 U_\theta}{\partial\theta^2}+\frac{\partial^2 U_\theta}{\partial z^2}-\frac{U_\theta}{r^2}+\frac{2}{r^2}\frac{\partial U_r}{\partial\theta}\right) \quad (5.5b)$$

$$\rho\left(U_r\frac{\partial U_z}{\partial r}+U_\theta\frac{\partial U_z}{r\partial\theta}+U_z\frac{\partial U_z}{\partial z}\right)$$
$$=F_z-\frac{\partial P}{\partial z}+\mu\left(\frac{\partial^2 U_z}{\partial r^2}+\frac{1}{r}\frac{\partial U_z}{\partial r}+\frac{1}{r^2}\frac{\partial^2 U_z}{\partial\theta^2}+\frac{\partial^2 U_z}{\partial z^2}\right) \quad (5.5c)$$

Moreover, if the flow is axi-symmetrical around z-axis, then the above equations are reduced to:

$$\rho_f\left(U_r\frac{\partial U_r}{\partial r}+V_z\frac{\partial U_r}{\partial z}-\frac{U_\theta^2}{r}\right)=F_r-\frac{\partial P}{\partial r}+\mu\left(\frac{\partial^2 U_r}{\partial r^2}+\frac{1}{r}\frac{\partial U_r}{\partial r}+\frac{\partial^2 U_r}{\partial z^2}-\frac{U_r}{r^2}\right) \quad (5.6a)$$

$$\rho\left(U_r\frac{\partial U_\theta}{\partial r}+U_z\frac{\partial U_\theta}{\partial z}+\frac{U_rU_\theta}{r}\right)=F_\theta+\mu\left(\frac{\partial^2 U_\theta}{\partial r^2}+\frac{1}{r}\frac{\partial U_\theta}{\partial r}+\frac{\partial^2 U_\theta}{\partial z^2}-\frac{U_\theta}{r^2}\right) \quad (5.6b)$$

$$\rho_f\left(U_r\frac{\partial U_z}{\partial r}+U_z\frac{\partial U_z}{\partial z}\right)=F_z-\frac{\partial P}{\partial z}+\mu\left(\frac{\partial^2 U_z}{\partial r^2}+\frac{1}{r}\frac{\partial U_z}{\partial r}+\frac{\partial^2 U_z}{\partial z^2}\right) \quad (5.6c)$$

For the rotational flow, the Navier-Stokes equation is key when representing the characteristics of rotational flow in the boundary layer in the vortex chamber (Ogawa, 1992). The radial velocity $U_r$ is small in comparison with $U_\theta$ and $U_z$ and thus negligible in the aforementioned equations. Based on the assumptions of free vortex type in the outer zone and forced vortex type in the core zone of the chamber along with Eq.(5.1c), the terms of $\partial^2 U_\theta / \partial z^2$ and $\partial^2 U_z / \partial z^2$ can be eliminated from the governing equations. Then, the governing equations for vortex chamber flow can be written as:

$$\frac{\partial P}{\partial r} = \rho_f \frac{U_\theta^2}{r} \tag{5.7}$$

$$\frac{\partial^2 U_\theta}{\partial r^2} + \frac{1}{r}\frac{\partial U_\theta}{\partial r} - \frac{U_\theta}{r^2} = \frac{1}{\mu}\left(\frac{1}{r}\frac{\partial P}{\partial \theta} - F_\theta\right) \tag{5.8}$$

$$\frac{\partial^2 U_z}{\partial r^2} + \frac{1}{r}\frac{\partial U_z}{\partial r} = \frac{1}{\mu}\left(\frac{\partial P}{\partial z} - F_z\right) \tag{5.9}$$

## 5.4 Solutions to Governing Equations

### 5.4.1 Tangential Velocity Component ($U_\theta$)

When a fluid is tangentially forced into a confined vortex chamber, a Rankine-like tangential velocity profile is generated. The tangential velocity profile in the chamber changes from a type of free vortex to a type of forced vortex when the flow approaches the central axis of rotation. The tangential velocity does not vary significantly along the height of the chamber (Vatistas et al, 1986; Vatistas et al, 1988;

Ogawa, 1993). For a given inflow rate, the tangential velocity mainly depends upon the radial coordinate ( r ), rather than the vertical coordinate (z).

The fluid motion in the tangential direction is governed by Eq.(5.8). The external forces exerted on the rotational flow system in the tangential direction ($F_\theta$) are the pressure force generated from the inflow and frictional resistance forces generated from the chamber surface. For an equilibrium system, the resultant external force should be equal to zero. Then Eq. (5.9) becomes:

$$\frac{\partial^2 U_\theta}{\partial r^2} + \frac{1}{r}\frac{\partial U_\theta}{\partial r} - \frac{U_\theta}{r^2} = 0 \tag{5.10}$$

The general solution for Eq.(5.10) is as follows:

$$U_\theta = C_1 r \tag{5.11a}$$

$$U_\theta = \frac{C_2}{r} \tag{5.11b}$$

where $C_1$ and $C_2$ are constants. This solution is exactly same as the form of Rankine's combined vortex model. By comparing Eqs.(5.11a) and (5.11b) with Rankine's tangential velocity solution, i.e.: Eq.(4.6) and Eq.(4.10) discussed in Chapter 4, then tangential velocity distribution in the forced vortex zone and the free vortex zone can be expressed as follows, respectively:

Forced Vortex Region (r = 0 to $R_2$)

$$U_\theta = \omega r \tag{5.12}$$

Free Vortex Region (r = $R_2$ to $R_1$)

$$U_\theta = \frac{\omega R_2^2}{r} \tag{5.13}$$

where $U_\theta$ is the tangential velocity at radius r in vortex chamber; $R_2$ is the radius at the maximum tangential velocity (see Fig.4.2); and $\omega$ is the angular velocity of the core. The angular velocity can be determined by Eq.(4. 43) developed in Chapter 4 based on the law of conservation of momentum:

$$\omega = \left(\frac{\lambda_2}{\lambda_1}\right)^{1/2} Q \tag{4.43}$$

in which

$$\lambda_1 = \frac{(H_o + R_1/3)R_1^2}{2(R_1 - R_{IN})R_{IN}^2} + \left(\frac{K_L}{f_\theta}\right) \tag{4.43a}$$

$$\lambda_2 = \frac{1}{\pi^2}\left(\frac{K_L}{f_\theta}\right)\left(\frac{R_1^2}{R_{IN}^4 R_2^4}\right)\left(\frac{1}{2} + \ln\frac{R_1}{R_2}\right)^{-2} \tag{4.43b}$$

where $K_L$ is the local loss coefficient at inlet pipe exit; $f_\theta$ is the friction factor in the tangential direction in the chamber.

### 5.4.2 Vertical Velocity ($U_z$)

The fluid motion in the vertical direction in the chamber is governed by Eq.(5.9). The right-hand side of Eq.(5.10) is the pressure gradient in the vertical direction and body force exerted on the fluid. In practical operation of liquid-solid separation system, the vertical velocity ($U_Z$) in a vortex chamber is very small. To simplify the problem and achieve an analytical solution, the fluid viscosity (μ) is assumed to be a constant. Therefore, the terms in the right hand side of Eq.(5.9) are constant. Then the general solution of Eq.(5.9) can be expressed as:

$$U_z = C_1 + C_2 \ln r + \frac{1}{4\mu}\left(\frac{\partial p}{\partial z} - F_z\right) r^2 \tag{5.14}$$

where $C_1$ and $C_2$ are constants. In terms of physical conditions, the velocity at r = 0 must be finite though the vertical velocity at the center of the chamber can not be determined. Therefore, for this equation to be true, $C_2 = 0$ (Fox and McDonald, 1985). Then Eq.(5.15) becomes:

$$U_z = C_1 + \frac{1}{4\mu}\left(\frac{\partial p}{\partial z} - F_z\right) r^2 \tag{5.15}$$

According to the boundary condition that $U_Z = 0$ at $r = R_1$, the constant $C_1$ can be determined by:

$$C_1 = -\frac{1}{4\mu}\left(\frac{\partial p}{\partial z} - F_z\right)R_1^2 \tag{5.16}$$

Substituting Eq.(5.16) into Eq.(5.15) and rearranging gives:

$$U_z = -\frac{1}{4\mu}\left(\frac{\partial p}{\partial z} - F_z\right)\left(R_1^2 - r^2\right) \tag{5.17}$$

In terms of the law of conservation of mass, the total outflow rate must be equal to the inflow rate (Q). Then the following relationship is obtained:

$$Q = \int_0^{R_1} U_z 2\pi r dr = -\frac{1}{4\mu}\left(\frac{\partial p}{\partial z} - F_z\right)\left(\frac{\pi R_1^4}{2}\right) \tag{5.18}$$

Rearranging Eq. (5.18) gives:

$$-\frac{1}{4\mu}\left(\frac{\partial p}{\partial z} - F_z\right) = \frac{2Q}{\pi R_1^4} \tag{5.19}$$

By substituting Eq.(5.19) into Eq.(5.17) and rearranging, the vertical velocity distribution can be expressed as:

$$U_z = \frac{2Q}{\pi R_1^2}\left[1-\left(\frac{r}{R_1}\right)^2\right] \tag{5.20}$$

This equation indicates that for a given radius of r the vertical velocity component is proportional to the inflow rate Q; while for a given inflow rate Q the vertical velocity distribution only depends upon the radius r.

Moreover, the ratio of flow rates passing through free vortex region ($Q_1$) and forced vortex region ($Q_2$) can be determined by:

$$\frac{Q_1}{Q} = \frac{1}{Q}\int_{R_2}^{R_1} U_z 2\pi r dr = \frac{\left(R_1^2 - R_2^2\right)^2}{R_1^4} = \left[1-\left(\frac{R_2}{R_1}\right)^2\right]^2 \tag{5.21}$$

and

$$\frac{Q_2}{Q} = \frac{1}{Q}\int_{0}^{R_2} U_z 2\pi r dr = \frac{2R_1^2 R_2^2}{R_1^4} = 2\left(\frac{R_2}{R_1}\right)^2 - \left(\frac{R_2}{R_1}\right)^4 \tag{5.22}$$

## 5.5 Case Analysis and Discussions

### 5.5.1 Prediction of Tangential Velocity Distribution

The tangential velocity distribution in a vortex chamber can be described by Eqs.(5.12) and (5.13):

$$U_\theta = \omega r \qquad (r = 0 \quad to \quad R_2) \tag{5.12}$$

$$U_\theta = \frac{\omega R_2^2}{r} \qquad (r = R_2 \quad to \quad R_1) \tag{5.13}$$

The angular velocity can be estimated by Eq.(4.43), which is reproduced as follows:

$$\omega = \left(\frac{\lambda_2}{\lambda_1}\right)^{1/2} Q \tag{4.40}$$

in which

$$\lambda_1 = \frac{(H_o + R_1/3)R_1^2}{2(R_1 - R_{IN})R_{IN}^2} + \left(\frac{K_L}{f_\theta}\right) \tag{4.40a}$$

$$\lambda_2 = \frac{1}{\pi^2}\left(\frac{K_L}{f_\theta}\right)\left(\frac{R_1^2}{R_{IN}^4 R_2^4}\right)\left(\frac{1}{2} + \ln\frac{R_1}{R_2}\right)^{-2} \tag{4.40b}$$

For a vortex chamber with diameter of $D_1 = 2R_1 = 127$ mm, inlet pipe diameter $D_{IN} = 2$ $R_{IN} = 12.7$mm; and height $H_0 = 175$ mm, the calculated angular velocities for various inflow rates based on the selected chamber configuration are shown in Table 5.1.

Figure 5.2 shows the predicted tangential velocity distribution for three inflow rates selected from Table 5.1. This figure indicates that for a given flow rate Q, the tangential velocity in the core region of the chamber (forced vortex region) increases with an increasing radius of r; while in the outer region of the chamber (free vortex region) the tangential velocity decreases with increasing the radius of r. For a given radius of r, the tangential velocity increases with increasing the inflow rate. The maximum tangential

velocity occurs at the boundary of forced vortex zone and free vortex zone. The maximum tangential velocities for flow rates of Q = 46.5 ml/sec and 130.6 ml/sec are 0.23 m/sec and 0.65 m/sec, respectively.

**Table 5.1 Calculated Angular Velocities for Various Inflow Rates**

| Q (ml/sec) | 46.5 | 56.6 | 84.7 | 90.8 | 105.6 | 130.6 | 196.8 |
|---|---|---|---|---|---|---|---|
| $K_L$ | 1.00 | 1.00 | 1.00 | 1.00 | 1.00 | 0.99 | 0.96 |
| D = 4 Rh | 0.107 | 0.107 | 0.107 | 0.107 | 0.107 | 0.107 | 0.107 |
| e/D | 0.09 | 0.09 | 0.09 | 0.09 | 0.09 | 0.09 | 0.09 |
| $f_\theta$ | 0.037 | 0.037 | 0.037 | 0.037 | 0.037 | 0.037 | 0.037 |
| $\omega$ (1/s) | 4.61 | 5.61 | 8.39 | 8.99 | 10.46 | 12.89 | 19.15 |

### 5.5.2 Prediction of Vertical Velocity Distribution

For a vortex chamber with diameter of $D_1 = 2R_1 = 127$ mm, inlet pipe diameter $D_{IN} = 2\ R_{IN} = 12.7$mm; and height $H_0 = 175$ mm, the vertical velocity distribution can be estimated by Eq.(5.20):

$$U_z = \frac{2Q}{\pi R_1^2}\left[1-\left(\frac{r}{R_1}\right)^2\right] \tag{5.20}$$

Figure 5.3 shows the predicted vertical velocity for different inflow rates. It shows that vertical velocity increases with increasing inflow rate. The maximum vertical velocities

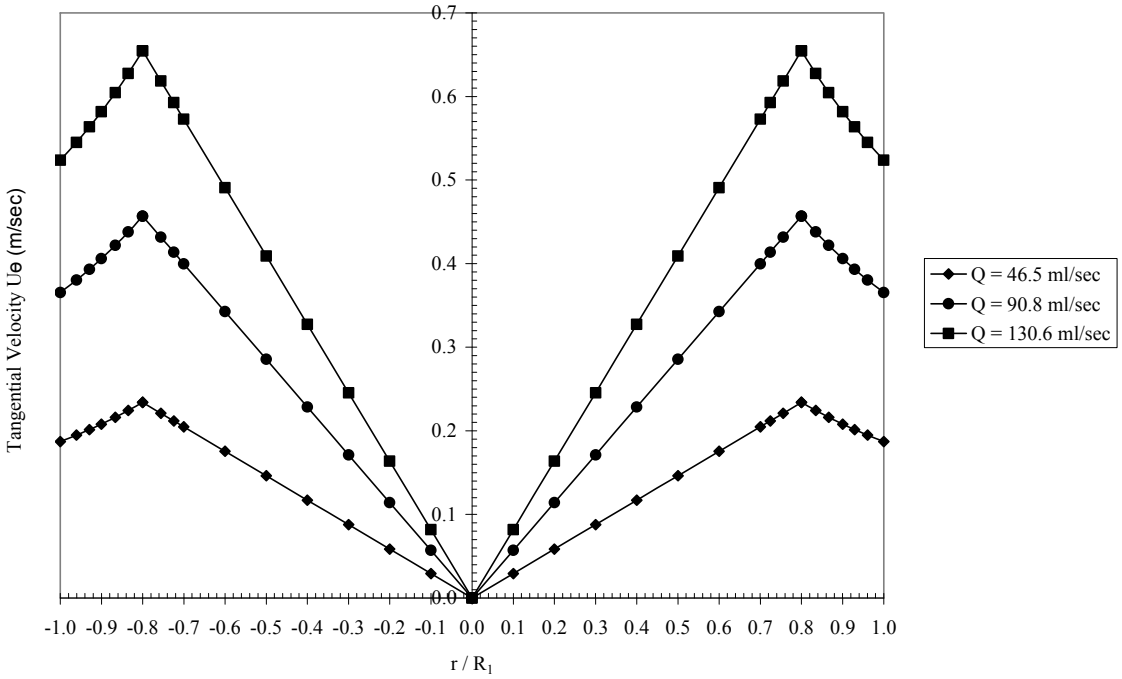


Fig. 5.2 Predicted Tangential velocity Distribution for Various Inlow Rates Q

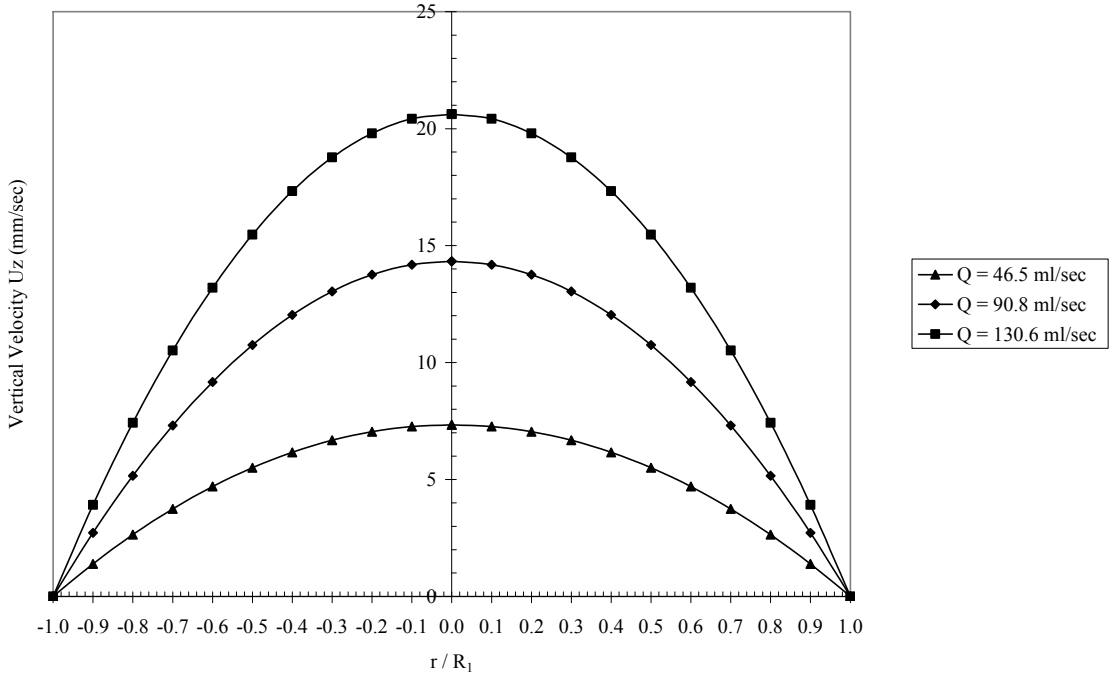


Fig. 5.3 Vertical Velocity Distribution for various Flow Rates

for Q = 46.5 ml/sec and 130.6 ml/sec are 7.4 mm/sec and 20.6 mm/sec, respectively. With a decreasing inflow rate, the shape of the curves become flat and lower. For the purpose of solid-liquid separation, the lower maximum vertical velocity and uniform distribution is desired.

## 5.6 Conclusions

A mathematical model, based on the Navier-Stokes governing equations coupled with the boundary conditions in a vortex chamber as well as the angular velocity, has been developed to describe the flow patterns for a selected vortex chamber model. The case analysis indicates that for a given location in the chamber the predicted tangential and vertical velocities increase with an increasing inflow rate. The maximum tangential velocity occurs at the boundary between the forced vortex region and free vortex region; while the maximum vertical velocity occurs at the center of the chamber.

# Chapter 6

# Dynamic Analysis of Particle Motion in a One-Dimensional Upward Uniform Steady Flowfield

The purpose of this chapter is to examine the characteristics of particle motion in a one-dimensional upward uniform steady fluid flow and investigate the mechanisms of solid-liquid separation. Based on the governing equation of particle motion in an upward uniform steady fluid flow, new particle settling velocity formulae have been derived in this study. The obtained analytical results were compared with accepted literature such as Cheng's formula. Good agreement was observed. The resulting equations developed in this chapter are useful when illustrating the most common aspects of multiphase fluid dynamics for solid-liquid separation.

## 6.1 General Equation of Particle Motion

The prediction of particle settling velocity and trajectory in fluid flow is of a considerable concern in many fields, such as gas-solid and liquid-solid separation. However, the prediction of particle motion requires not only a detailed understanding of fluid motion, but also the forces acting on a particle. A particle moving in a fluid with an initial velocity will be either decelerated or accelerated by the action of various forces. To investigate the hydrodynamic characteristics of particle motion, examine the effect of various forces acting on a particle, and thereby predict the trajectories of particle motion in a fluid flowfeild, numerous study results from previous investigators must be

considered and borrowed (Boothroyd, 1971; Maxey & Riley, 1983; Auton, 1987; Auton, et al, 1988; Sridhar & Katz, 1994; Legendre & Magnandet, 1998; Kurose & Komori; Coimbra, and Rangel, 1998; Coimbra and Kobayashi, 2002; Bagchi & Balachandar, 2002 & 2003; Candelier et al, 2004; Sobral et al, 2007; Iso and Kamemoto, 2008).

In terms of completed studies, when a solid particle is moving in fluid, the major forces considered on the particle include body forces, drag force, lift force, pressure force, inertia (added mass) force, and Bassett force. Therefore the general fundamental equation of particle motion is generally written as:

$$m_p \frac{d\vec{U}_p}{dt} = \vec{F}_{body} + \vec{F}_D + \vec{F}_I + \vec{F}_L + \vec{F}_p + \vec{F}_B \tag{6.1}$$

Where $m_p$ is the particle mass; $U_p$ is the particle absolute velocity; $F_{body}$ is the body forces which are proportional to particle mass; $F_D$ is the drag force; $F_I$ is the inertia force; $F_L$ is the lift force; $F_p$ is the pressure force; and $F_B$ is the Bassett force.

Once the velocity-time relation of particle motion has been obtained, the distance traveled by a particle can be determined by integrating the velocity / time relationship. It can be mathematically expressed as:

$$x = \int_{t_o}^{t} U_{p,x} dt + x_o \tag{6.2a}$$

$$y = \int_{t_o}^{t} U_{p,y} dt + y_o \tag{6.2b}$$

$$z = \int_{t_o}^{t} U_{p,z}\, dt + z_o \tag{6.2c}$$

where x, y and z are the distances of particle traveled in the x, y, and directions, respectively; and $U_{p,x}, U_{p,y}$, $U_{p,z}$ are particle velocity components in the x, y, and z directions, respectively.

### 6.1.1 Body Forces ( $\vec{F}_{body}$ )

Here the body forces are represented by the gravitational force ($F_g$) which acts in the direction of the gravity acceleration vector (g) or centrifugal force ($F_c$) which acts in the direction of centrifugal acceleration vector ($a_c$), such that:

$$\vec{F}_{body} = \vec{F}_g = m_p \vec{g} \tag{6.3}$$

For the vertical component, the net gravitational force can be expressed as:

$$F_g = m_p \left(1 - \frac{\rho_f}{\rho_p}\right) g \tag{6.3a}$$

### 6.1.2 Drag Force ( $\vec{F}_D$ )

A general expression for the drag force can be expressed as:

$$\vec{F}_D = \frac{1}{2} C_D \rho_f A_p \left(\vec{U}_f - \vec{U}_p\right)^2 \tag{6.4}$$

where $\rho_f$ is the fluid density; $A_p$ is the particle projected area; $U_f$ and $U_p$ are the fluid and particle velocities, respectively; $C_D$ is the drag coefficient which is related to the Reynolds number. The flows around the suspended bodies are generally divided into three categories: laminar, transition, and turbulent. At the region of low Reynolds number ($R_{ep} \leq 1.0$), streamline exists around the particle. The drag coefficient for spherical particles can be approximated as:

$$C_D = \frac{24}{R_{ep}} \tag{6.5}$$

where $R_{ep}$ is the Reynolds number which is defined as:

$$R_{ep} = \frac{\rho_f \left|U_f - U_p\right| d}{\mu} \tag{6.6}$$

where $\mu$ is dynamic viscosity of fluid. For spherical particles with a medium to high range Reynolds number, experimental data must be used to obtain the drag coefficient $C_D$ which can be found in various references (Lapple & Shephered, 1940; Morsi & Alexander, 1972). For the spherical particles with the Reynolds number of $R_{ep}$ = 500 to 20000, the average value of $C_D$ is about 0.44

For practical purpose, it is more convenient to use an analytical expression for $C_D$, many theoretical expressions and empirical curve fits have been suggested since the early part of last century. Boothroyd (1971) has listed ten such analytical expressions which fitted for the parts or entire range of Reynolds number. Several of them are described as follows.

**Oseen-Type Solutions**

Based on the Navier-Stokes equations, Oseen (1927) derived an equation to calculate the drag coefficient:

$$C_D = \frac{24}{R_{ep}}\left(1+\frac{3}{16}R_{ep}\right) \tag{6.7}$$

Further, based on the Oseen's solution, Goldstein (1929) proposed a more complete solution for the range of $R_{ep}<2$:

$$C_D = \frac{24}{R_{ep}}\left(1+\frac{3}{16}R_{ep}-\frac{19}{1280}R_{ep}^2+\frac{71}{20480}R_{ep}^3\right) \tag{6.8}$$

**Schiller and Nauman's Solution**

Schiller et al. (1933) proposed a solution that shows a good agreement with the experimental data for $R_{ep} < 800$:

$$C_D = \frac{24}{R_{ep}}\left(1 + 0.150 R_{ep}^{0.687}\right) \tag{6.9}$$

**Dallavalle's Solution**

Dallavalle (1943) proposed a simple equation that the entire range of experimental data can be represented with a fair degree of accuracy as:

$$C_D = \frac{24.4}{R_{ep}} + 0.4 \tag{6.10}$$

**Morsi and Alexander's Solution**

Morsi and Alexander (1972) presented a method to calculate the drag coefficient $C_D$ by fitting the measured $C_D$ with Reynolds number. To obtain the accuracy the experimental data curve was divided into a number of regions within the error of 1-2%. The equation they suggested for drag coefficient approximation in that region is:

$$C_D = \frac{K_1}{R_{ep}} + \frac{K_2}{R_{ep}^2} + K_3 \tag{6.11}$$

where $K_1$, $K_2$, and $K_3$ are constants which can be determined by fitting the experimental data at three points. The obtained values of $K_1$, $K_2$, and $K_3$ by Morris and Alexander (1972) are shown in Table 6.1.

**Table 6.1 Fitting Values of $K_1$, $K_2$ and $K_3$ for Drag Coefficient $C_D$**

| $R_{ep}$ | $K_1$ | $K_2$ | $K_3$ |
|---|---|---|---|
| $R_{ep} < 0.1$ | 24.0 | 0.0 | 0.0 |
| $0.1 < R_{ep} < 1.0$ | 22.73 | 0.0903 | 3.69 |
| $1.0 < R_{ep} < 10.0$ | 29.1667 | -3.8889 | 1.222 |
| $10.0 < R_{ep} < 100.0$ | 46.5 | -116.67 | 0.6167 |
| $100.0 < R_{ep} < 1000.0$ | 98.33 | -2778.0 | 0.3644 |
| $1000.0 < R_{ep} < 5000.0$ | 148.62 | -47500.0 | 0.357 |
| $5000.0 < R_{ep} < 10000.0$ | -490.546 | 578700.0 | 0.46 |
| $10000.0 < R_{ep} < 50000.0$ | -1662.5 | 5416700.0 | 0.5191 |

(Source: Moris & Alexander, 1972)

An advantage in using this equation is that the simple exponent may lead to integral forms of the equations to solve for the governing equations of particle motion. Thus, Morsi and Alexander's solution may be a good approach to approximate the drag coefficient. In this study, this equation will be used to approximate the drag coefficient.

### 6.1.3 Inertia Force ( $\vec{F}_I$ )

**Added Mass Force:** If the particle acceleration is different from that of the flowfield, then an additional relative acceleration ( $d\vec{U}_f / dt - d\vec{U}_p / dt$ ) arises. Some fluid near the particle surface must be accelerated or decelerated from the fluid velocity to the particle velocity, and thus an additional force acts on the particle. The portion of the surrounding fluid which is carried along with the particle due to the surface conditions should possess the same acceleration as that of the particle. This "carried mass" is referred to as the "added mass" or "virtual mass", and equals one-half the mass of the displaced fluid. The

added mass force is normally expressed as (see Boothroyd, 1971; Maxey & Riley, 1983; Auton et al, 1988; Coimbra & Rangel, 1998; Bagchi & Balachandar, 2003):

$$\vec{F}_A = \frac{1}{2} m_f \left( \frac{d\vec{U}_f}{dt} - \frac{d\vec{U}_p}{dt} \right) \tag{6.12}$$

where $m_f$ is displaced fluid mass by the particle. For a spherical particle Eq.(6.12) can be written as:

$$\vec{F}_A = \frac{\pi d^3 \rho_f}{12} \left( \frac{d\vec{U}_f}{dt} - \frac{d\vec{U}_p}{dt} \right) \tag{6.13}$$

### 6.1.4 Pressure Force ( $\vec{F}_p$ )

The pressure force exerted on a spherical particle due to the pressure gradient in the fluid can be expressed as (see Maxey & Riley, 1983; Sridhar & Katz, 1994; Bagchi & Balachandar, 2003)

$$\vec{F}_p = \frac{\pi d^3 \rho_f}{6} \frac{D\vec{U}_f}{Dt} \tag{6.14}$$

In a steady uniform fluid flowfield, the vertical component ( $F_{p,Z}$ ) is the buoyancy force which has been considered in Eq.(6.2a), and is reproduced as follows:

$$F_{p,Z} = \frac{\pi d^3}{6} \rho_f g \tag{6.14a}$$

### 6.1.5 Lift Force ( $\vec{F}_L$ )

In general the lift force in a shear flow is generated from the velocity gradient in the flow and from the rotation of particle (Magnus effect). For a spherical particle moving in a viscous flow with small Reynolds number, the expression of the shear-induced lift force derived by Saffman (1965) is:

$$F_L = C_L \rho_f \nu^{0.5} d^2 V_r \left( \frac{dU_f}{dz} \right)^{0.5} \tag{6.15}$$

where $C_L$ is lift coefficient (=1.615 for viscous flow); ν is kinematic viscosity; $V_r$ is the relative velocity; and $dU_f/dz$ is the velocity gradient. For the steady uniform flow the lift force is identically zero.

In 1917, Taylor, based on the study of motion of a solid body in a rotating flow system and the assumption that the flow system and the solid body have the same angular velocity, proposed an expression of lift force (see Rijin, 1990):

$$F_L = C_L \rho_f \forall V_r \left( \frac{dU_f}{dz} \right) \tag{6.15a}$$

where $C_L$ is the lift coefficient ($\approx 0.5$); $\forall$ is the particle volume. For a steady uniform flow this lift force is identically zero.

For the lift force arising from the rotation of particle in a viscous flow, Rubinov & Keller (1961) obtained the following expression:

$$F_L = C_L \rho_f d^3 V_r \omega \tag{6.15b}$$

where $C_L$ is the lift coefficient (= 0.39); ω is the angular velocity of the particle. But for a viscous flow, Saffman's theoretical analysis (1965) indicated that the lift force arising from the particle rotation is less by an order in magnitude than that arising from shear effect. Therefore, the lift force due to particle rotation effect can be neglected.

Auton (1987) obtained an expression to calculate the lift force on a sphere in an inviscid rotational flow with weak vorticity:

$$\vec{F}_L = C_L \frac{\pi d^3 \rho_f}{6} \left(\vec{U}_f - \vec{U}_p\right) \times \vec{\Omega} \tag{6.15c}$$

where the lift coefficient $C_L$ for spherical particle is 0.5; $\vec{\Omega}$ is the ambient vorticity. Later Auton et al (1988) presented a general expression for the net force on a sphere in inviscid unsteady non-uniform rotational flow:

$$\vec{F} = \frac{\pi d^3 \rho_f}{6} \left\{ \left[ \left(1 + C_M\right) \frac{D\vec{U}_f}{Dt} - C_M \frac{d\vec{U}_p}{dt} \right] + C_L \left(\vec{U}_f - \vec{U}_p\right) \times \vec{\Omega} \right\} \tag{6.15d}$$

where $C_M$ and $C_L$ are the added-mass and the inviscid lift coefficients. For a spherical particle, both of them are 0.5. For steady flow the force on the sphere in the inviscid limit can be written as (Auton, et al, 1988; Bagchi & balachandar, 2002):

$$\vec{F} = m_f (1 + C_M)\vec{U}_f \cdot \nabla \vec{U}_f + m_f C_{IL}(\vec{U}_f - \vec{U}_p) \times \vec{\Omega} \tag{6.15e}$$

where $m_f$ is the mass of fluid displaced by the sphere; and $C_{IL}$ is the inviscid lift coefficient, and for a sphere it is 0.5 provided that the vorticity is weak.

Bagchi & Balachander's investigation (2002 and 2002a) indicated that the lift force acting on a rigid spherical particle in a vortex is less than that in a linear shear flow; the rotational contribution is only about 4 – 14% of the total lift force and it can be considered to be only of secondary importance. More recently, Iso and Kamemoto (2008), based on the Lagrangian-Lagrangian method developed a numerical simulation scheme by combining a vortex method and a particle trajectory method. Their analysis indicated that the total lift force of Magnus and Saffman is only 4% of the drag force, and is approximately a hundredth smaller than the drag force. This is based in part that the surrounding flowfield gradients and particle spin are so small that particle lift can be neglected. Therefore, to simplify the problem, the lift force is neglected in this research.

### 6.1.6 Basset Force ($\vec{F}_B$)

The Basset force is the additional force acting on the particle due to the deviation of the flow pattern around the particle from steady-state conditions (Boothroyd, 1971; Rudinger, 1980). The Basset force is responsible for the modification of the drag force

due to the unsteadiness of the near flow field as the particle moves through the fluid (Coimbra and Rangel, 1998). The Basset force is expressed as (Maxey & Riley, 1983):

$$\vec{F}_B = \frac{3}{2} d^2 \sqrt{\pi \rho_f \mu} \int_{t_o}^{t} \frac{d\vec{U}_f / dt' - d\vec{U}_p / dt'}{\sqrt{t - t'}} \tag{6.16}$$

Unfortunately, there is no exact analytical solution for history forces due to the complexity of this expression. However, many studies with numerical methods or the Laplace transform approach (Yang & Leal, 1991; Michaelides, 1992; Mei et al, 1994; Thomas, 1997; Coimbra & Rangel, 1998; Coimbra & Kobayashi, 2002; Bagchi and Balachandar, 2003; Candelier et al, 2004) have found that the history force is not sensitive to the "long-term history" as it tends to be weak, and generally insignificant if the particle-fluid density ratio is high ($\rho_p / \rho_f \geq 1$), and thus negligible.

The study by Coimbra and Rangel (1998), based on their numerical example, showed that for an air bubble with a diameter of 100 μm it approximately takes 0.4 milliseconds (ms) to reach 90% of its terminal velocity with the history contribution when released from rest in glycerin; while without the history contribution it is about 2.2 microseconds (μs) to reach 90% of its terminal velocity. Numerical calculation show that results with Basset force overestimate the particle motion, i.e., the Basset term contribution is negative to particle motion. On the other hand, for the same particle size with density 20 times more than glycerin, it also takes approximately 0.4 ms to reach 90% of its terminal velocity with the contribution of history drag; while without the

Basset term contribution, it takes approximately 0.1 ms. This indicates that Basset force contribution is not so strong and negligible for heavy particles.

More recently, Candelier et al (2004) conducted a study to investigate the effect of Basset force on the radial migration of a Stokes particle in a solid-body rotation flow field. Their study also shows that the contribution of the Basset force is always negative that is agreement with the statement by Coimbra and Rangel (1998). Based on their analysis, they concluded that the radial component of the Basset term is more sensitive to the "short-term history", and less sensitive to the "long-term history". Therefore, to simplify the problem, the Bassett force is neglected in this research due to its insignificant effect on the motion of heavy particles.

## 6.2 Governing Equation of Particle Motion in a One-Dimensional Upward Uniform Steady Flowfield

### 6.2.1 Assumptions that Simplify the Dynamics

Though the general equations of particle motion in fluid flow are easy to establish, the complexity of the solid-liquid particle systems makes it difficult to obtain the analytical solutions for particle motion. In order to simply the problem, the following assumptions are made:

- The particles have a spherical shape
- The particle concentration is so low that presence of particles does not affect the fluid flow
- Particle-particle interactions are negligible; the behavior of each particle can be treated alone.

### 6.2.2 Governing Equation of Particle Motion

To simply the problem, the secondary forces are neglected in this study. The considered forces acting on a spherical particle are the net gravitational force ( $F_g$ ), drag force ( $F_D$ ), and inertia force (added mass) ( $F_I$ ) only as shown in Fig.6.1.

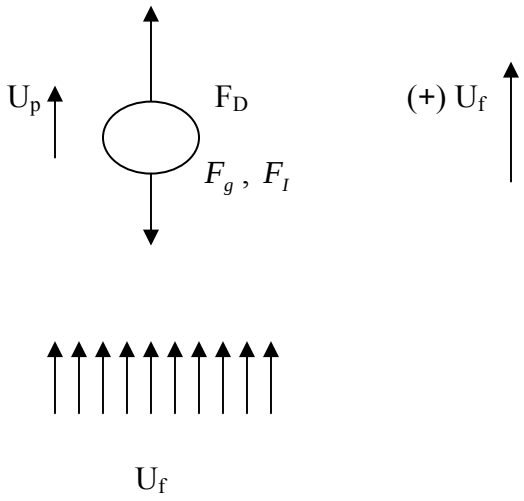


**Fig.6.1 Forces Acting on a Particle**

Therefore the governing equation of particle motion can be written as:

$$m_p \frac{dU_p}{dt} = F_D - F_g - F_I \tag{6.17}$$

The net gravitational force ( $F_g$ ) can be represented by Eq.(6.3a) as follows:

$$F_g = m_p\left(1-\frac{\rho_f}{\rho_p}\right)g \tag{6.17a}$$

In terms of Eq.(6.4), the drag force ( $F_D$ ) can be expressed as:

$$F_D = \frac{1}{2}C_D\rho_f A\left(U_f - U_p\right)^2 \tag{6.17b}$$

According to Eq.(6.12), in a one-dimensional uniform steady fluid flow the added mass force ( $F_I$ ) can be written as follows:

$$F_I = \frac{1}{2}m_f\frac{dU_p}{dt} \tag{6.17c}$$

By substituting Eqs.(6.17a), (9.17b) and (6.17c) into Eq.(6.17), the governing equation of particle motion can be expressed as:

$$\left(m_p + 0.5\,m_f\right)\frac{dU_p}{dt} = \frac{1}{2}C_D\rho_f A\left(U_f - U_p\right)^2 - m_p\left(1-\frac{\rho_f}{\rho_p}\right)g \tag{6.18}$$

For a spherical particle, the particle mass ( $m_p$ ) can be determined by:

$$m_p = \frac{\pi}{6}d^3\rho_p \tag{6.19}$$

While the added mass ( $m_f$ ) can be expressed as:

$$m_f = \frac{\pi}{6} d^3 \rho_f \tag{6.20}$$

The projected area (A) of a spherical particle is

$$A = \frac{\pi}{4} d^2 \tag{6.21}$$

Substituting Eqs.(6.19), (6.20) and (6.21) into Eq.(6.18) and rearranging yields:

$$\frac{dU_p}{dt} = \frac{3C_D}{4d}\left(\frac{\rho_f}{\rho_p + 0.5\rho_f}\right)\left(U_f - U_p\right)^2 - \left(\frac{\rho_p - \rho_f}{\rho_p + 0.5\rho_f}\right)g \tag{6.22}$$

## 6.3 Solutions to Governing Equation

### 6.3.1 Particle Motion in the Stokes' Flow

**Particle settling velocity** For low Reynolds numbers ( $R_{ep} \le 1.0$ ), the flow is known as the Stokes flow. By substituting Eqs.(6.5) and (6.6) into Eq.(6.22) and rearranging, the governing equation for a spherical particle becomes:

$$\frac{dU_p}{dt} = -\frac{18\mu}{\left(\rho_p + 0.5\rho_f\right)d^2}U_p + \left[\frac{18\mu}{\left(\rho_p + 0.5\rho_f\right)d^2}U_f - \left(\frac{\rho_p - \rho_f}{\rho_p + 0.5\rho_f}\right)g\right] \tag{6.23}$$

Integrating Eq.(6.23) and rearranging yields:

$$U_p = U_f - \frac{(\rho_p - \rho_f)g}{18\mu} d^2 + C_0 e^{-\frac{t}{\tau_v}} \tag{6.24}$$

where $\tau_v$ is called the velocity relaxation time of the motion with the dimension of time. It is given by (Rudinger, 1980; Svarovsky, 1981), but there is not the term of $0.5\rho_f$ in their expression:

$$\tau_v = \frac{(\rho_p + 0.5\rho_f)d^2}{18\mu} \tag{6.25}$$

and $C_0$ is the integration constant. It can be determined by the initial conditions that $U_p = U_{po}$ at t = 0:

$$C_0 = (U_{p0} - U_f) + \frac{(\rho_p - \rho_f)g}{18\mu} d^2 \tag{6.26}$$

Therefore the general equation of particle motion can be expressed as:

$$U_p = U_f - \frac{(\rho_p - \rho_f)g}{18\mu} d^2 + \left[ (U_{po} - U_f) + \frac{(\rho_p - \rho_f)g}{18\mu} d^2 \right] e^{-\frac{t}{\tau_v}} \tag{6.27}$$

Moreover, if we assume that $U_{po} = U_f$ at t = 0, then Eq.(6.27) can be further reduced to:

$$U_p = U_f - \frac{(\rho_p - \rho_f)g}{18\mu} d^2 + \left[ \frac{(\rho_p - \rho_f)g}{18\mu} d^2 \right] e^{-\frac{t}{\tau_v}} \tag{6.28}$$

In terms of Stokes' particle settling formula, the terminal settling velocity of a spherical particle in quiescent fluid can be expressed as:

$$U_{stoke} = \frac{(\rho_p - \rho_f)g}{18\mu} d^2 \tag{6.29}$$

Substituting Eq.(6.29) into Eq.(6.28) and rearranging gives:

$$U_p = U_f - U_{stoke} \left[ 1 - e^{-\frac{t}{\tau_v}} \right] \tag{6.30}$$

when $t \to \infty$ (actually, for sand particles with diameter of 100 micron, it takes within 0.005 seconds to approach its terminal settling velocity), the particle will reach its terminal velocity ($U_{pt}$):

$$U_{pt} = U_f - U_{stoke} \tag{6.30a}$$

Further, if $U_f = 0$, (i.e. the particle settles in the quiescent fluid), then Eq.(6.30a) reduces to the Stokes' terminal falling velocity of Eq.(6.29).

**Particle trajectory** By integrating Eq.(6.30) with respect to time t from t = 0 t = t, the particle trajectory as a function of time can be determined by:

$$Z = \left(U_f - U_{stoke}\right)t - \tau_v U_{stoke}\left[e^{-\frac{t}{\tau_v}t} - 1\right] \tag{6.31}$$

In some cases, it would be more convenient to obtain the distance (Z) as a function of particle velocity. To obtain such relationship, Eq. (6.23) can be rewritten in the following form:

$$U_p \frac{dU_p}{dZ} = -\frac{18\mu}{\left(\rho_p + 0.5\rho_f\right)d^2}U_p + \left[\frac{18\mu}{\left(\rho_p + 0.5\rho_f\right)d^2}U_f - \left(\frac{\rho_p - \rho_f}{\rho_p + 0.5\rho_f}\right)g\right] \tag{6.32}$$

Substituting Eq.(5.25) into Eq.(6.32) and rearranging gives:

$$\tau_v U_p \frac{dU_p}{dZ} = -U_p + \left(U_f - U_{stoke}\right) \tag{6.33}$$

Eq.(6.33) can be further expressed as:

$$\int_{Z_0}^{Z} dZ = \int_{U_{p0}}^{U_p} (-\tau_v) \frac{U_p}{U_p + (U_{stoke} - U_f)} dU_p \tag{6.34}$$

Integrating Eq.(6.34) yields:

$$Z - Z_0 = \tau_v \left\{ (U_{p0} - U_p) + (U_{stoke} - U_f) \ln \left[ \frac{U_p + (U_{stoke} - U_f)}{U_{p0} + (U_{stoke} - U_f)} \right] \right\} \tag{6.35}$$

If the initial condition is that $Z_0 = 0$ and $U_{p0} = U_f$ at t = 0 then the above equation becomes:

$$Z = \tau_v \left\{ (U_f - U_p) + (U_{stoke} - U_f) \ln \left[ \frac{U_p + (U_{stoke} - U_f)}{U_{stoke}} \right] \right\} \tag{6.36}$$

### 6.3.2 Particle Motion in the Transitional Flow and Turbulent Flow

Stokes' law is applied when viscosity is the controlling factor in the resistance of the fluid. For very high Reynolds numbers, the contribution of this resistance to drag is only about 5% of the total drag force. Rundinger (1980) pointed out that "the range of Reynolds number of interest in gas-particle flow rarely exceeds a few hundred". In general, the range of Reynolds number in liquid-solid flows could not be more than that of gas-particle flow. Therefore, in this section, only the intermediate range of Reynolds numbers is considered. The Morsi and Alexander's solution is used to approximate the

drag coefficient $C_D$. For a spherical particle, the general governing equation of particle motion can be described by Eq.(6.22):

$$\frac{dU_p}{dt} = \frac{3C_D}{4d}\left(\frac{\rho_f}{\rho_p + 0.5\rho_f}\right)\left(U_f - U_p\right)^2 - \left(\frac{\rho_p - \rho_f}{\rho_p + 0.5\rho_f}\right)g \tag{6.22}$$

In the intermediate range of Reynolds numbers, the drag coefficient $C_D$ can be estimated with the formula proposed by Moris & Alexander (1972):

$$C_D = \frac{K_1}{R_{ep}} + \frac{K_2}{R_{ep}^2} + K_3 \tag{6.10}$$

Substituting Eqs.(6.10) and (6.5) into Eq.(6.22) and rearranging gives:

$$\frac{dU_p}{dt} = A_I U_p^2 - B_I U_p + C_I \tag{6.37}$$

in which

$$A_I = \left(\frac{3}{4d}\right)\left(\frac{\rho_f}{\rho_p + 0.5\rho_f}\right)K_3 \tag{6.37a}$$

$$B_I = \left(\frac{3}{4d}\right)\left(\frac{\rho_f}{\rho_p + 0.5\rho_f}\right)\left(2K_3 U_f + \frac{K_1\mu}{\rho_f d}\right) \tag{6.37b}$$

$$C_I = \left(\frac{3}{4d}\right)\left(\frac{\rho_f}{\rho_p + 0.5\rho_f}\right)\left[K_3 U_f^2 + \left(\frac{K_1 \mu}{\rho_f d}\right)U_f + \frac{K_2 \mu^2}{\rho_f^2 d^2}\right] - \left(\frac{\rho_p - \rho_f}{\rho_p + 0.5\rho_f}\right)g \qquad (6.37c)$$

This is a Riccati equation with constant coefficient. To solve this equation, a mathematical method presented by Morsi and Alexander (1972) is followed. Then Eq.(6.37) can be further written as the following form:

$$\frac{dU_p}{(U_p - \eta_1)(U_p - \eta_2)} = A_I \, dt \qquad (6.38)$$

where $\eta_1$ and $\eta_2$ are the roots of the right hand side of Eq.(6.37) which are as follows:

$$\eta_{1,2} = \left(\frac{B_I}{2A_I}\right) \pm \sqrt{\left(\frac{B_I}{2A_I}\right)^2 - \left(\frac{C_I}{A_I}\right)} \qquad (6.38a)$$

**Case I for $\eta_1 = \eta_2$**

**Particle settling velocity** If the roots of $\eta_1$ and $\eta_2$ are identical, then the general solution of Eq. (6.38) can be written as follows:

$$U_p = \eta_1 + \left[\frac{U_{p0} - \eta_1}{1 - A_I(t - t_0)(U_{p0} - \eta_1)}\right] \qquad (6.39)$$

If we further assume that $U_{po} = U_f$ at $t_o = 0$, then the above equation becomes:

$$U_p = \eta_1 + \left[ \frac{U_f - \eta_1}{1 - A_I \left( U_f - \eta_1 \right) t} \right] \tag{6.39a}$$

**Particle trajectory** The distance of particle motion as a function of time can be obtained by integrating Eq.(6.39a):

$$Z = \eta_1 t - \frac{1}{A_I} \ln \left[ 1 - A_I \left( U_f - \eta_1 \right) t \right] \tag{6.40}$$

In order to obtain the distance as a function of particle velocity, Eq.(6.38) for the case of $\eta_1 = \eta_2$ can be expressed as:

$$\frac{U_p}{\left( U_p - \eta_1 \right)^2} dU_p = A_I \, dz \tag{6.41}$$

Integrating Eq.(6.41) and rearranging yields:

$$Z - Z_0 = \frac{1}{A_I} \left\{ \ln \left[ \frac{U_p - \eta_1}{U_{p0} - \eta_1} \right] - \frac{\eta_1 \left( U_{p0} - U_p \right)}{\left( U_p - \eta_1 \right) \left( U_{p0} - \eta_1 \right)} \right\} \tag{6.42}$$

If the initial conditions are that $U_{po} = U_f$ and $Z_0 = 0$ at $t_o = 0$, then Eq.(6.42) becomes:

$$Z = \frac{1}{A_I}\left\{\ln\left[\frac{U_p - \eta_1}{U_f - \eta_1}\right] - \frac{\eta_1\left(U_f - U_p\right)}{\left(U_p - \eta_1\right)\left(U_f - \eta_1\right)}\right\} \tag{6.43}$$

**Case II for** $\eta_1 \neq \eta_2$

**Particle settling velocity** If the roots of $\eta_1$ and $\eta_2$ are not identical, then the general form of the solution for Eq.(6.38) is as follows:

$$U_p = \frac{\eta_1\left(U_{p0} - \eta_2\right) - \eta_2\left(U_{p0} - \eta_1\right)e^{A_I(\eta_1 - \eta_2)(t - t_0)}}{\left(U_{p0} - \eta_2\right) - \left(U_{p0} - \eta_1\right)e^{A_I(\eta_1 - \eta_2)(t - t_0)}} \tag{6.44}$$

Moreover, if we further assume that $U_{po} = U_f$ at $t_o = 0$, then the above equation becomes:

$$U_p = \frac{\eta_1\left(U_f - \eta_2\right)e^{-A_I(\eta_1 - \eta_2)t} - \eta_2\left(U_f - \eta_1\right)}{\left(U_f - \eta_2\right)e^{-A_I(\eta_1 - \eta_2)t} - \left(U_f - \eta_1\right)} \tag{6.44a}$$

In terms of Eq.(6.44a), when $t \to \infty$, the particle will reach its terminal velocity ($U_{pt}$):

$$U_{pt} = \eta_2 = \left(\frac{B_I}{2A_I}\right) - \sqrt{\left(\frac{B_I}{2A_I}\right)^2 - \left(\frac{C_I}{A_I}\right)} \tag{6.45}$$

Substituting $A_I$, $B_I$ and $C_I$ into the above equation and rearranging gives:

$$U_{pt} = U_f + \left(\frac{K_1}{2K_3}\right)\left(\frac{\mu}{\rho_f d}\right) - \sqrt{\left[\left(\frac{K_1}{2K_3}\right)^2 - \frac{K_2}{K_3}\right]\left(\frac{\mu}{\rho_f d}\right)^2 + \frac{4gd}{3K_3}\left(\frac{\rho_p}{\rho_f} - 1\right)} \qquad (6.45a)$$

By setting $U_f = 0$ and changing the sign of Eq.(6.45a), the terminal settling velocity in the quiescent fluid can be expressed as:

$$U_{pt} = \sqrt{\left[\left(\frac{K_1}{2K_3}\right)^2 - \frac{K_2}{K_3}\right]\left(\frac{\mu}{\rho_f d}\right)^2 + \frac{4gd}{3K_3}\left(\frac{\rho_p}{\rho_f} - 1\right)} - \left(\frac{K_1}{2K_3}\right)\left(\frac{\mu}{\rho_f d}\right) \qquad (6.46)$$

**Particle trajectory** The distance of particle motion as a function of time can be determined by integrating Eq.(6.44a) with time (t):

$$z = \eta_2\, t - \frac{1}{A_I}\ln\left[\frac{\left(U_f - \eta_2\right)e^{-A_I(\eta_{I1}-\eta_2)t} - \left(U_f - \eta_1\right)}{\eta_1 - \eta_2}\right] \qquad (6.47)$$

Similarly, in order to obtain the distance of particle motion as a function of particle velocity, Eq.(6.38) can be expressed as the following form:

$$\frac{U_p}{\left(U_p - \eta_1\right)\left(U_p - \eta_2\right)} dU_p = A_I\, dz \qquad (6.48)$$

Integrating Eq.(6.48) and rearranging yields:

$$Z - Z_0 = \frac{1}{A_I(\eta_1 - \eta_2)}\left\{\eta_1 \ln\left[\frac{U_p - \eta_1}{U_{p0} - \eta_1}\right] - \eta_2 \ln\left[\frac{U_p - \eta_2}{U_{p0} - \eta_2}\right]\right\} \tag{6.49}$$

Similarly, if the initial conditions are that $U_{po} = U_f$ and $Z_0 = 0$ at $t_o = 0$, then the above equation reduces to:

$$Z = \frac{1}{A_I(\eta_1 - \eta_2)}\left\{\eta_1 \ln\left[\frac{U_p - \eta_1}{U_f - \eta_1}\right] - \eta_2 \ln\left[\frac{U_p - \eta_2}{U_f - \eta_2}\right]\right\} \tag{6.49a}$$

## 6.4 Result Analysis and Discussions

### 6.4.1 Terminal Settling Velocity in Quiescent Fluids

#### 6.4.1.1 Particle motion in the Stokes' flow

For a spherical particle with a Reynolds number of $R_{ep} \le 1$, viscous resistance is the main influence on particle motion. The particle settling velocity derived in this study is same as Stokes' formula (Eq.(6.29)). It is reproduced in the present notation as follows:

$$U_{sphere} = \frac{(\rho_p - \rho_f)g}{18\mu} d^2 \tag{6.50}$$

#### 6.4.1.2 Particle motion in the transitional and turbulent Flow

In the transitional and turbulent flow, the terminal settling velocity for a spherical particle can be determined with Eq.(6.46).

$$U_{pt} = \sqrt{\left[\left(\frac{K_1}{2K_3}\right)^2 - \frac{K_2}{K_3}\right]\left(\frac{\mu}{\rho_f d}\right)^2 + \frac{4gd}{3K_3}\left(\frac{\rho_p}{\rho_f} - 1\right)} - \left(\frac{K_1}{2K_3}\right)\left(\frac{\mu}{\rho_f d}\right) \qquad (6.46)$$

The constants of $K_1$, $K_2$ and $K_3$ can be determined with Table 6.2 which obtained by Moris and Alexander (1972) by fitting the drag coefficient curve. In terms of the range of Reynolds numbers, the simple form of the terminal settling velocity formula can be derived by substituting the values of $K_1$, $K_2$ and $K_3$ into Eq.(6.46). They are as follows:

**(1) For** $1 \prec \mathrm{R}_{ep} \leq 10$

In the range of Reynolds number $1 \prec R_{ep} \leq 10$, the constants of $K_1$, $K_2$ and $K_3$ are 29.167, -3.889, and 1.222 respectively (see Table 6.2). By substituting these values into Eq.(6.46) and rearranging, the terminal settling velocity for spherical particles ($U_{sphere}$) can be expressed as:

$$U_{spheret} = \sqrt{145.61\left(\frac{\nu}{d}\right)^2 + 1.09\,g\left(\frac{\rho_p}{\rho_f} - 1\right)d} - 11.93\left(\frac{\nu}{d}\right) \qquad (6.51)$$

**(2) For** $10 \prec \mathrm{R}_{ep} \leq 100$

For Reynolds number in the range of $10 \prec R_{ep} \leq 100$, the values of $K_1$, $K_2$ and $K_3$ are 46.500, -116.67, and 0.617 respectively (see Table 6.2). Substituting these values into Eq.(6.46) and rearranging gives:

$$U_{spheret} = \sqrt{1609.05\left(\frac{\nu}{d}\right)^2 + 2.16\,g\left(\frac{\rho_p}{\rho_f} - 1\right)d} - 37.68\left(\frac{\nu}{d}\right) \tag{6.52}$$

**(3) For** $100 \prec \mathrm{R}_{ep} \leq 1000$

Similarly, in the range of Reynolds number of $100 \prec R_{ep} \leq 1000$, the values of $K_1$, $K_2$ and $K_3$ are 98.33, -2778.0, and 0.3644 respectively (see Table 6.2). Substituting them into Eq.(6.46) and rearranging yields:

$$U_{spheret} = \sqrt{25827.01\left(\frac{\nu}{d}\right)^2 + 3.66\,g\left(\frac{\rho_p}{\rho_f} - 1\right)d} - 134.92\left(\frac{\nu}{d}\right) \tag{6.53}$$

As stated in Section 6.3.2, the range of Reynolds number in liquid-solid flows rarely exceeds a few hundred, and thus the above ranges of Reynolds number could cover the common applied ranges in liquid-solid separation systems. For Reynolds numbers greater than 1000, the same approaches can be followed to get the solution.

### 6.4.2 Determination of Particle Limits

#### 6.4.2.1 Particle size limits in an upward uniform steady fluid flow (water)

As the particle terminal settling velocity formulae are derived based on the different ranges of Reynolds numbers; the Reynolds number must be known. Therefore, for practical purpose it is necessary to show the range of the Reynolds numbers which correspond to the equivalent particle sizes. As the Reynolds number is a function of the relative particle settling velocity, particle diameter, fluid viscosity, and fluid density, for a given range of Reynolds number and a given constant upward fluid velocity ( $U_f$ ) there must have a relative range of particle sizes to match it. Assuming that the range of Reynolds number is $R_1 \le R_{ep} \prec R_2$, then following relationship can be obtained:

$$R_1 \le \frac{\rho_f \left| U_f - U_p \right| d}{\mu} \prec R_2 \tag{6.54}$$

By substituting the particle terminal settling velocity formulae of Eqs.(6.50), (6.51), (6.52) and (6.53) into Eq.(6.54) respectively, the corresponding ranges of particle sizes can be determined for each range of Reynolds number. Tables 6.2 to 6.5 show the calculated particle size limits for spherical sand particles based on different ranges of Reynolds numbers and various fluid velocities.

Table 6.2 shows the calculated upper limit of spherical sand particle sizes in the Stokes' flow. The first row is the upward fluid (water) velocity ($U_f$). The second row is the calculated particle terminal velocity in still water with Stokes formula; while the third row is the calculated upper limit of spherical sand particle size in the Stokes' flow for various upward fluid velocities. This table indicates that the upper limit of particle size

**Table 6.2 Upper Limit of Spherical Sand Particles for** $R_{ep} \leq 1.0$

| $U_f$ (mm/sec) | 0.0 | 5.0 | 10.0 | 15.0 | 20.0 | 25.0 | 50.0 | 100.0 |
|---|---|---|---|---|---|---|---|---|
| $U_{sphere}$ (mm/s)* | 9.7 | 6.6 | 4.4 | 2.8 | 1.9 | 1.3 | 0.4 | 0.1 |
| $d_{max}$ (μm) | 104 | 86 | 70 | 56 | 46 | 38 | 20 | 10 |
| Rep | 1.0 | 1.0 | 1.0 | 1.0 | 1.0 | 1.0 | 1.0 | 1.0 |

(* Obtained by Eq.(6.50) based on $T = 20^o c$ )

**Table 6.3 Upper Limits of Sand Spheres for** $1.0 \prec R_{ep} \leq 10.0$

| $U_f$ (mm/sec) | 0.0 | 5.0 | 10.0 | 15.0 | 20.0 | 25.0 | 50.0 | 100.0 |
|---|---|---|---|---|---|---|---|---|
| $U_{sphere}$ (mm/s)* | 37.5 | 34.7 | 32.1 | 29.6 | 27.3 | 25.0 | 16.2 | 7.6 |
| $d_{max}$ (micron) | 267 | 252 | 238 | 225 | 212 | 200 | 151 | 93 |
| $R_{ep}$ | 10.0 | 10.0 | 10.0 | 10.0 | 10.0 | 10.0 | 10.0 | 10.0 |

(* Obtained by Eq.(6.51) based on $T = 20^o c$ )

**Table 6.4 Upper Limits of Sand Spheres for** $10.0 \prec R_{ep} \leq 100.0$

| $U_f$ (mm/sec) | 0.0 | 5.0 | 10.0 | 15.0 | 20.0 | 25.0 | 50.0 | 100.0 |
|---|---|---|---|---|---|---|---|---|
| $U_{sphere}$ (mm/s)* | 126.4 | 124.1 | 121.8 | 119.5 | 117.3 | 115.1 | 104.6 | 86.1 |
| $d_{max}$ (micron) | 793 | 776 | 760 | 745 | 730 | 715 | 648 | 538 |
| $R_{ep}$ | 100.0 | 100.0 | 100.0 | 100.0 | 100.0 | 100.0 | 100.0 | 100.0 |

(* Obtained by Eq.(6.52) based on $T = 20^o c$ )

**Table 6.5 Upper Limit of Sand Spheres for** $100.0 \prec R_{ep} \leq 1000.0$

| $U_f$ (mm/sec) | 0.0 | 5.0 | 10.0 | 15.0 | 20.0 | 25.0 | 50.0 | 100.0 |
|---|---|---|---|---|---|---|---|---|
| $U_{sphere}$ (mm/s)* | 360.9 | 358.9 | 356.9 | 355.0 | 353.0 | 351.1 | 341.5 | 323.4 |
| $d_{max}$ (micron) | 2776 | 2753 | 2731 | 2708 | 2686 | 2664 | 2559 | 2367 |
| $R_{ep}$ | 1000.0 | 1000.0 | 1000.0 | 1000.0 | 1000.0 | 1000.0 | 1000.0 | 1000.0 |

(* Obtained by Eq.(6.53) based on $T = 20^o c$ )

decreases with increasing upward fluid velocity ($U_f$). However, for $U_f = 0.0$ (quiescent water), the Stokes' formula could be applied to the particle sizes up to 100 micron.

Tables 6.3 to 6.5 show the calculated upper limits for spherical sand particles in the transitional flow. These tables indicate that the upper limits increase with an increasing Reynolds number. In the still water ($U_f = 0.0$), the upper limits of particle sizes also increase with an increasing Reynolds number.

Figure 6.2, which was a plot of Eq.(6.54) coupled with Eqs.(6.50), (6.51), (6.52), and (6.53), shows the predicted upper and lower limits for spherical sand particles in the Stokes' flow and the transitional flow. The horizontal axis represents the upward constant fluid (water) velocity ($U_f$); while the vertical axis represents the size of the spherical sand particle (d). This figure indicates that in the Stokes flow (i.e., $R_{ep} < 1.0$) the predicted particle limits decreases with increasing the fluid velocity ($U_f$); while over this range (i.e., in the ranges of $1 < R_{ep} < 10$, $10 < R_{ep} < 100$, and $100 < R_{ep} < 1000$) the predicted particle limits for each range of Reynolds number increase with increasing the fluid velocity ($U_f$). However, when the Reynolds number is greater than 100, the effect of increasing fluid velocity on the particle size limits is small.

This figure graphically shows the relationship between the upper and lower limits of particle sizes, ranges of Reynolds numbers, and the upward constant fluid velocity. For a given fluid velocity of $U_f$ and a particle size, the range of Reynolds numbers under the given conditions can quickly be determined with this figure. In terms of the range of Reynolds numbers, the particle settling velocity formula, which would be used to calculate the particle settling velocity, can easily be determined.

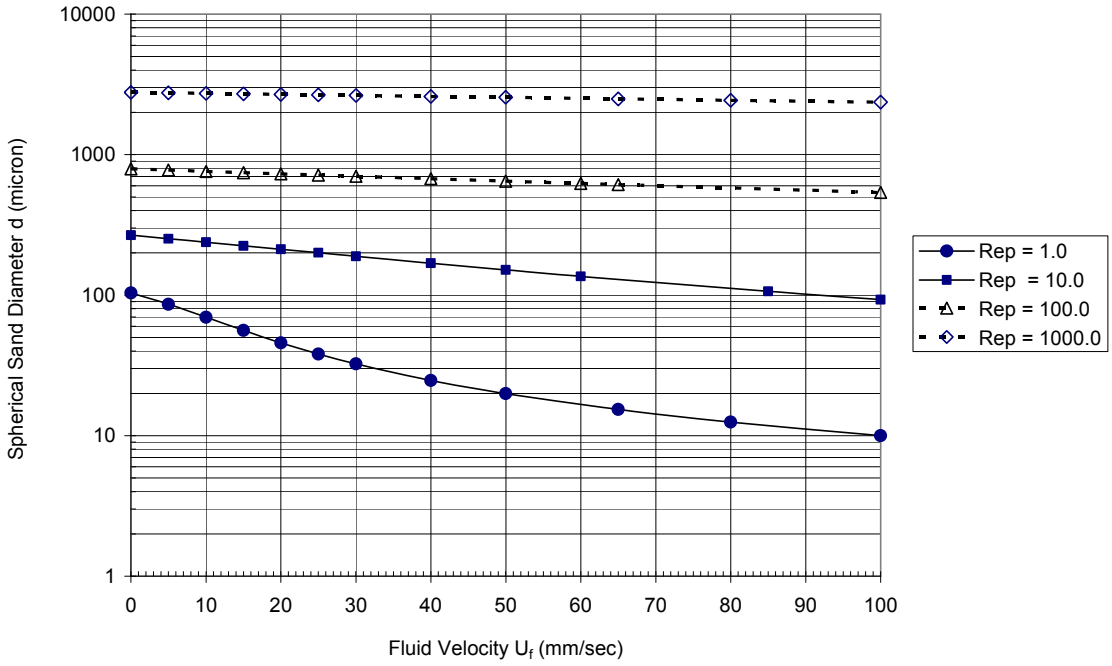


Fig. 6.2 Predicted Limits of Sapherical Sand Particle in an Upward Uniforrm Steady Fluid Flow (water)

### 6.4.2.2 Particle size limits in quiescent water

In the second columns (with $U_f = 0.0$) of Tables 6.3 to 6.6, we can find that for spherical sand particles settling in quiescent water, the following relationships are true:

$$R_{ep} \le 1.0 \quad \Leftrightarrow \quad d \le 104\,\mu m \tag{6.54a}$$

$$1.0 \prec R_{ep} \le 10.0 \quad \Leftrightarrow \quad 104 \prec d \le 267\,\mu m \tag{6.54b}$$

$$10.0 \prec R_{ep} \le 100.0 \quad \Leftrightarrow \quad 267 \prec d \le 793\,\mu m \tag{6.54c}$$

$$100.0 \prec R_{ep} \le 1000.0 \quad \Leftrightarrow \quad 793 \prec d \le 2780\,\mu m \tag{6.54d}$$

Therefore, by means of these equivalent relationships, the conditions for Eqs.(6.50), (6.51), (6.52), and (6.53) can be rewritten as follows:

If $d \le 104$ μm**:**
$$U_{sphere} = \frac{(\rho_p - \rho_f)g}{18\mu} d^2 \tag{6.50}$$

If $104 \le d < 267$ μm:
$$U_{spheret} = \sqrt{145.61\left(\frac{\nu}{d}\right)^2 + 1.09\,g\left(\frac{\rho_p}{\rho_f} - 1\right)d} - 11.93\left(\frac{\nu}{d}\right) \tag{6.51}$$

If $267 \le d < 793$ μm:
$$U_{spheret} = \sqrt{25827.01\left(\frac{\nu}{d}\right)^2 + 3.66\,g\left(\frac{\rho_p}{\rho_f} - 1\right)d} - 134.92\left(\frac{\nu}{d}\right) \tag{6.52}$$

If $793 \le d < 2776$ μm:
$$U_{spheret} = \sqrt{25827.01\left(\frac{\nu}{d}\right)^2 + 3.66\,g\left(\frac{\rho_p}{\rho_f} - 1\right)d} - 134.92\left(\frac{\nu}{d}\right) \tag{6.53}$$

### 6.4.3 Comparison of this Study with Cheng's Formula

#### 6.4.3.1 Stokes' flow

Cheng (1997) proposed a general formula to predict the terminal settling velocity of natural sediment particles in the present notation:

$$U_{natural} = \frac{\nu}{d}\left\{\sqrt{25 + 1.2\left[\left(\frac{\rho_p}{\rho_f} - 1\right)\frac{g}{\nu^2}\right]^{2/3} d^2} - 5\right\}^{1.5} \tag{6.55}$$

This formula can be applied to a wide range of Reynolds numbers from the Stokes flow to the turbulent regime. Figure 6.3a shows the predicted terminal settling velocities for the spherical sand particles in a quiescent water with Stokes's formula of Eq. (6.29) Cheng's formula of Eq.(6.55). This figure indicates that the results derived from Cheng's formula are far lower (about 25-30%) than that from Stoke' formula. This is because, Cheng's formula was developed for predicting the terminal settling velocity of natural sediment particles instead of the spherical particles. Unfortunately, Cheng's formula does not explicitly account for the value of shape factor. Therefore, if Chen's formula is used to predict the settling velocity of spherical particles, it should be corrected by a shape factor. For natural sand particles the average shape factor is approximately 0.7 (Graf, 1971; Van Rijin, 1993; Jimenez and Madsen, 2003). Here a shape factor of 0.71 is applied to Cheng's original formula. By dividing Cheng's original formula by a shape factor of 0.71, then Cheng's terminal settling velocity for spherical particles can be expressed as follows:

$$U_{sphere} = \left(\frac{1}{0.71}\right)\left(\frac{\nu}{d}\right)\left\{\sqrt{25 + 1.2\left[\left(\frac{\rho_p}{\rho_f} - 1\right)\frac{g}{\nu^2}\right]^{2/3} d^2} - 5\right\}^{1.5} \tag{6.55a}$$

Fig.6.3b shows the comparison of the results derived from Stokes's formula and Cheng's modified formula (i.e., Eq.(6.55a)). This figure indicates that the predicted results from Cheng's modified formula have a good agreement with that from Stokes' formula (i.e., Eq. (6.50). The maximum percent difference between them is about 5.4 %.

On the contrary, if Stokes' formula is used to predict the terminal settling velocity of natural sediment particles, it must be corrected with a shape factor of 0.71 as follows:

$$U_{natural} = (0.71)\frac{(\rho_p - \rho_f)g}{18\mu} d^2 \tag{6.50a}$$

Fig.6.3c shows the comparison of the results for natural sediment particles derived from Stokes' modified formula (i.e., Eq.(6.50a)) and Cheng's original formula (i.e., Eq.(6.55)). This comparison indicates that the predicted results from Stokes' modified formula agree with Cheng's formula. This analysis reveals that the Stokes' formula can not be directly applied to predict the terminal settling velocities of natural sediment particles even in the range of Stokes flow.

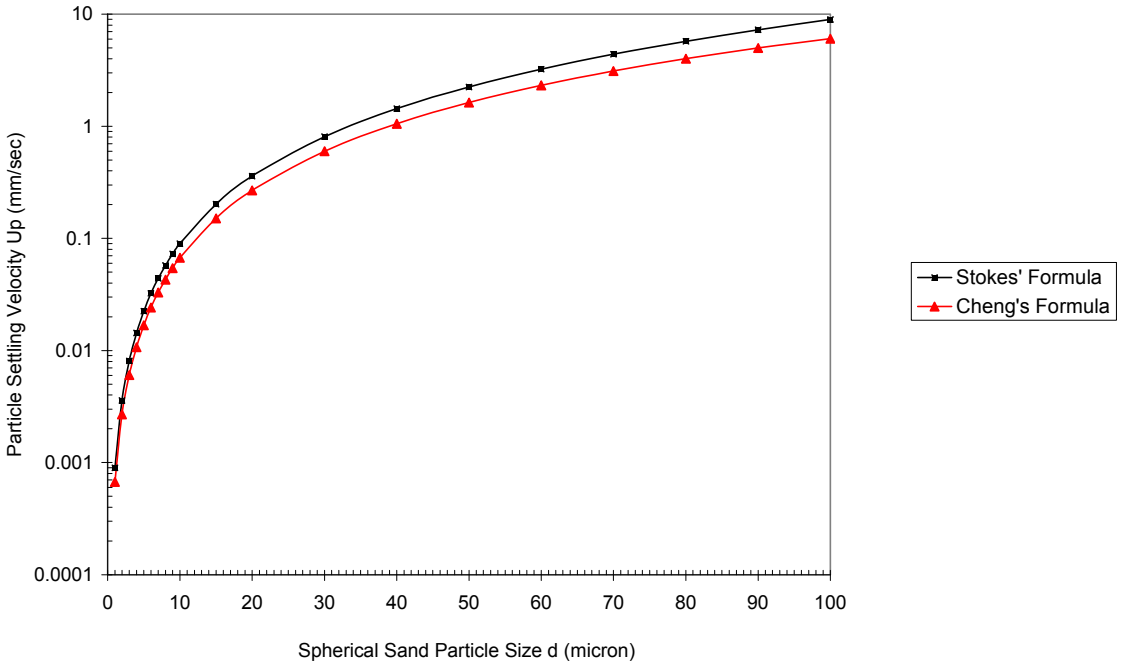


Figure 6.3a Comparison of the Predicted Results Derived from Stokes' Formula and Cheng's Formula for Spherical Sand particles in the Stokes Flow.

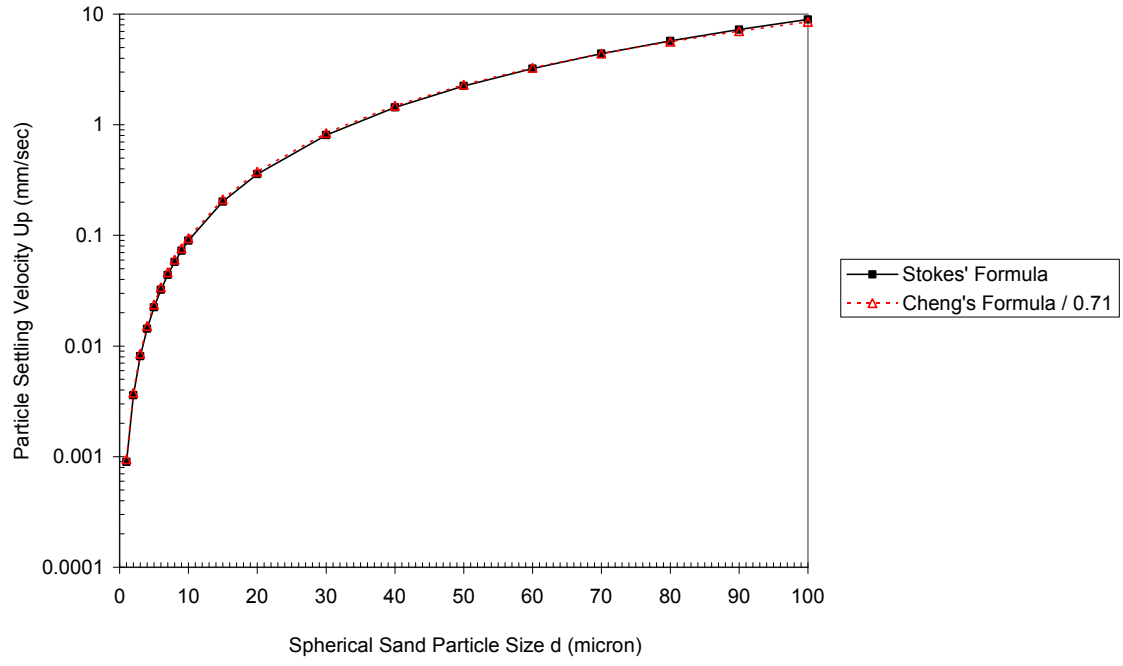


Figure 6.3b Comparison of the Predicted Results Derived from Stokes' Formula and Cheng's Modified Formula for Spherical Sand Particles in the Stokes Flow.

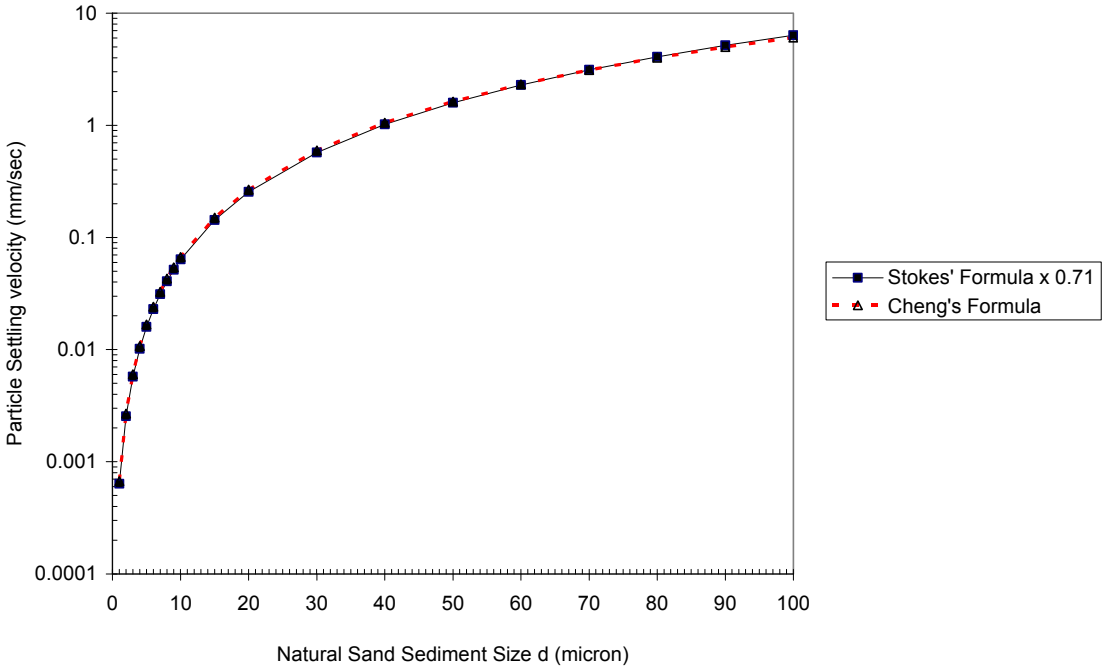


Fig.6.3c Comparison of the Predicted Results Derived from Stokes' Modified Formua and Cheng's Formula for Natural Sediment Particles in the Stokes Flow

### 6.4.3.2 Transitional flows

As the terminal settling velocity formulae derived in this study are based on the spherical particles, they must also be corrected by a shape factor prior to predicting the terminal settling velocity of natural sediment particles. Similar to the last section, here a shape factor of 0.75 is applied to Eq.(6.51). Then Eq.(6.51) becomes:

$$U_{natural} = 0.75\left\{\sqrt{145.61\left(\frac{\nu}{d}\right)^2 + 1.09\,g\left(\frac{\rho_p}{\rho_f} - 1\right)d} - 11.93\left(\frac{\nu}{d}\right)\right\} \tag{6.51a}$$

Fig. 6.4 shows the comparison of the predicted results obtained from Eq.(6.51a) and Cheng's formula for natural sediment particles with diameters ranging from 100 micron to 300 micron. This figure indicates that the predicted results from Eq.(6.51a) agree with that from Cheng's formula. The maximum percent difference between the two equations is about 4 %. Therefore, Eq.(6.51a) could be used to predict the terminal settling velocity of natural sediment particles with a particle size in the range of d = 100 to 300 microns.

Similarly, if Eq.(6.52) is used to predict the terminal settling velocity of natural sediment particles, it must be corrected by a shape factor. By multiplying it by a shape factor of 0.76, Eq.(6.52) becomes:

$$U_{natural} = 0.76\left\{\sqrt{25827.01\left(\frac{\nu}{d}\right)^2 + 3.66\,g\left(\frac{\rho_p}{\rho_f} - 1\right)d} - 134.92\left(\frac{\nu}{d}\right)\right\} \tag{6.52a}$$

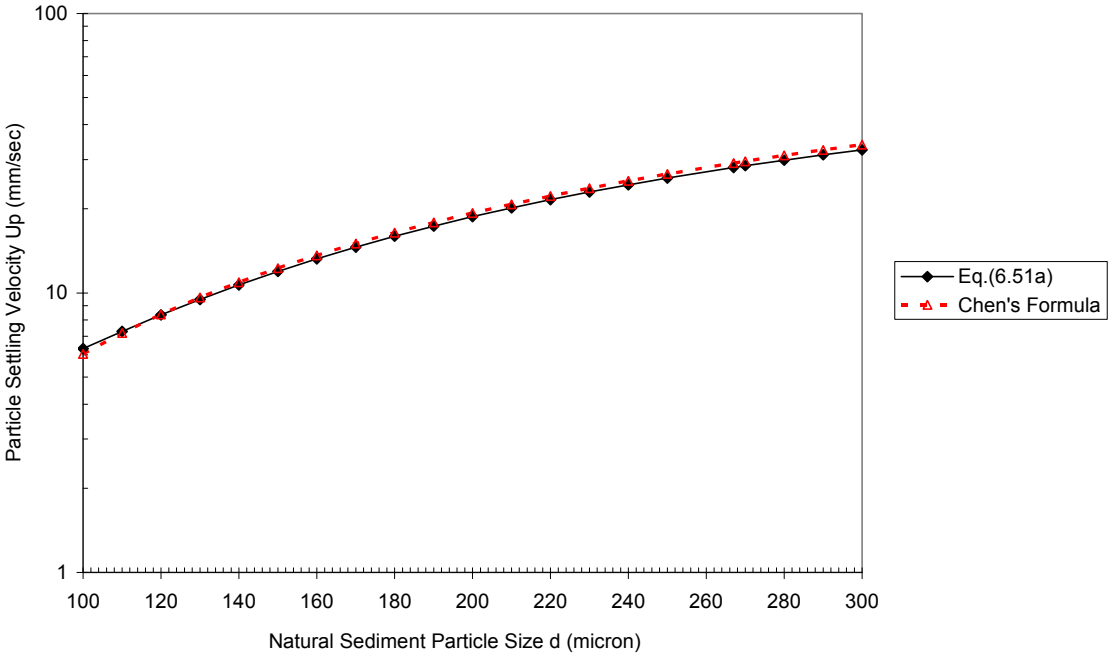


Figure 6.4 Comparison of Predicted Results for Natural Sediment Particiles Ranging from 100 to 300 micron

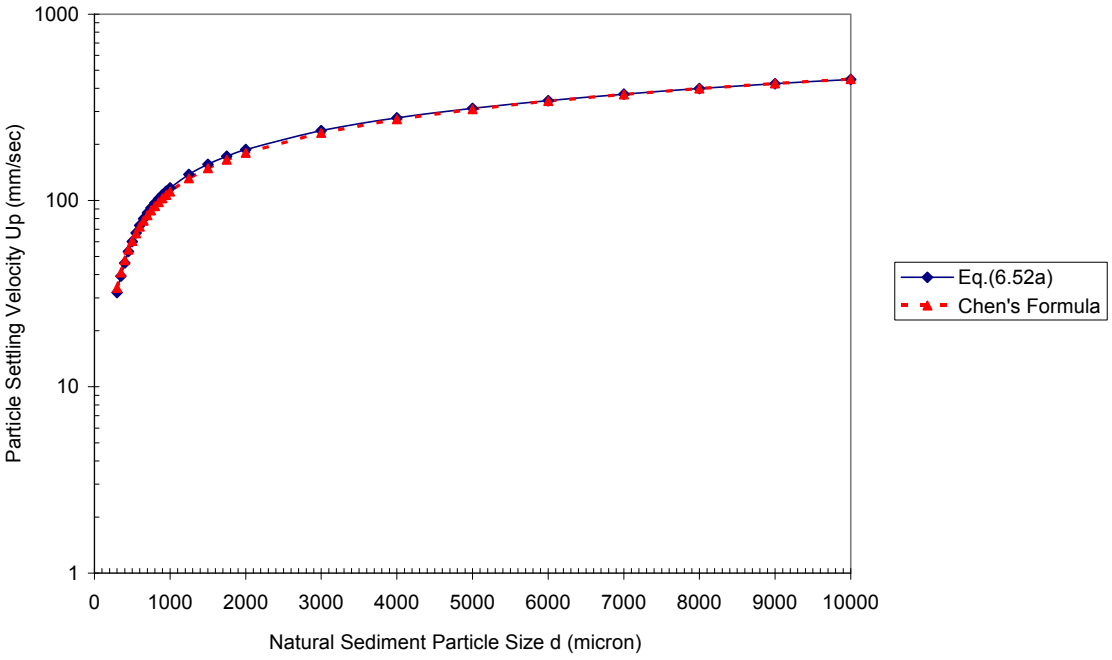


Figure 6.5 Comparison of Predicted Results for Natural Sediment Particiles with Diameters Larger than 300 micron

Fig. 6.5 shows the comparison of the predicted results obtained from Eq.(6.52a) and Cheng's formula for natural sediment particles with diameters larger than 300 microns. This figure indicates that the predicted results from Eq.(6.52a) agree with that from Cheng's formula. Comparison reveals that the maximum percent difference between both of them is about 5 %. Therefore, Eq.(6.52a) could be applied to predict the terminal settling velocities for natural sediment particles with diameters grater than 300 microns.

#### 6.4.3.3 Summary of terminal settling velocity formulae proposed by this study

In terms of the above analysis, the following equations derived in this study are suggested to predict the terminal settling velocity for spherical sand particles and natural sediment particles in the quiescent fluid.

**Spherical Sand Particles:**

For $d \le 100\mu m$,

$$U_{sphere} = \frac{(\rho_p - \rho_f)g}{18\mu} d^2 \tag{6.50}$$

For $100\mu m \prec d \le 270\mu m$,

$$U_{spheret} = \sqrt{145.61\left(\frac{\nu}{d}\right)^2 + 1.09\, g\left(\frac{\rho_p}{\rho_f} - 1\right)d} - 11.93\left(\frac{\nu}{d}\right) \tag{6.51}$$

For $270\mu m \prec d \le 790\mu m$,

$$U_{spheret} = \sqrt{25827.01\left(\frac{\nu}{d}\right)^2 + 3.66\,g\left(\frac{\rho_p}{\rho_f} - 1\right)d} - 134.92\left(\frac{\nu}{d}\right) \tag{6.52}$$

For $790\mu m \prec d \leq 2770\mu m$,

$$U_{spheret} = \sqrt{25827.01\left(\frac{\nu}{d}\right)^2 + 3.66\,g\left(\frac{\rho_p}{\rho_f} - 1\right)d} - 134.92\left(\frac{\nu}{d}\right) \tag{6.53}$$

**Natural Sediment Particles:**

For $d \leq 100\mu m$:

$$U_{natural} = (0.71)\frac{(\rho_p - \rho_f)g}{18\mu}d^2 \tag{6.50a}$$

For $100\mu m \prec d \leq 300\mu m$,

$$U_{natural} = 0.75\left\{\sqrt{145.61\left(\frac{\nu}{d}\right)^2 + 1.09\,g\left(\frac{\rho_p}{\rho_f} - 1\right)d} - 11.93\left(\frac{\nu}{d}\right)\right\} \tag{6.51a}$$

For $d \succ 300\mu m$:

$$U_{natural} = 0.76\left\{\sqrt{25827.01\left(\frac{\nu}{d}\right)^2 + 3.66\,g\left(\frac{\rho_p}{\rho_f} - 1\right)d} - 134.92\left(\frac{\nu}{d}\right)\right\} \tag{6.52a}$$

### 6.4.4 Response of Particle Motion in One-Dimensional Upward Uniform Steady Fluid Flow

In this section the response of a spherical particle to a one-dimensional upward uniform steady fluid (water) flow is investigated. In practice, the range of Reynolds numbers in liquid-solid flow rarely exceed a few hundred, the particle motion in only the Stokes' and transitional flow are investigated in the present study.

#### 6.4.4.1 Particle motion in the Stokes flow

In the Stokes' flow, the particle velocity and trajectory in a one-dimensional upward uniform steady flow can be described by Eqs.(6.30) and (6.31):

$$U_p = U_f - U_{stoke}\left[1 - e^{-\frac{t}{\tau_v}}\right] \tag{6.30}$$

$$Z = \left(U_f - U_{stoke}\right)t - \tau_v U_{stoke}\left[e^{-\frac{t}{\tau_v}t} - 1\right] \tag{6.31}$$

in which

$$\tau_v = \frac{\left(\rho_p + 0.5\rho_f\right)d^2}{18\mu} \tag{6.25}$$

$$U_{stoke} = \frac{\left(\rho_p - \rho_f\right)g}{18\mu}d^2 \tag{6.29}$$

According to Table 6.2, for a given upward uniform steady fluid flow (water) with $U_f$ = 5.0 mm/sec and under the condition of $R_{ep} \le 1.0$, the upper size limit of sand spheres is 86 micron. Over this limit, the Stokes' law no longer holds.

Figure 6.6a shows the variation of the predicted particle velocities with time in an upward steady uniform fluid flow (water) with $U_f$ = 5.0 mm/sec. The vertical axis represents the predicted velocity of particle motion in the vertical direction; while the horizontal axis represents the time at time t. This figure indicates that the unsteady state of the particles motion is very short. For particles with diameters ranging from d = 50 to 85 microns, the time required to reach their terminal velocity range from 5 to 10 milliseconds. After this time range, particles with diameters less than 74.6 microns will move steadily upward in the fluid; while particles with diameters greater than that of 74.63 microns will move steadily downwards to settle. However, particles with the diameters close to 74.63 microns will be suspended in the fluid flowfield.

Figure 6.6b shows the predicted particle trajectories in an upward uniform steady fluid flow (water) with $U_f$ = 5.0 mm/sec. The vertical axis represents the predicted distance (Z) of particles traveled at time (t) in the vertical direction; while the horizontal axis represents the time of the particles traveled in the fluid flowfield. This figure indicates that particles with diameters less than the critical diameter of 74.68 microns will move directly upward; while particles with diameters greater than that of 74.68 microns will move first upward with a very short distance (within several microns, except for particle sizes close to the critical diameter of 74.63 microns), then move downward to the bottom to settle.

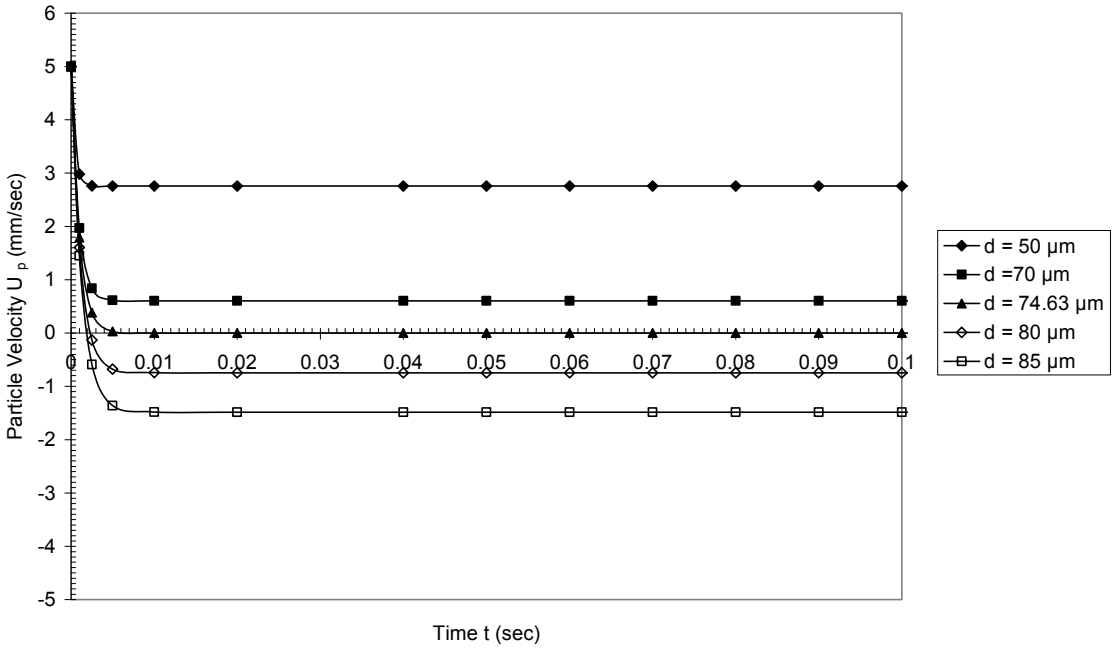


Figure 6.6a Particle Velocity in an Upward Uniform Steady Fluid (water) Flow with $U_f$ = 5.0 mm/sec Based on Rep < 1.0.

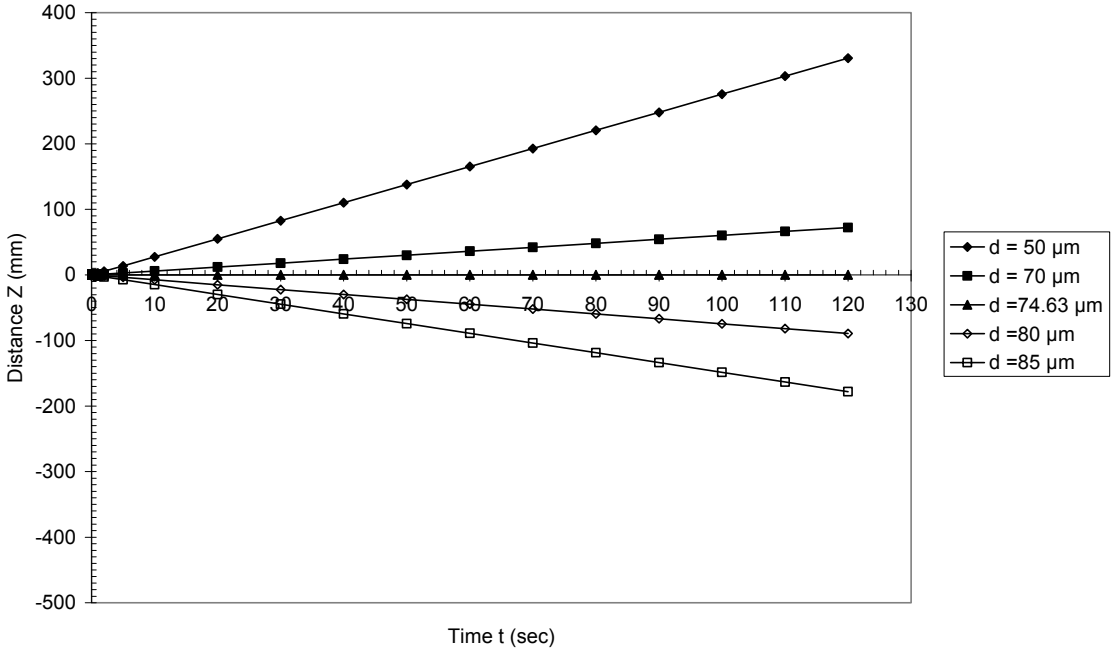


Figure 6.6b Particle Trajectory in an Upward Uniform Steady Fluid (water) Flow with with $U_f$ = 5.0 mm/sec Based on Rep < 1.0

#### 6.4.4.2 Particle motion in the intermediate Reynolds number range

In the intermediate range of Reynolds numbers, the Stokes drag law no longer holds. For spherical sand particles moving in a given upward uniform steady fluid flow, the particle motion in the intermediate range of Reynolds number can be described by Eqs.(6.44a) and (6.47):

$$U_p = \frac{\eta_{I1}\left(U_f - \eta_{I2}\right) - \eta_{I2}\left(U_f - \eta_{I1}\right) e^{A_I(\eta_{I1}-\eta_{I2})t}}{\left(U_f - \eta_{I2}\right) - \left(U_f - \eta_{I1}\right) e^{A_I(\eta_{I1}-\eta_{I2})t}} \tag{6.44a}$$

$$z = \eta_{I2}\, t - \frac{1}{A_I} \ln\left[\frac{\left(U_f - \eta_{I2}\right) e^{-A_I(\eta_{I1}-\eta_{I2})t} - \left(U_f - \eta_{I1}\right)}{\eta_{I1} - \eta_{I2}}\right] \tag{6.47}$$

in which

$$\eta_{I1,2} = \left(\frac{B_I}{2A_I}\right) \pm \sqrt{\left(\frac{B_I}{2A_I}\right)^2 - \left(\frac{C_I}{A_I}\right)} \tag{6.38a}$$

$$A_I = \left(\frac{3}{4d}\right)\left(\frac{\rho_f}{\rho_p + 0.5\rho_f}\right) K_3 \tag{6.37a}$$

$$B_I = \left(\frac{3}{4d}\right)\left(\frac{\rho_f}{\rho_p + 0.5\rho_f}\right)\left(2K_3 U_f + \frac{K_1 \mu}{\rho_f d}\right) \tag{6.37b}$$

$$C_I = \left(\frac{3}{4d}\right)\left(\frac{\rho_f}{\rho_p + 0.5\rho_f}\right)\left[K_3 U_f^2 + \left(\frac{K_1 \mu}{\rho_f d}\right) U_f + \frac{K_2 \mu^2}{\rho_f^2 d^2}\right] - \left(\frac{\rho_p - \rho_f}{\rho_p + 0.5\rho_f}\right) g \tag{6.37c}$$

In the range of Reynolds number of $1.0 \prec R_{ep} \leq 10.0$, the constants of $K_1$, $K_2$ and $K_3$ are 29.167, -3.889, and 1.222 respectively (see Table 6.1). In terms of Tables 6.2 and 6.3 or

Fig.6.2, for a given upward uniform steady fluid (water) flow with $U_f$ = 10.0 mm/sec and under the condition of $1.0 \prec R_{ep} \leq 10.0$, the size limit of the sand spheres range from d = 70 to d = 238 micron.

Figures 6.7a and 6.7b show the variations of the predicted particle velocities and trajectories with time in an upward steady uniform fluid (water) flow with $U_f$ = 10.0 mm/sec. This two figures indicate that the unsteady state of the particles motion in the transitional flow is very short (within the range of t = 10 to 20 milliseconds for particles sizes ranging from d = 100 to 200 microns). After these time range, the particles with diameter less that of 112.5 microns will move steadily upward with the fluid; while particles with diameters grater than that of 112.5 microns will move steadily downwards to settle. But, particles with diameters close to112.5 microns will suspend in the fluid flowfield.

From the above two case analysis, it is true that the unsteady state of particle motion in an upward uniform steady fluid (water) flowfield is very short for heavy particles. The time required by spherical sand particles, with diameters ranging from 100 to 200 microns, to reach their terminal velocity is within 10 to 20 milliseconds. The result from this case analysis agrees with that obtained by Coimbra and Rangel (1998).

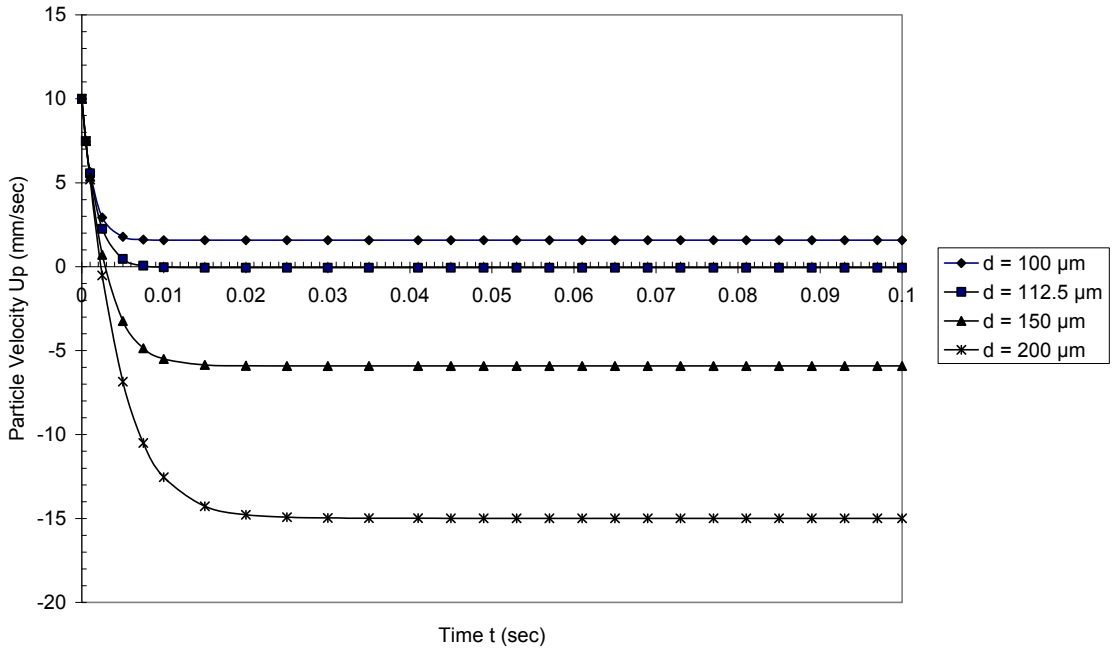


Fig. 6.7a Particle Velovity in an Upward Uniform Fluid (water) Flow with $U_f$ = 10.0 mm/sec Based on 1.0< Rep<10.0.

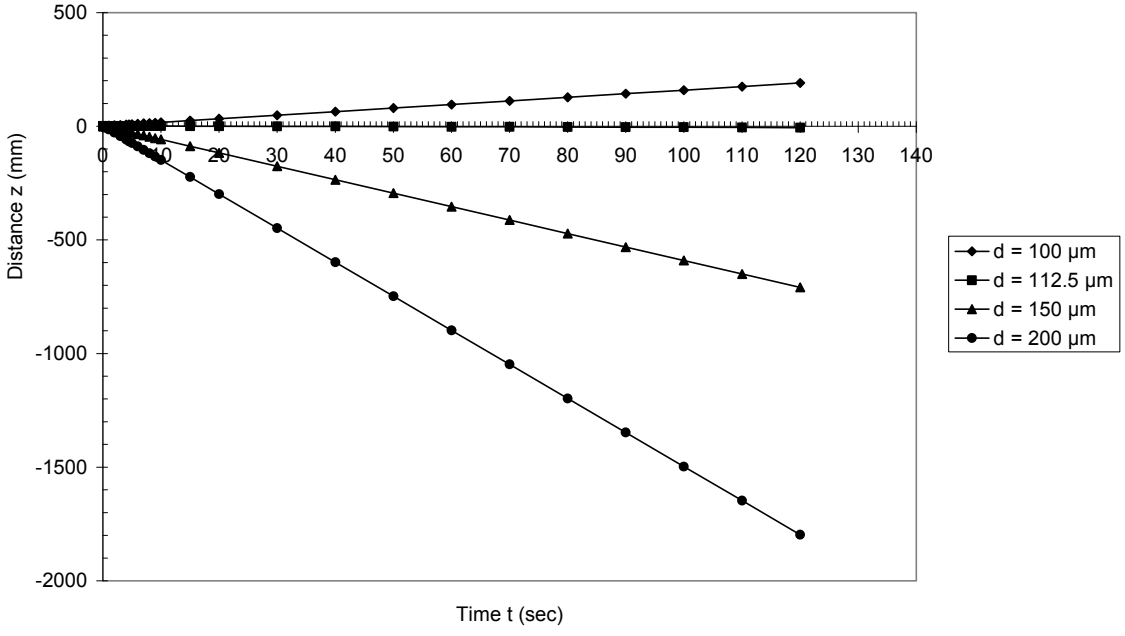


Figure 6.7b Distance of Particle Traveled in an Upward Uniform Fluid (water) Flow with $U_f$ = 10.0 mm/sec based on 1.0<Rep<10.0

## 6.5 Conclusions

### 6.5.1 Particle Motion in the Upward Uniform Steady Fluid Flow

Based on the forces balance on a spherical particle, the general solution for particle motion in an upward uniform steady fluid flow has been developed. The case analysis indicates that for heavy particles the unsteady state of particles motion in an upward steady uniform fluid (water) flow is very short (within 0.02 seconds for sand spheres with diameters up to 200 microns). After this time range, particles with diameters less than the suspended critical diameter ($d_c$) will move directly upward with the fluid; while particles with diameters larger than that of the suspended critical diameter will move downward to settle. The magnitude of the suspended critical particle diameter (dc) is dependant upon the magnitude of the upward fluid velocity ($U_f$).

### 6.5.2 Terminal Settling Velocity

In this study, the new terminal settling velocity formulae for both spherical and natural sand particles have been derived. The case analysis indicates that particle terminal settling velocity formulae developed for spherical particles can not be directly applied to natural sediment particles. The equations must be corrected by a shape factor prior to predicting the terminal settling velocity of natural sediment particles.

The comparison of the predicted results from Eqs.(6.50a), (6.51a), and (6.52a) developed in this study with Cheng's formula showed that they have good agreement with Cheng's formula. This means that these simple equations are applicable to predict the terminal settling velocity of the natural sediment particles.

# Chapter 7

# Particle Trajectories in a Vortex Chamber Flow

The purpose of this chapter is to investigate the characteriscs of particle motion in a confined vortex chamber flowfield, and thus to examine the mechanisms of solid-liquid separation for the selected vortex chamber model. Based on the governing equations of particle motion coupled with the vortex chamber flow patterns derived in Chapter 5, the analytical solutions of particle trajectory in a confined vortex chamber flowfield have been derived. The resulting basic equations developed in this chapter will be useful to illustrate the most common aspects of solid-liquid separating mechanisms in practical engineering.

## 7.1 Problem Description and Assumptions

The knowledge of particle motion in a rotational flowfield is critical for the performance evaluation of particulate-involved operating systems (such as gas-solid or liquid-solid separators). The understanding and ability to predict the pattern of particle motion is of considerable value for the purpose of design or improved operation. However, there are too many factors that may affect the motion of particles in the rotational flowfield, and thereby in some cases prevent any reasonable theoretical approach. The works by previous investigators (Lapple and Shepherd, 1940; Kriebel, 1961; Boothroyd, 1971; Morsi & Alexander, 1972; Svarovsky, 1977, 1981 & 1984; Rudinger, 1980) have shown that though the general governing equations of particle motion in a rotational flowfield are easy to formulate, the analytical solutions are very

difficult to obtain due to the complexity of the simultaneous non-linear equations of particles motion. In a general case to obtain analytical solutions, the governing equations must be simplified to formulate a realistic manner based on some assumptions.

The objective of this study, based on the governing equations of particle motion and some assumptions, is to derive the analytical solutions of particle motion in a confined rotational flowfield. In order to obtain the analytical solutions of the governing equation of particle motion, the following assumptions are made:

- The particles have a spherical shape
- The particle concentration is so low that the presence of particles does not affect the fluid flow
- Particle-particle interactions are negligible; the behavior of each particle can treated alone
- The fluid is incompressible, steady and axi-symmetrical about z-axis
- The tangential flow velocity distribution is a type of Rankine-like profile

## 7.2 Physical Model

Consider a cylindrical vortex chamber with a tangential inlet pipe, but without underflow exit (see Figure 7.1). In this system, the flow tangentially enters the chamber to generate a rotational flowfield around the vertical axis (z), and then flows out along the top edge of the vortex chamber. The velocity of fluid flow in this confined vortex chamber is resolved into three components: tangential ($U_{f,\theta}$), axial ($U_{f,z}$) and radial ($U_{f,r}$). However, the radial velocity is small compared with the tangential velocity and

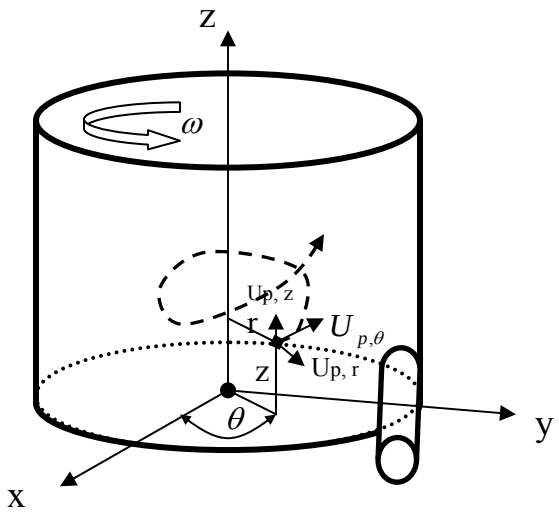


**Figure 7.1 Schematic Illustration of Particle Trajectory in a Vortex Chamber**

axial velocity, and thus negligible (Rudinger, 1980; Svarovsky, 1981; Vatistas, et al, 1986; Vatistas, et al, 1988; Ogawa, 1992).

Particles of low concentration are introduced into the vortex chamber with the tangential inflow. The response of the particles motion depends upon not only the flow patterns, but also the properties of the fluid. The particles in the confined vortex chamber will be either accelerated or decelerated by the influence of the external forces acting on them. The particle velocity components in the tangential, radial, and vertical directions are denoted by $U_{p,\theta}$, $U_{p,r}$, $U_{p,z}$, respectively (see Figure.7.1). In most cases, it is desirable to find the paths of particle motion that can be described by the individual components in the directions of interest.

## 7.3 Particle Trajectories

The principle of liquid-solid separation in a confined vortex chamber is somewhat different from gas-solid separation in a dust collector or a cyclone. For gas-solid separation in a dust collector, the centrifugal force generated by the higher tangential gas inflow is the dominant force in comparison with the gravitational force; and thus the separation mainly depends upon the centrifugal force. The fine particles are transported to the wall surface of the device to settle by the centrifugal effect. In a dust collector, the major concern is over the particle trajectory in the $(r, \theta)$ plane, rather than the (r, z) plane.

Conversely, for liquid-solid separation, as the rotational flowfield in a confined vortex chamber is generated by the momentum transfer from the tangential inflow, the generated tangential flow velocity is low compared with that in a dust collector, and thus centrifugal effect is not strong. The mechanism of particle separation depends upon the

combined effect of the gravitational force and centrifugal force. For a suspended particle in a confined vortex chamber located at radius of r, it will move simultaneously downward, outward (radial), and forward (tangential) if its terminal settling velocity $U_p$ is greater than the vertical upward flow velocity $U_{z,r}$. Also, there is a possibility the particle will move simultaneously upward, outward, and forward if its terminal settling velocity is less than the vertical upward flow velocity.

For solid-liquid separation in a confined vortex chamber, the present work is concerned about the particle trajectories in the (z, r) plane, and not the (r, θ) plane. Hence, if the flow pattern in a rotational flowfield is known, the particle trajectory in the (z, r) plane can be predicted by considering the relationships between flowfield and particle motion in radial, tangential, and vertical directions.

### 7.3.1 Particle Trajectory in the Tangential Direction

For a spherical particle suspended in a rotational flowfield, the force acting on the suspended particle in the tangential direction is the drag force only, and the particle takes a very short time to reach its terminal velocity (within 0.002 seconds for particles with a diameter of 200 microns, see Chapter 6). As a result, the particle's tangential velocity component quickly approaches the tangential fluid velocity component (i.e.: $U_{p,\theta} = U_{f,\theta}$). The particle's tangential velocity component in the forced vortex region (core of the chamber) and free vortex region (outer region of the chamber) can be expressed as:

$$U_{p,\theta} = \omega r \qquad (r = 0 \quad to \quad R_2) \tag{7.1a}$$

and

$$U_{p,\theta} = \frac{\omega R_2^2}{r} \qquad \left(r = R_2 \quad to \quad R_1\right) \tag{7.1b}$$

where $U_{p,\theta}$ and $U_{f,\theta}$ are the particle and fluid velocities in the tangential direction at radius of r. Then, the particle trajectories in the tangential direction can be written as:

$$\theta = \omega t \qquad \left(r = 0 \quad to \quad R_2\right) \tag{7.2a}$$

and

$$\theta = \frac{\omega R_2^2}{r^2} t \qquad \left(r = R_2 \quad to \quad R_1\right) \tag{7.2b}$$

where θ is the angle of particles traveled in the rotational flowfield.

### 7.3.2 Particle Trajectory in the Radial Direction

Since the radial fluid velocity is small compared to the tangential and vertical velocity (Rudinger, 1980; Svarovsky, 1981; Vatistas, et al, 1986; Vatistas, et al, 1988; Ogawa, 1992), it can be neglected (i.e.: $U_{f,r} = 0$). Moreover, to further simplify the problem, the Stokes' law is applied to calculate the drag force in the radial direction. By considering the centrifugal force, drag force and gradient pressure force acting on a particle in the radial direction, the governing equation of the particle motion in the radial direction can be written as (Boothroyd, 1971; Maxey and Rilley, 1983):

$$m_p \frac{dU_{p,r}}{dt} = m_p \frac{U_{p,\theta}^2}{r} - m_f \frac{U_{f,\theta}^2}{r} - \frac{1}{2} C_D \rho_f A_p U_{pr}^2 \tag{7.3}$$

where $m_p$ is the mass of particle, and $m_f$ is the mass of fluid with the same volume of particle. On the right-hand side of Eq.(7.3), the first term is the centrifugal force; the second term is the pressure gradient force in the radial direction; the third term is the drag force. For a spherical particle, if Stokes's law applies, then the above equation can be further written as:

$$\frac{dU_{p,r}}{dt} = -\frac{18\mu}{\rho_p d^2} U_{p,r} + \left(1 - \frac{\rho_f}{\rho_p}\right) \frac{U_{p,\theta}^2}{r} \tag{7.3a}$$

#### 7.3.2.1 Particle motion in the forced vortex region

By substituting Eq.(7.1a) into Eq.(7.3a) and rearranging, the governing equation of particle motion in the forced vortex region (core of the chamber) can be expressed as:

$$\frac{dU_{p,r}}{dt} = -\frac{18\mu}{\rho_p d^2} U_{p,r} + \left(1 - \frac{\rho_f}{\rho_p}\right) \omega^2 r \tag{7.4}$$

The general solution for Eq.(7.4) is:

$$U_{p,r} = \frac{\omega^2 d^2 r \left(\rho_p - \rho_f\right)}{18\mu} \left(1 - e^{-\frac{18\mu}{\rho_p d^2} t}\right) \tag{7.5}$$

Since the last term in the Eq.(7.5) decays very fast with time, thus it is negligible. Then Eq.(7.5) reduces to:

$$U_{p,r} = \frac{\omega^2 d^2 \left(\rho_p - \rho_f\right)}{18\mu} r \tag{7.6}$$

In terms of the definition of velocity, Eq. (7.6) can be expressed as:

$$\frac{dr}{dt} = U_{p,r} = \frac{\omega^2 d^2 \left(\rho_p - \rho_f\right)}{18\mu} r \tag{7.7}$$

By integrating the above equation, the distance of particle traveled in the radial direction can be written as

$$r = r_0 e^{\frac{\omega^2 d^2 \left(\rho_p - \rho_f\right)}{18\mu}(t - t_0)} \tag{7.8}$$

where $r_0$ is the initial distance of particle from origin at time $t_0$. If further assuming that the particle initial distance is $r_0$ at $t_0 = 0$, then Eq.(7.9) reduces to:

$$r = r_0 e^{\frac{\omega^2 d^2 \left(\rho_p - \rho_f\right)}{18\mu} t} \tag{7.9}$$

Moreover, for the gas-solid flow system, as the density of gas is greatly less than that of solid (i.e., $\rho_f << \rho_p$), the pressure gradient force term is negligible in the governing equation. then the above equation is reduced to:

$$r = r_0 e^{\frac{\rho_p \omega^2 d^2}{18\mu} t} \tag{7.9a}$$

Eq.(7.9a) is similar to the result derived by Kriebel (1961) for small particles in a gas centrifuge. In some cases, it is desirable to know the time required for a particle moving from radius of r = $r_o$ to r = r. From Eq.(7.10), the time can be expressed as:

$$t_r = \frac{18\mu}{\omega^2 d^2 \left(\rho_p - \rho_f\right)} \ln\left(\frac{r}{r_0}\right) \tag{7.10}$$

Further for the gas-solid flow system, the pressure term is negligible. Then the above equation reduces to:

$$t_r = \frac{18\mu}{\rho_p \omega^2 d^2} \ln\left(\frac{r}{r_0}\right) \tag{7.10a}$$

#### 7.3.2.2 Particle motion in the free vortex region

By substituting Eq.(7.1b) into Eq.(7.3a) and rearranging, the governing equation for particle motion in the free vortex region (outer region of the chamber) can be expressed as:

$$\frac{dU_{p,r}}{dt} = -\frac{18\mu}{\rho_p d^2} U_{p,r} + \left(1 - \frac{\rho_f}{\rho_p}\right) \frac{\omega^2 R_2^4}{r^3} \tag{7.11}$$

The general solution for Eq.(7.11) is:

$$U_{p,r} = \frac{\omega^2 d^2 \left(\rho_p - \rho_f\right)}{18\mu} \left(\frac{R_2^4}{r^3}\right) \left(1 - e^{-\frac{18\mu}{\rho_p d^2} t}\right) \tag{7.12}$$

As the last term in Eq.(7.12) decays very fast with time, and thus negligible. Then Eq.(7.12) reduces to:

$$U_{p,r} = \frac{\omega^2 d^2 \left(\rho_p - \rho_f\right)}{18\mu} \left(\frac{R_2^4}{r^3}\right) \tag{7.13}$$

In terms of the definition of velocity, Eq. (7.13) can be expressed as:

$$\frac{dr}{dt} = U_{p,r} = \frac{\omega^2 d^2 \left(\rho_p - \rho_f\right)}{18\mu} \left(\frac{R_2^4}{r^3}\right) \tag{7.14}$$

By integrating the above equation, the distance of particle traveled in the radial direction can be expressed as:

$$r = \left[ r_0^4 + \frac{2\omega^2 d^2 \left(\rho_p - \rho_f\right) R_2^4}{9\mu} \left(t - t_0\right) \right]^{1/4} \tag{7.15}$$

where $r_0$ is the initial distance of particle from origin at time $t_0$. If further assuming that the particle initial distance is $r_0$ at $t_0$ = 0, then Eq.(7.15) reduces to:

$$r = \left[ r_0^4 + \frac{2\omega^2 d^2 \left(\rho_p - \rho_f\right) R_2^4}{9\mu} t \right]^{1/4} \tag{7.16}$$

For gas-solid flow system, the pressure gradient force term is negligible in the governing equation, then the above equation is reduced to:

$$r = \left[ r_0^4 + \frac{2\rho_p \omega^2 d^2 R_2^4}{9\mu} t \right]^{1/4} \tag{7.16a}$$

By rearranging Eq.(7.16), the time required for a particle moving from radius of $r = r_0$ to r = r can be expressed as:

$$t_r = \frac{9\mu\left(r^4 - r_0^4\right)}{2\omega^2 d^2 \left(\rho_p - \rho_f\right) R_2^4} \tag{7.17}$$

For the gas-solid flow system, the pressure term is negligible, then the above equation reduces to:

$$t_r = \left(\frac{9\mu}{2\rho_p \omega^2 d^2}\right)\left(\frac{r^4 - r_0^4}{R_2^4}\right) \tag{7.17a}$$

### 7.3.3 Particle Trajectories in the (z, r) Plane

For a suspended particle distant r from the origin and moving vertically at velocity ($U_{p,z}$), tangentially at velocity ($U_{p,\theta}$), and radially at velocity ($U_{p,r}$), the governing equation of particle motion in the vertical direction can be expressed as:

$$m_p \frac{dU_{p,z}}{dt} = \frac{1}{2} C_{D,z} \rho_f A_p \left(U_{f,z} - U_{p,z}\right)^2 - m_p \left(\frac{\rho_p - \rho_f}{\rho_p}\right) g \tag{7.18}$$

As the vertical velocity ($U_{f,z}$) distribution in a vortex chamber is not uniform, but a function of radius r for a steady rotational flow, the equations of particle trajectory derived from one-dimensional upward constant flow can not be directly used to predict the particle trajectories in the (z, r) plane. For a suspended particle in a confined vortex chamber distant r from origin, it will move simultaneously forward (tangential), outward (radial), and downward (or upward).

According to the dynamic analysis of a single particle in one-dimensional upward uniform flow (see Chapter 6), the unsteady state of particle motion is very short (i.e., the time required for a particle to reach its terminal velocity). To simplify the problem, the unsteady effect on particle motion from one location to another is neglected in this study; and the particle terminal velocity ($U_s$) is directly used to estimate the particle trajectory

in the (z, r) plane. Therefore, in terms of the vertical flow velocity ($U_{f,z}$) distribution and the particle terminal settling velocity ($U_s$) coupled with the particle motion in the radial direction, the particle trajectory can be determined. The vertical distance of a particle traveled in the vortex chamber from time $t_0$ to t can be expressed as:

$$Z_t - Z_{t_0} = \int_{t_0}^{t} \left(U_{f,z} - U_s\right) dt \tag{7.19}$$

where $Z_0$ and $Z_t$ are the vertical coordinates of particle motion at time $t_0$ and t; $U_s$ is the particle terminal settling velocity in the quiescent water; and $U_{z,r}$ is the vertical fluid flow velocity distribution in the vortex chamber, which can be determined by the vortex models developed in Chapter 5. The particle trajectory in the (z, r) plane is determined as follows.

**Forced Vortex Region (** $r = 0$ *to* $R_2$ **):**

In terms of the vortex model derived in Chapter 5, the vertical fluid velocity distribution in a confined vortex chamber could be described by Eq.(5.20):

$$U_{z,r} = \frac{2Q}{\pi R_1^2}\left[1 - \left(\frac{r}{R_1}\right)^2\right] \tag{5.20}$$

Substituting Eq.(5.20) into Eq.(7.19) gives:

$$Z_t - Z_{t_0} = \int_{t_0}^{t} \left(U_{z,r} - U_s\right) dt = \int_{t_0}^{t} \left\{ \frac{2Q}{\pi R_1^2} \left[ 1 - \left( \frac{r}{R_1} \right)^2 \right] - U_s \right\} dt \tag{7.20}$$

The distance of particle traveled in the radial direction could be described by Eq.(7.9). By differentiating Eq.(7.9) with respect to time t and rearranging, the following relationship is obtained:

$$dt = \frac{18\mu}{\left(\rho_p - \rho_f\right)\omega^2 d^2} \frac{dr}{r} \tag{7.21}$$

Substituting Eq.(7.21) into Eq.(7.20) and rearranging, the following integral transform is obtained:

$$Z_r - Z_{r_0} = \int_{r_0}^{r} \left[ \frac{18\mu}{\left(\rho_p - \rho_f\right)\omega^2 d^2} \right] \left\{ \frac{2Q}{\pi R_1^2} \left[ 1 - \left( \frac{r}{R_1} \right)^2 \right] - U_s \right\} \frac{dr}{r} \tag{7.22}$$

Integrating Eq.(7.22) and rearranging gives:

$$Z_r - Z_{r_0} = \frac{18\mu}{\left(\rho_p - \rho_f\right)\omega^2 d^2} \left\{ \left( \frac{2Q}{\pi R_1^2} - U_s \right) \ln\left( \frac{r}{r_0} \right) - \left( \frac{Q}{\pi R_1^2} \right) \left[ \left( \frac{r}{R_1} \right)^2 - \left( \frac{r_0}{R_1} \right)^2 \right] \right\} \tag{7.23}$$

**Free Vortex Region (** $r = R_2$ *to* $R_1$ **):**

Similarly, in the free vortex region the vertical distance of particle traveled from time t to $t_0$ can be determined by Eq.(7.20):

$$Z_t - Z_{t_0} = \int_{t_0}^{t} \left(U_{z,r} - U_s\right) dt = \int_{t_0}^{t} \left\{ \frac{2Q}{\pi R_1^2} \left[ 1 - \left( \frac{r}{R_1} \right)^2 \right] - U_p \right\} dt \tag{7.20}$$

Differentiating Eq.(7.17) with respect to time (t) and rearranging gives:

$$dt = \frac{18\mu}{\left(\rho_p - \rho_f\right)\omega^2 d^2 R_2^4} \left(r^3 dr\right) \tag{7.24}$$

By substituting Eq.(7.24) into Eq.(7.20) and rearranging, the following integral transform is obtained:

$$Z_r - Z_{r_0} = \int_{r_0}^{r} \left[ \frac{18\mu}{\left(\rho_p - \rho_f\right)\omega^2 d^2} \right] \left\{ \frac{2Q}{\pi R_1^2} \left[ 1 - \left( \frac{r}{R_1} \right)^2 \right] - U_s \right\} \left( \frac{r^3}{R_2^4} \right) dr \tag{7.25}$$

Integrating Eq.(7.25) and rearranging yields:

$$Z_r - Z_{r_0} = \left[ \frac{18\mu}{\left(\rho_p - \rho_f\right)\omega^2 d^2} \right] \left\{ \left( \frac{2Q}{\pi R_1^2} - U_s \right) \left( \frac{r^4 - r_0^4}{4R_2^4} \right) - \left( \frac{Q}{\pi R_1^2} \right) \left( \frac{r^6 - r_0^6}{3R_1^2 R_2^4} \right) \right\} \tag{7.26}$$

## 7.4 Case Analysis and Discussions

For a confined vortex chamber with chamber diameter of $D_1 = 127$ mm, inlet pipe diameter of $D_{IN} = 12.7$ mm, and chamber height of $H_0 = 175$ mm, the particle trajectory in the (z, r) plane can be described by Eqs.(7.23) and (7.26):

$$Z_r - Z_{r_0} = \frac{18\mu}{(\rho_p - \rho_f)\omega^2 d^2}\left\{\left(\frac{2Q}{\pi R_1^2} - U_p\right)\ln\left(\frac{r}{r_0}\right) - \left(\frac{Q}{\pi R_1^2}\right)\left[\left(\frac{r}{R_1}\right)^2 - \left(\frac{r_0}{R_1}\right)^2\right]\right\} \tag{7.23}$$

$$Z_r - Z_{r_0} = \left[\frac{18\mu}{(\rho_p - \rho_f)\omega^2 d^2}\right]\left\{\left(\frac{2Q}{\pi R_1^2} - U_p\right)\left(\frac{r^4 - r_0^4}{4R_2^4}\right) - \left(\frac{Q}{\pi R_1^2}\right)\left(\frac{r^6 - r_0^6}{3R_1^2 R_2^4}\right)\right\} \tag{7.26}$$

**Angular Velocity (ω)** For a given flow rate Q, the angular velocity of the fluid flow around the z axis can be determined by the Eq.(4.43) derived in Chapter 4:

$$\omega = \left(\frac{\lambda_2}{\lambda_1}\right)^{1/2} Q \tag{4.43}$$

in which

$$\lambda_1 = \frac{(H_o + R_1/3)R_1^2}{2(R_1 - R_{IN})R_{IN}^2} + \left(\frac{K_L}{f_\theta}\right) \tag{4.43a}$$

$$\lambda_2 = \frac{1}{\pi^2}\left(\frac{K_L}{f_\theta}\right)\left(\frac{R_1^2}{R_{IN}^4 R_2^4}\right)\left(\frac{1}{2} + \ln\frac{R_1}{R_2}\right)^{-2} \tag{4.43b}$$

**Terminal Settling Velocity ($U_s$)** Cheng's settling velocity formula derived for the natural sediment particles can be applied to a wide range of Reynolds numbers from the Stokes flow to the turbulent flow, here his formula is used to predict the sand particle settling velocity:

$$U_s = \frac{\nu}{d}\left\{\sqrt{25 + 1.2\left[\left(\frac{\rho_p}{\rho_f} - 1\right)\frac{g}{\nu^2}\right]^{2/3} d^2} - 5\right\}^{1.5} \tag{7.27}$$

Figures 7.2 to 7.5 show the predicted particle trajectories in the (z, r) plane for particles injected from six different locations of $r_0 = R_1/100$, $R_1/10$, $R_1/5$, $R_1/4$, $R_1/3$, and $R_1/2$. These figures only display the trajectories for particles with diameters that could arise a height that is same as the chamber height. For a given flow rate and a given injection location, particles with diameters less than that indicated in these figures will escape from the chamber; while particles with diameter greater than that indicated in these figures will be captured by the chamber.

These figures indicate that for a given flow rate, the particle sizes which could be captured by the chamber decrease with increasing the injection locations from the core to the outer region of the chamber. However, by comparing these figures, it is found that for the injection locations ($r_o$) near the core of the chamber with a radius about 10% of the chamber radius ($R_1$), the sizes of the particle, which could be captured by the chamber, increase with increasing flow rate; over this region, the particle sizes that can be captured by the chamber first increase and then decrease with increasing inflow rate.

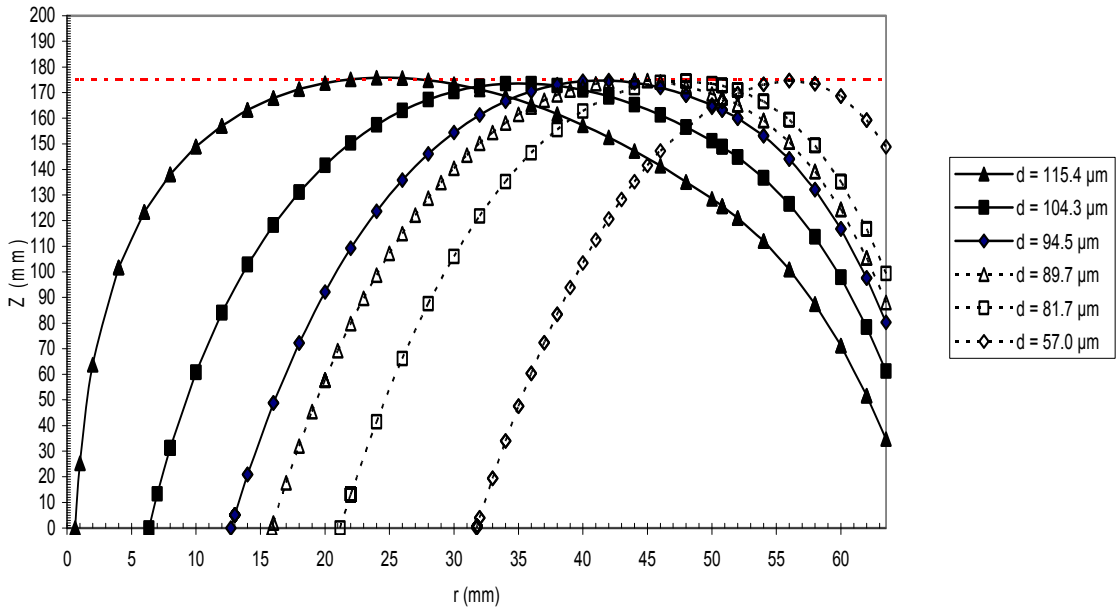


Figure 7.2 Particle Trajectories in the plane (z, r) Based on Q = 46.5 ml/s for Particles Injected from $r_o = R_t/100$, $R_t/10$, $R_t/5$, $R_t/4$, $R_t/3$, and $R_t/2$, respectively.

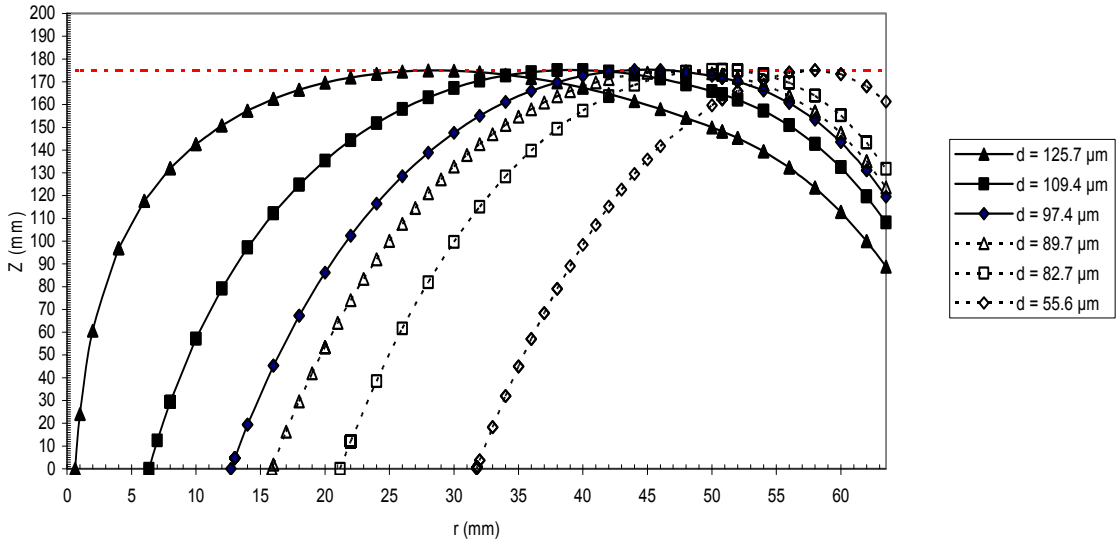


Figure 7.3 Particle Trajectories in the plane (z, r) Based on Q = 56.6 ml/s for Particles Injected from $r_o = R_t/100$, $R_t/10$, $R_t/5$, $R_t/4$, $R_t/3$, $R_t/2$, respectively.

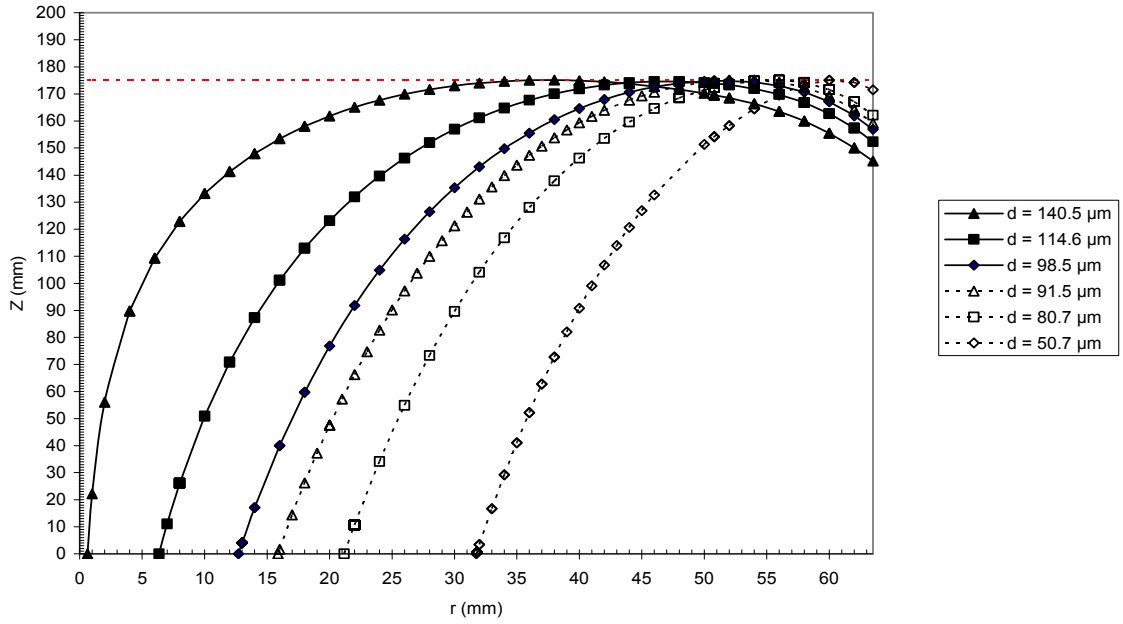


Figure 7.4 Particle Trajectories in the plane (z, r) Based on Q = 84.7 ml/s for Particles Injected from $r_o = R_1/100$, $R_1/10$, $R_1/5$, $R_1/4$, $R_1/3$, and $R_1/2$, respectively.

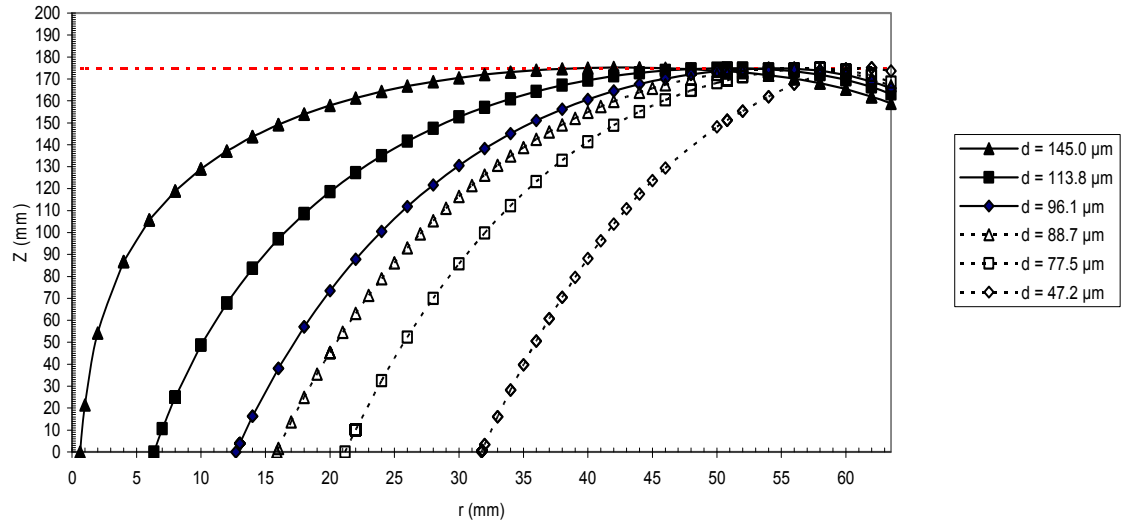


Figure 7.5 Particle Trajectories in the plane (z, r) Based on Q = 105.6 ml/s for Particles Injected from $r_o = R_1/100$, $R_1/10$, $R_1/5$, $R_1/4$, $R_1/3$, and $R_1/2$, respectively.

## 7.5 Conclusions

Based on the governing equations of particle motion in a rotational flowfield coupled with the vortex flow pattern developed in Chapter 5, the particle trajectory in a confined vortex flow has been derived in this study. Case analysis indicates that the particle trajectory in a confined vortex chamber is governed by the combined effect of the centrifugal force and the gravitational force. The centrifugal effect becomes significant when magnitude of the inflow rate (Q) is increased. The critical particle diameter which can be captured by the chamber increases with increasing magnitude of the inflow rate. This means that the removal efficiency decreases with increasing inflow rate.

# Chapter 8

# Investigation of Unit Sizing Formula

In this chapter, based on the particle trajectory equation in the (z, r) plane derived in Chapter 7 coupled with the angular velocity formula derived in Chapter 4, a unit sizing formula for a confined vortex chamber with tangential inflow, but without baseflow exit has been derived. The comparison of the predicted removal efficiency from this formula to the experimental result indicated that the predicted result agrees with the experimental data. This means that the equation derived in this study is applicable to unit performance evaluation and sizing for vortex separators with a similar configuration.

## 8.1 Introduction

In current practice, the widely used treatment technologies for liquid-solid separation include the gravitational settling method and hydrodynamic separation method. Gravitational separation is a conventional treatment process to remove solids from liquids. In this treatment process, particles with density greater than that of water move downwards to settle, while particles with density less than that of water move upwards to float on the water surface. This is the major mechanisms of pollutant removal in wastewater and stormwater treatment systems. Sedimentation removal rate is a function of detention time, solid terminal settling velocity and overflow rate in the treatment device (Wanielista and Yousel, 1993; Andoh and Smisson, 1994; Sincero and Sincero, 1996).

Unlike the conventional treatment technology that only rely on gravity settling, solid removal in a confined vortex separator relies on not only gravity settling, but also secondary flows which transport settling solids to the center of vortex chamber to settle (Andoh and Smisson, 1994; Wong, 1997; Minton, 2005). Though many types of hydrodynamic separators have been developed for wastewater and stormwater treatment, so far not much fundamental study exists due to the complexity of the problem. Design specifications of commercial devices are almost based on the semi-empirical equations or scaling laws (such as Froude scaling and Hazen scaling) that are suitable for each manufacturer.

The accurate prediction of particle removal efficiency in a hydrodynamic separator is critical either for the purpose of unit design or improved operation. The purpose of this chapter is to develop a unit sizing formula for a selected vortex separator in this study (see Fig.8.1).

## 8.2 Vortex Chamber Physical Model

The physical model considered in this chapter is same as that described in the previous chapters. For convenient referencing, it is reproduced as follows (Fig. 8.1). The main symbols for unit dimensions are also shown in Fig.8.1. Liquid-solid flow is forced tangentially into the vortex chamber by a fluid pressure difference between the chamber inlet and outlet, and flows out along the top edge of the chamber.

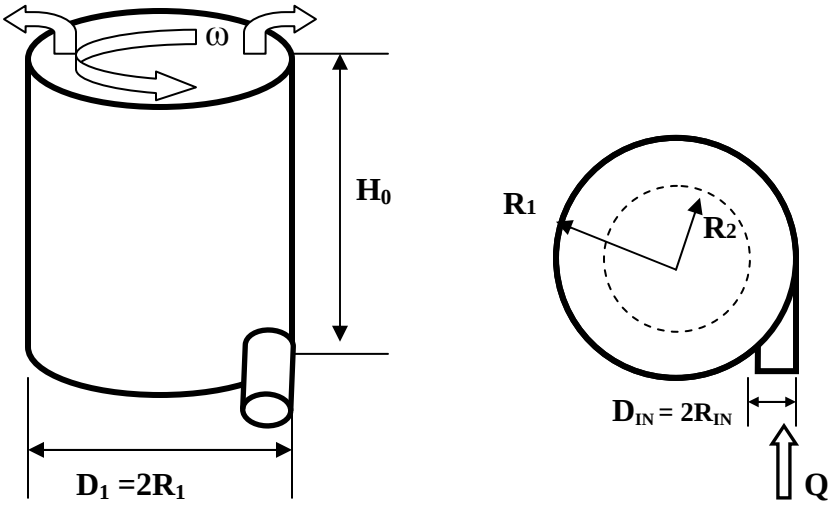


**(a) Perspective View** **(b) Top View**

**Fig. 8.1 Schematic Illustration of the Vortex Chamber Model**

## 8.3 Determination of Sizing Formula

The particle trajectories in the (z, r) plane of a confined vortex chamber can be predicted by Eq.(7.23) derived in Chapter 7. It is reproduced as follows:

$$Z_r - Z_{r_0} = \frac{18\mu}{(\rho_p - \rho_f)\omega^2 d^2}\left\{\left(\frac{2Q}{\pi R_1^2} - U_s\right)\ln\left(\frac{r}{r_0}\right) - \left(\frac{Q}{\pi R_1^2}\right)\left[\left(\frac{r}{R_1}\right)^2 - \left(\frac{r_0}{R_1}\right)^2\right]\right\} \quad (7.23)$$

where $r_o$ and $Z_{r_o}$ are initial location of particles in the radial and vertical directions respectively in the chamber. For a given height of vortex chamber with inflow rate Q, if the maximum height that a suspended particle could rise from the bottom of the chamber ($Z_{r_o} = 0$) is less than that of the chamber height, then this particle could be captured by the chamber. To find this maximum height that a suspended particle could rise, differentiating Eq.(7.23) with respect to r and setting it to zero (i.e., $dz_r/dr = 0$) yields:

$$r_{Z_{max}} = R_1\sqrt{1 - \frac{1}{2}\left(\frac{U_s}{U_{OR}}\right)} \quad (8.1)$$

where $r_{Z_{max}}$ is the location where a particle could rise its maximum height if it is injected from a point at r = $r_o$ in the chamber, and it is a function of the particle diameter d and the flow rate Q; $U_s$ is the particle terminal settling velocity; and $U_{OR}$ is the chamber overflow rate and is defined as follows:

$$U_{OR} = \frac{Q}{\pi R_1^2} \tag{8.2}$$

By substituting (8.2) into Eq.(7.23) and replacing r with $r_{z\max}$, then maximum height that a particle could rise can be expressed as:

$$Z_{\max} = \frac{18\mu}{(\rho_p - \rho_f)\omega^2 d^2}\left\{(2U_{OR} - U_s)\ln\left(\frac{r_{z_{\max}}}{r_0}\right) - U_{OR}\left[\left(\frac{r_{z_{\max}}}{R_1}\right)^2 - \left(\frac{r_0}{R_1}\right)^2\right]\right\} \tag{8.3}$$

where $Z_{\max}$ is the maximum height that a suspended particle could rise from the bottom of the chamber ($Z_{r_o} = 0$). Further, if we set the maximum height ($Z_{\max}$) that a particle could rise to chamber height of $H_o$, then the following relationship is obtained:

$$H_o = \frac{18\mu}{(\rho_p - \rho_f)\omega^2 d^2}\left\{(2U_{OR} - U_s)\ln\left(\frac{r_{z_{\max}}}{r_0}\right) - U_{OR}\left[\left(\frac{r_{z_{\max}}}{R_1}\right)^2 - \left(\frac{r_0}{R_1}\right)^2\right]\right\} \tag{8.4}$$

For a given design flow rate Q and the desired removal efficiency, the unit dimensions can be determined with this equation coupled with the angular velocity (ω) formula, and particle terminal settling velocity ($U_s$) formula. The determination of angular velocity (ω), particle terminal settling velocity ($U_s$) and the injection location are described as follows:

**Angular Velocity (**ω) The angular velocity (ω) in the above equation is a function of flow rate Q and the unit geometrical dimensions, and it can be determined by Eq.(4.43) derived in Chapter 4. It is reproduced as follows:

$$\omega = \left(\frac{\lambda_2}{\lambda_1}\right)^{1/2} Q \tag{4.43}$$

in which

$$\lambda_1 = \frac{(H_o + R_1/3)R_1^2}{2(R_1 - R_{IN})R_{IN}^2} + \left(\frac{K_L}{f_\theta}\right) \tag{4.43a}$$

$$\lambda_2 = \frac{1}{\pi^2}\left(\frac{K_L}{f_\theta}\right)\left(\frac{R_1^2}{R_{IN}^4 R_2^4}\right)\left(\frac{1}{2} + \ln\frac{R_1}{R_2}\right)^{-2} \tag{4.43b}$$

where $K_L$ is the local loss coefficient at inlet pipe exit, and is approximately equal to 1.0 for sudden expansion in pipe flow. $f_\theta$ is the fraction factor in the tangential direction of the vortex chamber, and it is constant for turbulent rough flow (Street, et al., 1996). But for the unit sizing purpose, it is more convenient to express $f_\theta$ as the following form (Street, et al., 1996):

$$f_\theta = \frac{8 g n^2}{R_h^{1/3}} \tag{8.5}$$

where n is the Manning roughness coefficient. $R_h$ is the hydraulic radius for flow in the tangential direction, and it is defined as:

$$R_h = \frac{R_1 H_o}{2H_o + R_1} \tag{8.6}$$

Substituting Eq.(8.6) into Eq.(8.5) gives:

$$f_\theta = 8 g n^2 \left( \frac{2H_0 + R_1}{H_o R_1} \right)^{1/3} \tag{8.7}$$

By substituting Eq.(8.7) into Eq.(4.43) and replacing $R_2$ with $(R_1 - 2R_{IN})$ in Eq.(4.43), the angular velocity can be rewritten as:

$$\omega = \left( \frac{\lambda_2}{\lambda_1} \right)^{1/2} Q \tag{8.8}$$

in which

$$\lambda_1 = \frac{(H_o + R_1/3) R_1^2}{2(R_1 - R_{IN}) R_{IN}^2} + \frac{K_L}{8 g n^2} \left( \frac{H_o R_1}{2H_0 + R_1} \right)^{1/3} \tag{8.8a}$$

$$\lambda_2 = \left( \frac{K_L}{8\pi^2 g n^2} \right) \left( \frac{H_o R_1}{2H_0 + R_1} \right)^{1/3} \left[ \frac{R_1^2}{R_{IN}^4 (R_1 - 2R_{IN})^4} \right] \left[ \frac{1}{2} + \ln \left( \frac{R_1}{R_1 - 2R_{IN}} \right) \right]^{-2} \tag{8.8b}$$

**Particle Terminal Settling Velocity ($U_s$)** The particle settling velocity is a function of particle diameter as well as fluid and particle properties. It can be determined by Cheng's formula (1997):

$$U_s = \frac{\nu}{d}\left\{\sqrt{25 + 1.2\left[\left(\frac{\rho_p}{\rho_f} - 1\right)\frac{g}{\nu^2}\right]^{2/3} d^2} - 5\right\}^{1.5} \tag{8.9}$$

**Particle Injection Location ($r_o$)** From the case analysis of particle trajectory described in Chapter 7, it was found that for a given flow rate Q, the critical particle sizes ($d_c$) which could be captured by the chamber varies with the particle injection location of $r_o$. In real operation, the particles enter into the vortex chamber through the inflow, then the secondary flow currents transport the particles to the central zone of the chamber bottom to settle or re-suspend. For high inflow rates, almost all of the particles fed from the inflow pipe would be transported to the core region of the chamber floor by the strong secondary flow currents. Typically, a cone shape of sedimentation accumulation is formed in the central zone, while for very low inflow rate the shape of sedimentation accumulation is almost flat due to the weak secondary flow currents. Therefore, it is very difficult to determine the exact particle injection or re-suspended locations ($r_o$) in the bottom of chamber.

However, the degree of particles migration ($r_o$) from the periphery of the chamber to the central zone relies on the strength of the secondary flow currents; while the strength of secondary flow currents depends on the magnitude of inflow rate (Q). Hence, there must exist relationships between the inflow rate and the degree of particle migration ($r_o$) from chamber periphery to central zone. To simplify the problem, here we use the chamber's Reynolds number to represent the inflow flow parameter. It is defined as follows:

$$R_e = \frac{U_{OR} D_1}{\nu} = \frac{2Q}{\pi R_1 \nu} \tag{8.10}$$

In terms of the above analysis, as the degree of particle migration ($r_o$) should be a function of inflow rate and unit sizes, it can be determined inversely with the experimental data obtained in Chapter 3 coupled with Eq.(8.4) and particle size distribution (PSD). For a given inflow rate and measured particle removal efficiency, the critical particle size that could be captured by the chamber can be found from PSD curve. By substituting it into Eq.(8.4), the corresponding average particle injection location ($r_o/R_1$) can be obtained. By plotting the calculated chamber Reynolds number with Eq.(8.10) against the calculated particle injection location ($r_o/R_1$) with Eq.(8.4), and fitting it to a logarithmic curve (see Fig.8.2), the following relationship (with a correlation factor of $R^2 = 0.9908$) is obtained:

$$\frac{r_o}{R_1} = -0.3981 \, \mathrm{Ln}(\mathrm{Re}) + 2.7536 = -0.3981 \, \mathrm{Ln}\left( \frac{2Q}{\pi R_1 \nu} \right) + 2.7536 \tag{8.11}$$

For a given Q and chamber radius $R_1$, if the calculated value of ($r_o/R_1$) is negative that means the particle is injected from the center of the chamber, then set $r_o$ to a value closing to zero, for example, $r_o$ = 100 micron (0.1 mm).

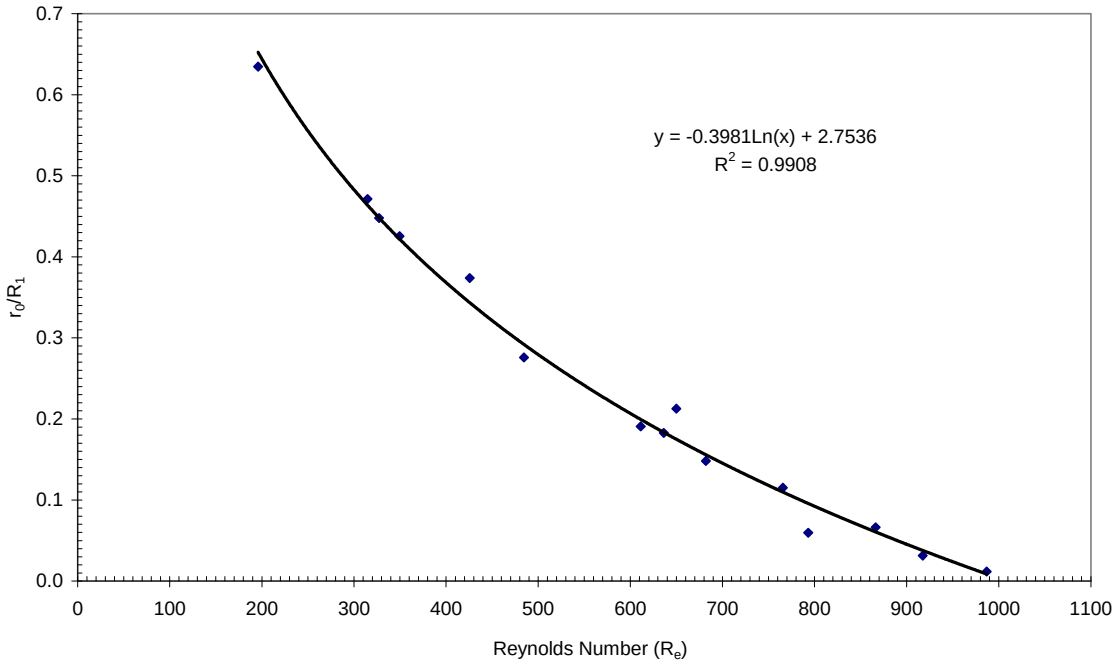


Fig.8.2 Relationship Between Particle Injection Location ($r_o/R_1$) and Chamber Reynolds Number ($R_e$)

## 8.4 Comparison of Predicted Results with Experimental Results

For a confined vortex chamber with diameter of $D_1$ = 127 mm, height of $H_o$ = 175 mm, and inlet pipe diameter of $D_{IN}$ = 12.7 mm, Figure 8.3 shows the comparison of the predicted removal efficiency with Eq.(8.4) to the experimental results presented in the Tables 3.2, 3.3, and 3.4 of Chapter 3. This figure indicates that the predicted results of Eq.(8.4) coupled with the PSD curve agrees with the measured results. The difference between the measured data and the predicted results ranges from 0.2% to 3.6%.

Figure 8.4 shows the comparison of the predicted removal efficiency with Eq.(8.4) to the experimental results presented in the Table 3.5 of Chapter 3 based on the chamber height of $H_o$ = 120 mm. This figure also indicates that the predicted results with Eq.(8.4) agree with the measured results. The maximum difference between the predicted results and the experimental results is about 3.6%. The above analysis reveals that Eq.(8.4) is applicable to the unit performance evaluation for types of vortex chambers selected in this study, and thus it can be used for unit sizing.

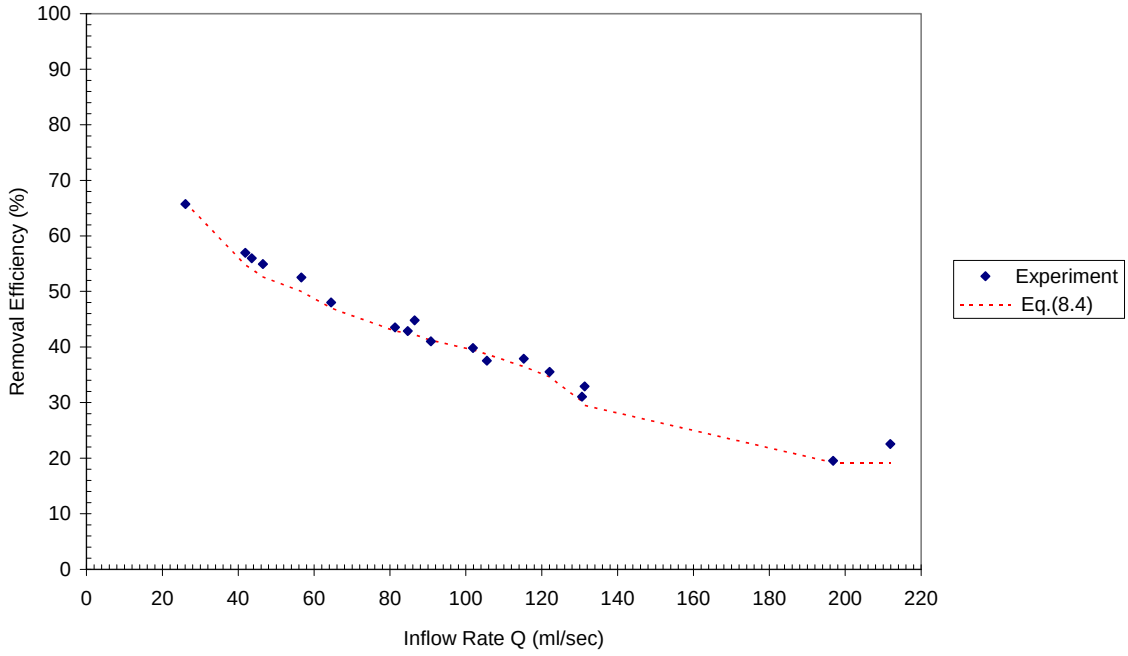


Fig. 8.3 Comparison of Predicted Removal Effeciency with Experimental Data Based on Chamber Heigh $H_0$ = 175 mm

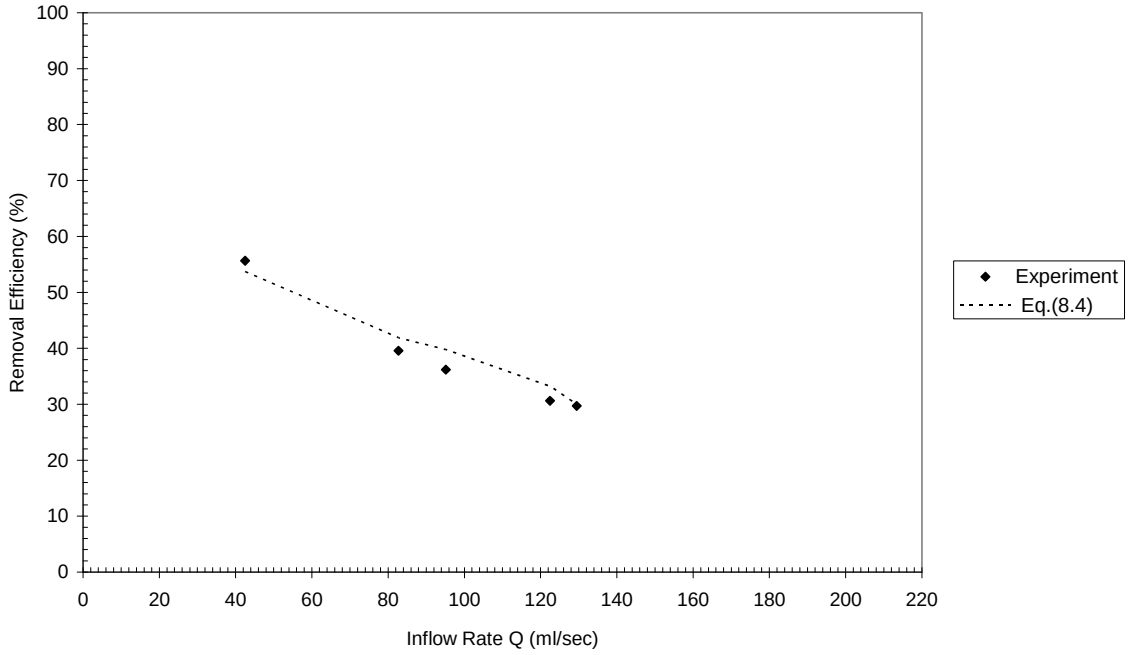


Fig. 8.4 Comparison of Predicted Removal Effeciency with Experimental Data Based on Chamber Heigh $H_0$ = 120 mm

## 8.5 Sizing Example

The unit sizing procedures using equations developed in this study is quite simple. For a given design fluid (water) flow rate and a desired particle removal efficiency, as well as the particle size distribution curve, the detailed unit sizing procedures are illustrated as follows.

**Example 1:** Given:

- Design flow rate Q = 0.01 $m^3$/sec (162gpm)
- Desired particle removal efficiency $E_T$ = 50% ( PSD: d = 80 μm)
- The specific gravity of sand particle $\rho_p / \rho_f = 2.65$
- The kinematic viscosity of water (@ 20°C) $\nu = 1.003 \times 10^{-6}$ $m^2$/sec
- The acceleration of gravity g = 9.81 m/$sec^2$

**Determine the size of the vortex chamber.**

**Solution:**

**(1) Estimation of Chamber Diameter $D_1$ (= 2 $R_1$)**

From Eq.(8.1), if the location ( $r_{z_{max}}$ ) of maximum height that a particle could rise exists, then the following condition must be satisfied:

$$r_{z_{max}} = R_1 \sqrt{1 - \frac{1}{2}\left(\frac{U_s}{U_{OR}}\right)} \succ 0 \qquad (8.12)$$

Rearranging the above equation yields:

$$U_{OR} \succ \frac{1}{2} U_s \tag{8.13}$$

If Cheng's formula is used to predict the particle settling velocity, then the following relationship can be obtained:

$$\frac{Q}{\pi R_1^2} \succ \frac{1}{2}\frac{\nu}{d}\left\{\sqrt{25 + 1.2\left[\left(\frac{\rho_p}{\rho_f} - 1\right)\frac{g}{\nu^2}\right]^{2/3} d^2} - 5\right\}^{1.5} \tag{8.14}$$

For a given design flow rate of Q = 0.01 $m^3$/sec and a desired removal efficiency of $E_T$ = 50%, the critical particle size d that could be captured by the chamber can be determined from the particle size distribution curve (Fig. 3.3), and it is d = 80 microns. The specific gravity for sand particle is $\rho_p / \rho_f$ = 2.65. The kinematic viscosity of water at 20°C is $\nu = 1.003 \times 10^{-6}$ $m^2$/sec. The acceleration of gravity is g = 9.81 m/$sec^2$. By substituting the values of Q, d, $\rho_p / \rho_f$, g and $\nu$ into Eq. (8.14), the calculated chamber radius $R_1$ is as follows:

$$R_1 \prec 1.57\,\text{m} \qquad \text{Try} \qquad R_1 = 1.25\,\text{m}$$

**(2) Selection of Inlet Pipe Diameter $D_{IN}$ (= 2 $R_{IN}$)**

In terms of US EPA laboratory test results for swirl concentrator (Sullivan, et al., 1982), the small the inlet pipe size, the high removal efficiency could be achieved. For

practical operation, the reasonable ratio of chamber diameter $D_1$ to inlet pipe diameter $D_{IN}$ is $D_1/D_{IN}$ = 6 to 14. In this example, the ratio of $D_1/D_{IN}$ = 12.5 is selected to illustrate the sizing procedures. Therefore, the selected inlet pipe radius is:

$$R_{IN} = 0.10 \text{ m}$$

**(3) Calculation of $U_{OR}$, $U_S$, and $r_{z_{max}}$**

The chamber overflow rate, particle terminal settling velocity, and location of maximum height that a suspended particle could rise are determined as follows:

$$U_{OR} = \frac{Q}{\pi R_1^2} = \frac{0.01}{3.14 \times 1.25^2} = 0.00204\,\text{m/s} = 2.04\,\text{mm/s}$$

$$U_s = \frac{\nu}{d}\left\{\sqrt{25 + 1.2\left[\left(\frac{\rho_p}{\rho_f} - 1\right)\frac{g}{\nu^2}\right]^{2/3} d^2} - 5\right\}^{1.5}$$

$$= \frac{1.003 \times 10^{-6}}{80 \times 10^{-6}}\left\{\sqrt{25 + 1.2\left[\frac{(2.65-1) \times 9.81}{(1.003 \times 10^{-6})^2}\right] \times (53 \times 10^{-6})} - 5\right\}^{1.5}$$

$$= 0.00404\,\text{m/s} = 4.04\,\text{mm/s}$$

$$r_{z_{max}} = R_1\sqrt{1 - \frac{1}{2}\left(\frac{U_s}{U_{OR}}\right)} = 0.112 \text{ m}$$

**(4) Determination of Particle Injection Location ($r_o$)**

For the given design flow rate Q = 0.01 $m^3$/sec and the selected chamber radius $R_1$ = 1.25 m, the average particle injection location can be estimated by Eq.(8.8):

$$\frac{r_o}{R_1} = -0.3981\ \mathrm{Ln}\left(\frac{2Q}{\pi R_1 \nu}\right) + 2.7536$$

$$= -0.3981\ \ln\left(\frac{2\times 0.01}{3.14\times 1\times 1.003\times 10^{-6}}\right) + 2.7536 \qquad (8.8)$$

$$= -0.73 \prec 0$$

Set $r_o = 0.1$ mm

**(5) Determination of Chamber Height ($H_o$)**

By substituting the following values of

| | | |
|---|---|---|
| $\mu = 1.003 \times 10^{-3}$ Pa.s | $\rho_p = 2650$ kg/m$^3$ | $\rho_f = 1000$ kg/m$^3$ |
| $d = 80 \times 10^{-6}$ m | $U_{OR} = 2.04 \times 10^{-3}$ m/s | $Us = 4.04 \times 10^{-3}$ m/s |
| $R_1 = 1.25$ m | $R_{IN} = 0.10$ m | $r_{Z_{mam}} = 0.11$ m |
| $r_o = 0.0001$ m | $K_L = 1.0$ | $n = 0.01$ |
| $Q = 0.01$ m$^3$/s | | |

into Eq.(8.4) and Eq.(8.8) and solving these two equations by trial and error gives:

$\omega = 0.318$/sec

$H_o = 2.29\ \mathrm{m} \approx 2.30\ \mathrm{m}$

Therefore, based on the given design flow rate Q = 0.01m$^3$/sec and desired particle removal efficiency $E_T$ = 50%, the determined unit dimensions are as follows:

| | |
|---|---|
| Chamber Diameter | $D_1 = 2\ R_1 = 2.50$ m |
| Chamber Height | $H_o = 2.30$ m |
| Inlet Pipe Diameter | $D_{IN} = 2\ R_{IN} = 0.20$ m |

**Example 2** **Given**

Design flow rate Q = 0.02 $m^3$/sec (324 gpm)

Desired particle removal efficiency $E_T$ = 50% ( PSD: d = 80 μm)

The specific gravity of sand particle $\rho_p / \rho_f = 2.65$

The kinematic viscosity of water (@ 20°C) $\nu = 1.003 \times 10^{-6}$ $m^2$/sec

The acceleration of gravity g = 9.81 m/$sec^2$

Determine the size of the vortex chamber.

**Solution:**

Similarly, following the same procedures described in Example 1, the determined unit dimensions for the given design flow rate Q = 0.02$m^3$/sec and desired particle removal efficiency $E_T$ = 50% (d = 80 microns) are as follows:

| | |
|---|---|
| Chamber Diameter | $D_1 = 2\ R_1 = 2 \times 1.78$ m ≈ 3.60 m |
| Chamber Height | $H_o = 1.44$ m ≈ 1.45 m |
| Inlet Pipe Diameter | $D_{IN} = 2\ R_{IN} = 2 \times 0.14$ m ≈ 0.30 m |

## 8.6 Conclusions

Based on the particle trajectory equation derived Chapter 7, a unit sizing formula (Eq.(8.4)) for a confined vortex chamber with tangential inflow, but without baseflow exit has been developed. The comparison of the predicted results with experimental data reveals that the predicted result has a good agreement with the experimental data. The maximum difference between the predicted results and the measured results are less than 4%. This study shows that Eq.(8.4) coupled with PSD curve is applicable to unit performance evaluation and unit sizing for devices with the similar configuration of this study.

# Chapter 9

# Summary and Conclusions

In this research, experimental and theoretical investigation on particle removal efficiency was conducted to examine the mechanisms of solid - liquid separation in a confined vortex chamber, and thereby develop some fundamental basis for hydrodynamic separator sizing. The main achievements and findings obtained from this research are summarized and concluded, based on the experimental investigation and theoretical study, as follows:

**Experiment Investigation**

In the experimental section, in order to investigate the effect of the unit configuration on particle removal efficiency in the confined vortex chambers, four physical vortex models, three with varying inlet pipe elevation and one with lower chamber height, were tested.

The measured result analysis reveals the impact of inlet pipe elevation change on the particle removal efficiency is insignificant; while the change of the chamber height has a greater impact on particle removal efficiency.

This finding is very helpful for theoretical study as there are a lot of variables that may prevent any reasonable theoretic investigation. In terms of this finding, one variable (inlet pipe elevation) can be eliminated.

Based on gravitational separation method, a unit sizing formula for a vortex chamber with the ratio of chamber height to diameter equating to one was suggested.

The comparison of predicted results with this formula agrees with the experimental results. It is applicable to evaluation of unit performance and unit sizing.

**Theoretical Development**

In the theoretical development section, the following three topics have been covered by this research:

(1) determination of fluid flow patterns in a confined vortex chamber (Chapters 4 & 5).

(2) dynamic response of particle motion in a one-dimensional upward uniform steady fluid flow and vortex chamber flow (Chapters 6 &7).

(3) and derivation of unit sizing formula for a confined vortex separator.

The angular velocity of fluid motion around the common axis is an important factor to theoretically determine the flow patterns and particle trajectories in a rotational flowfield. In this research, a simple formula, based on the law of conservation of momentum and boundary conditions, was derived to determine the angular velocity for turbulent vortex flows. The visual observation with an object in the chamber found that the observed results were basically close to the predicted results.

Based on the Navier-Stokes governing equation and some basic assumptions, a vortex model to predict the flow patterns in a confined vortex chamber was derived in this study. This model can be used to describe the tangential and vertical velocity distributions in a confined vortex chamber with a tangential inflow pipe, but without the baseflow exit.

The dynamic response of particles in a one-dimensional upward uniform steady fluid flow, based on the balance of forces acting on a spherical particle, was examined. The case analysis showed that an unsteady state of particle motion exists for a very short time for sand particles (about 0.02 seconds). For solid-liquid separation in wastewater and stormwater treatment system, the effect of an unsteady state on particle motion can be neglected. In terms of the derived analytical solutions of particle velocity, a new particle terminal settling velocity formula for natural sediment particles was proposed. The comparison of predicted results with previous study indicated that it has a good agreement with that from previous study such as Cheng's formula.

In terms the flow pattern derived for a confined vortex chamber flow and the particle settling velocity, the particle trajectory equations in a confined vortex chamber have been derived. Based on the particle trajectory, a unit sizing formula was obtained in this research. Comparison of the predicted results with experimental data revealed that this formula has a good agreement with experimental data. Therefore, the final goals of the study were successfully achieved.

**Future Work**

This study has provided a fundamental approach for the unit performance evaluation. This approach covers an array of topics, namely, flow pattern, particle trajectory and unit performance evaluation. For vortex separators with different unit configuration or units with internal components, this fundamental approach is useful for the development of a unit performance formula.

Prior knowledge of flow patterns in a confined vortex chamber is critical to understand the mechanisms of solid-liquid separation. Therefore, experimental investigation on flow patterns, based on different types of vortex separators (including the type selected in this study) is emergent and necessary for the theoretical development in the future.

**REFERENCES**

Ahrens, J.P. (2000). "The fall-velocity equation." J. Waterway, Port, Coastal, and Ocean Engrg., 126(2),99-102.

Albertson, M.L.(1953). "Effect of Shape on Fall Velocity of Gravel Particles." Proc. 5th Hydr. Conf., Univ. of Iowa, Bull. No. 34, USA.

American Public Health Association, American Water Works Association, and Water Pollution Control Federation (1987). "Standard Methods for the Examination of Water and Wastewater." 17th ed. American Public Health Association, Inc., New York.

Andoh, R.Y.G. and Smisson, R.P.M. (1994). "High Rate Sedimentation in Hydrodynamic Separators." *2nd International Conference on Hydraulic Modeling Development and Application of Physical and Mathematical Models (Ed.A J Saul), Stratford, UK, 341-358.*

Andoh, R.Y.G. and Smisson, R.P.M. (1996). "The Practical Use of Wastewater Characterisation in Design." *Water Science and Technology* 33(9):127-134.

Andoh, R.Y.G. and Saul, A.J. (2003). "The Use of Hydrodynamic Separators and Screening Systems to Improve Water Quality." *Water Science and Technology* 47(4): 175-183.

Auton, T.R. (1987). "The Lift Force on a Spherical Body in a Rotational Flow." *J. Fluid Mech., vol. (183), pp*. 199-218.

Auton, T.R., Hunt, J.C.R., and Prud'homme, M. (1988). "The Force Exerted on a Body in Inviscid Unsteady Non-Uniform Rotational Flow." *J. Fluid Mech., vol.(197), pp.*241-257.

Avco Corporation (1970). "Storm Water Pollution from Urban Land Activity." PB195-281. Federal Water Quality Administration, Washington,D.C.

Bagchi, P., and Balachandar, S. (2002). "Shear versus Vortex-Induced Lift Force on a Rigid Sphere at Moderate Re." *J. Fluid Mech, Vol.(473),* pp. 379-388.

Bagchi, P. and Balachandar, S. (2002a). "Effect of free rotation on the motion of a solid sphere in linear shear flow at moderate Re." *Physics of Fluids, 14(8), pp*.2719-2737.

Bagchi, P. and Balachandar, S. (2003). "Inertial and Viscous Forces on a Rigid Sphere in Straining Flows at Moderate Reynolds Numbers." *J. Fluid Mech., Vol.(481), pp*.105-148.

Bagchi, P. and Balachandar, S. (2003). "Effect of Turbulence on the Drag and Lift of a Particle." *Physics of Fluids., 15(11), pp*.3496-3513.

Batchelor, G.K.(1967). An Introduction to Fluid Dynamics. Cambridge University Press UK.

BaySaver®, Inc.(2005). BaySaver® Separation System Technical and Design Mannual. Mount Airy, Maryland. http://www.baysaver.com/downloads/BaySeparator_tech_manual.pdf

Bhaduri, B., Minner, M. and Atalovich, S.(2001). "Long-Term Hydrological Impacts of Urbanization: A Tale of Two Models." *Journal of Water Resources and Management* 127(1):13-19.

Boothroyd, R.G. (1971). *Flowing Gas-Solids Suspensions*. Chapman and Hall Ltd. London.

Brown, P.P. and Lawler, D.F.(2003). "Sphere Drag and Settling Velocity Revisited." *Journal of Environmental Engineering,* 129(2):222-231.

Brueske, C.C. (2000). Technology Review: Ultra-Urban Stormwater Technologies. Department of Civil and Environmental Engineering, University of Washington, Seattle, WA. http://water.washington.edu/Research/Reports/ultraurbn.pdf

Burgers, J.M. (1948)." A Mathematical Model Illustrating the Theory of Turbulence." *Advances in Applied Mechanics*, Vol.(1), pp.171-199.

Carver, R.E.(edt.) (1971)."Procedures in Sedimentary Petrology". Wiley-Interssience, A Division of John Wiley and Sons, In., New York, Londin, Tokyo, 653pp.

Candelier, F., Angilella, J.R. and Souhar, M. (2004) " On the effect of the Boussinesq-Basset force on the radial migration of a Stokes Particle in a Vortex." *Physics of Fluids, 16(5), pp*.1765-1776.

Cheng, N.S. (1997a). "Simplified Settling Velocity Formula for Sediment Particle." *Journal of Hydraulic Engineering*, 123(2):149-152.

Cheng, N.S. (1997b). "Effect of Concentration on Settling Velocity of Sediment Particles." *Journal of Hydraulic Engineering*, 123(8):728-731.

Chorin, A.J. (1973). "Numerical Study of Slightly Viscous Flow." *J. Fluid Mech*. 57, 785-796.

Chorin, A.J. (1978). "Vortex Sheet Approximation of Boundary Layers" *J. Comput. Phys.* 27, 428-442.

Chorin, A.J. (1980). "Vortex Models and Boundary Layers Instability" *SIAM J. Sci. Stat. Comput*. 34, 1-21.

Chorin, A.J. (1990). "Hairpin Removal in Vortex Interactions." *J. Comput. Phys*. 91, 1-21.

Chorin, A.J. (1993). "Hairpin Removal in Vortex Interactions II." *J. Comput. Phys*. 107, 1-9.

Clift, R.; Grace, J.R.; and Weber, M.E. (1978). Bubbles, Drops, and Particles. Academic Presess, New York.

Coimbra, C.F.M. and Rangel, R.H.(1998) "General solution of the particle momentum equation in unsteady Stokes flows." *Journal of Fluid Mechanics, vol.370, pp.53-72*.

Coimbra, C.F.M. and Kobayashi, M.H.(2002) "On the viscous motion of a small particle in a rotating cyclinder." *Journal of Fluid Mechanics, vol.469, pp.257-286.*

Cottet, G.H. and Koumoutsakos P.D. 2000, Vortex Methods: Theory and Practice. Cambridge University Press.

Dallavalle, J. (1943). Micromeritics. Pitman, New York.

Deamer, A.P., R.A. Fenner, S. Edwards (1994). "Hydrodynamic Separators, dimensional analysis, and scaling laws". Ed. By Sau, A.J., 2nd International Conference on Hydraulic Modeling, Mechanical Engineering Publications Limited, London, United Kingdom.

Emanuel, G. (1994). Analytical Fluid Dynamics. CRC Press, Boca Raton, Florida.

EPA (1983). "Results of the Nationwide Urban Runoff Program, volume I – Final Report." U.S. Environmental Protection Agency, Water Planning Division, Washington D.C.

Escudier, M. P., Zehnder, J. B., and Maxworthy, T. (1980). "The Classification of Confined Vortex Flow Regimes." Vortex Flows. Ed. by Swift et al, ASCE, New York.

Faram, M.G. and Harwood, R. (2003). "A Method for the Numerical Assessment of Sediment Interceptors." *Water Science and Technology* 47(4): 167-174.

Faram, M.G., James, M.D., and Williams, C.A. (2004). "Wastewater Treatment Using

Hydrodynamic Vortex Separators." *CIWEM 2nd National Conference*, Wakefield, UK, pp. 79-87.

Field, R. and O'Connor, T.P. (1996). "Swirl Technology: Enhancement of Design, Evaluation and Application." *Journal of Environmental Engineering*, Vol. 122, No. 8, pp.741-748.

Fenner, R.A., and Tyack, J.N. (1997). "Scaling Laws for Hydrodynamic Separators." *Journal of Environmental Engineering*, Vol. 123 , No. 10. pp.1019-1029

Fenner, R.A., and Tyack, J.N. (1998). "Physical Modeling of Hydrodynamic Separators Operationg with Underflow." *Journal of Environmental Engineering*, Vol. 124 , No. 9. pp.881-886.

Fox, R.W. and McDonald, A.T. (1985). Introduction to Fluid Mechanics. 3rd Edition. John Wiley & Sons, Inc.

Goldstein, S. (1929) "The Steady Flow of Viscous Fluid Past a Fixed Spherical Obstacle at Small Reynolds Numbers." Proc. Roy. Soc. (London), vol.123A, 225.

Graf, W. H. (1971). Hydraulics of Sediment Transport. McGraw-Hill, New York.
Greenspan, H.P. (1980). The Theory of Rotating Fluids. Cambridge University Press, Cambridge, UK.

Gupta, A. K.; Lilley, D.G.; and Syred, N. (1984). Swirl Flows. ABACUS Press.

Guo, Q.(2005). "Development of Adjustment and Scaling Factors for Measured Suspended Solids Removal Performance of Stormwater Hydrodynamic Treatment Devices." Proceedings of the World Water & Environmental Resources Congress, May 15-19, 2005, Anchorage, Alaska, ASCE-EWRI.

Guo, Q. (2006) "Correlation of Total Suspended Solids (TSS) and Suspended Sediment Concentration (SSC) Test Methods." Final Report, Contract No: SR05-005. Rutgers, The State University of New Jersey.

Hallermeier, R.J. (1981). "Terminal Settling Velocity of Commonly Occuring Sand Grains " Sedimentology, 28(6): 859-865.

H.I.L. Technology, Inc. (2005). NJCAT Technology Verification. Hydro International. http://www.state.nj.us/dep/dsr/bscit/FinalVer_Hydro.pdf

Iso, Y. and Kamemoto (2008) "A Grid-Free Lagrangian Approach of Vortex Method and Particle Trajectory Tracking Method Applied to Internal Fluid-Solid Two-Phase Flows." Journal of Fluids Engineering, Vol. (130), pp. 011401-011409.

Kriebel, A.R. (1961) “Particle Trajectories in a Gas Centrifuge.” Journal of Basic Engineering, Vol.(83), Part 2, pp.333-340.

Jimenez J.A., and Madsen, O.S.(2003). A Simple Formula to Estimate Settling Velocity of Natural Sediments. Journal of Waterway, Port, Coastal and Ocean Engineering, 129(2):70-78.

Khader, M.S and Ayad, S.S. (1980,) Turbulent Confined Vortex Flow. Ed. by Swift et al, ASCE, New York.

Kriebel, A.R. (1961) “Particle Trajectories in a Gas Centrifuge.” Journal of Basic Engineering, Vol.(83), Part 2, pp.333-340.

Kurose, R. and Komori, S. (1999). “Drag and Lift Forces on a Rotating Sphere in a Linear Shear Flow.” *J. Fluid Mech., Vol.(384), pp*.183-206.

Lamb, S.H. (1945). Hydrodynamics, Dover Publication, New York.

Lapple, C.E., and Shepherd (1940). Calculation of Particle Trajectories” Industrial and Engineering Chemistry Research, 32(5) pp.605-617.

Leonard, A. (1975). “Numerical Simulation of Interacting Vortex Filaments.” Proceedings of the IV Intl. Conference on Numerical Methods of Fluid Dynamics, Springer-Verlag, New York.

Leonard, A. (1980). “Vortex Methods for Flow Simulation.” *J. Comput. Phys*. 37, 289-335.

Leonard, A. (1985). “Computing Three-dimensional Incompressible Flows with Vortex Elements.” *Ann. Rev. Fluid Mech.* 17, 523-559.

Legendre, D. and Magnaudet, J. (1998) “The Lift Force on a Spherical Bubble in a Viscous Linear Shear Flow.” *J. Fluid Mech., Vol.(368), pp*. 81-126.

Lin, C.C. (1943). On the Motion of Vortices in Two Dimensions. University of Toronto Studies. Applied Mathematics Series, No.5. The University of Toronto Press.

Lugt, H.J. (1983). Vortex Flow in Nature and Technology, John Wilry and Sons, New York.

Luyckx, G. and Berlamont, J. (2004).”Removal Efficiency of Swirl/Vortex Separators” *Urban Water Journal*, 1(3):251-260.

Marcu, B., Meiburg, E., and Newton, P.K. (1995). “Dynamics of Heavy Particles in a Burgers Vortex.” *Phys. Fluids* 7(2) pp.400-410.

Maxey, M.R. and Rilley, J.J. (1983) “Equation of Motion for a Small Rigid Sphere in a Non-uniform Flow.” *Phys. Fluids, 26(4), pp*.883-889.

Mei, R., Klausner, J.F. and Lawrence, C.J. (1994) “A Note on the History Force on a Spherical Bubble at Finite Reynolds Number.” *Physics of Fluids,* 6(1), pp. 418-420.

Meiburg, B.M.E and Newton, P.K. (1995). “ Dynamics of Heavy Particles in a Burgers Vortex”. *Phys. Fluids* 7(2): 400-410.

Michaelides, E. (1992) “A novel way of computing the Basset term in unsteady multiphase flow computations.” *Physics of Fluids A 4 (7),* pp. 1579-1582.

Minton, G. (2005). Stormwater Treatment. Resource Planning Associates, Seattle, Washington.

Morsi, S.A. and Alexander, A.J. (1972). An Investigation of Particle Trajectories in Two-Phase Flow Systems. Journal of Fluid Mechanics, Vol. 55, part 2, pp. 193-208.

Mosheim, J. (2006). “An Innovative Method for Modeling, Analysis, and Prediction of Structural Stormwater BMP Performance” Presented on Storm Con’06.

National Association of Counties Research Foundation (NACRF) and Federal Water Quality Administration (FWQA) (1970). “Urban Soil Erosion and Sediment Control”. PB-195-281, U.S. Government Printing Office, Washington, D.C.

New Jersey Department of Environmental Prodition (NJDEP) (2004). “ New Jersey Stormwater Best Management Practices Manual”. Divison of Watershed management, NJDEP, Trenton, NJ.

Nikora, V., Aberle, J., and Green M. (2004). “Sediment Flocs: Settling Velocity Flocculation Factor, and Optical Backscatter”. *Journal of Hydraulic Engineering*, 130(10):1043-1047.

Ogawa, A. (1984). Separation of Particles from Air and Gases. Volume I & II. CRC Press, Inc., Boca Raton, Florida.

Ogawa, A. (1993), Vortex Flow, CRC Press.

Oseen, C. (1927). Hydrodynamik, Chapter 10, Akademische Verlagsgesellschaft, Leipzig.

Osborne, L.L. and Wiley, M.J. (1998). “Empirical Relationships between land-use/cover and Stream Water Quality in an Agricultural Watershed”. *Journal of Environmental Management. Vol.(26):9-27.*

Peavy, H.S.; Rowe, D.R. and Tchobanoglous, G. (1985). Environmental Engineering. McGraw-/Hill Book Company, New York.

Pisano, W.C., Connick, D.J., and Aronson, G.L. (1984). ”Swirl and Helical Bend Regulator / Concentrator for Storm and Combined Sewer Overflow Control”. Rep. No. EPA-600/2-84/151. U.S. EPA, Cincinnati, Ohio.

Prus-Chacinski, T.M., and Wielogorski, J.W. (1967). “Secondary Motions Applied to Storm Sewage Overflows”. *Symposium on Storm Sewage Overflows.* Institute of Civil Engineers, London, UK.

Roesner, L.A. (1999). “Urban Runoff Pollution - Summary Thoughts – the State-of-Practice Today and for the 21st Century”. *Wat. Sci. Tech.* 39 (12): 353-360.

Roesner, L.A. and Brashear, R.W. 2001. Are Best-Management-Practice Criteria Really Environmentally Friendly? *Journal of Water Resources Planning and Management 127(3)*: 150-154.

Rudinger, G. (1980). Fundamentals of Gas-Particle Flow. Elsevier Scientific Publishing Company, New York.

Rosenhead, L. (1932). “The Point Vortex Approximation of a Vortex Sheet”. *Proc. R. Soc. London Ser*. A 134, 170-192.

Rubey, W.W. (1933). “Settling Velocities of Gravel, Sand, and Silt Particles”. *Americal Journal of Science.* Vol. XXV, No.145, pp325-338.

Rouse, H., (ed.) (1959). Advanced Mechanics of Fluids. John Wiley & Sons, New York.

Saffman, P.G. (1965) “The lift on a small sphere in a slow shear flow.” *Journal of Fluid Mechanics. Vol. (22), pp*.385-400.

Saffman, P.G. (1992). Vortex Dynamics, Cambridge University Press.

Saul, A.J., Ruff, S.J., Walsh, A.M., and Green, M.J. (1993).”Laboratory Studies of CSO Performance”. WRc Report No. UM 1421, October, UK.

Schiller, L. and Neuman, A. (1933) Uber die grundlegenden Berechungen bei der Schwerkraftaufbereitung. Ver. Deutt. Ing. 77, 318.

Sobral, Y.D., Oliveira, T.F. and Cunha (2007) “On the unsteady forces during the motion of a sedimenting particle.” *Powder Technology, Vol.(178),* pp.129-141.

Svarovsky, L. (1977). Solid-Liquid Separation. Butterworths, London.

Svarovsky, L. (1981). Solid-Gas Separation. Elsevier Scientific Publishing Company,

New York.

Svarovsky, L. (1984). Hydrocyclones. Technomic Publishing Co. INC., London

Schlichting, H. and Gersten, K. (2000). "Boundary Layer Theory". 7th ed., New York, Springer, Germany.

Shakespeare, W.J. and Levy, E.K. (1980). "Pressure Drop in a Confined Vortex with High Flow Rate". Vortex Flows. Ed. by Swift et al.

Shapiro, A.H. (1959). The Dynamics and Thermodynamics of Compressible Fluid Flow. The Ronald Press Company, New York.

Sharma, T., Kiran, P.V.S., Singh, T.P., Trivedi, A.V. and Navalgund, R.R. (2001). "Hydrologic Response of a Watershed to Land Use Changes: Aremote Sensing GIS Approach". International Journal of Remote Sensing 22(11):2095-2108.

Simons, D.B.; and Senturk, F. (1992). Sediment Transport Technology: Water and Sediment Dynamics. Water Resources Publications, Colorado, USA.

Sincero, A.P., and Sincero, G.A. (1996). "Environmental Engineering: A Design Approach". Prentice Hall, Upper Saddle River, New Jersey.

Smisson, B. (1967) Design, Construction and Performance of Vortex Overflows. *Symposium on Storm Sewage Overflows.* Institute of Civil Engineers, London, UK.

Stoke, G.G. (1851). On the effect of the Internal Friction of Fluids on the Motion of Pendulums: Trans. Cambridge Philos. Soc., 9, Pt. 2, [51-52]. Reprinted in Stokes, G.G. Mathematical and Physical Paper, 3, pp.59-60, 1901.

Stork, P., Bowling, L., and Wetherbee, P. and Lettenmaier, D. (1998)."Application of a GIS-based Distributed Hydrology Model for Prediction of Forest Harvest Effects on Peak Streamflow in the Pacific Northwest". Hydrological Process-An Internal Journal 12(6):889-904.

Street, R.L.; Watters, G.Z.; and Vennard, J.K. (1996). Elementary Fluid Mechanics. 7th Edition. John Wiley & Sons.

Sullivan, R.H., Cohn, M.M., Coombes, J.P. and Smisson, B.S. (1972). The Swirl Concentrator as a Combined Sewer Overflow Regulator Facility. Rep. No. EPA-R2-72-008 (NTIS PB 214 687). U.S. EPA, Edison, N.J.

Sullivan, R.H., Cohn, M.M., Ure, J.E., Parkinson, F.E., and Galiana, G. (1974).

"Relationship between diameter and height for design of a swirl concentrator as a combined sewer overflow regulator." Rep. No. EPA-670/2-74-039, U.S. EPA, Edison, N.J.

Sullivan, R.H.; Cohn, M.M.; Ure, J.E.; Parkinson, F.; Galiana, G.; Boericke, R.R.; Koch, C.; and Zielinski, P. (1978). The Swirl Primary Separator: Development and Pilot Demonstration. Rep. No. EPA-600/2-78-122. U.S. EPA, Cincinnati, OHio.

Sullivan, R.H., Ure, J.E., Parkinson, F., and Zielinski, P. (1982). "Design Manual-Swirl and helical bend pollution control devices." Rep. No. EPA-600/8-82/013, U.S. EPA, Edison, N.J.

Taylor, G.I. (1921). Experiments with Rotating Fluids. *Proc. Cambridge Phil. Soc*. **20**, 326-9. <p.2>

Taylor, G.I. (1921). Experiments with Rotating Fluids. *Proc. Roy. Soc*. A **100**. 114-21. <p.2.>

Thomas, P.J. (1997) "A numerical study of the influence of the Basset force on the statistics of LDV velocity data sampled in a flow region with a large spatial velocity gradient." *Experiments in Fluids, vol.(23), pp*.48-53.

U.S. Environmental Protection Agency (USEPA). 1983. USEPA, Results of the Nationwide Urban Runoff Program, Final Report. NTIS No. PB84-185545, Washington, D.C

Van Rijin, L.C. (1993). Principles of Sediment Transport in Rivers, Estuaries and Coastal Seas, AQUA Publications, The Netherlands.

Vatistas, G.H.; Lin, S.; Kwok, C.K. (1986) " Theoretical and experimental studies on vortex chamber flows." *AIAA Journal, Vol.(24), pp.635-642.*

Vatistas, G.H.; Lin, S.; Li, P.M. (1988) "A similar profile for the tangential velocity in vortex chambers." *Experiments in Fluids, Vol.(6), pp.135-137.*

Vortechnics, Inc. (2004). NJCAT Technology Verification. Vortechnics, Inc. http://www.state.nj.us/dep/dsr/bscit/VortechnicsVerification.pdf

Walker, D., Golden, J., Bingham, D., and Driscoll, E. (1993). "Manual: Combined sewer overflow control." Rep. No. EPA/625/R-93/007, U.S. EPA, Cincinnati, Ohio.

Wanielista, M.P. and Yousef, Y.A. (1993). Stormwater Management. John Wiley & Sons, INC. New York.

*Weiβ* , G.J. (1997)."Vortex Separator: Proposal of a dimensioning method." *Water Science and Technology*, 36(8-9):201-206.

*Weiβ*, G.J., and Michelbach, S. (1996). "Vortex separator: Dimensionless properties and calculation of annual separation efficiencies." *Water Science and Technology*, 33(9):277-284.

Whitaker, S. (1981). Introduction to Fluid Mechanics. Robert E. Krieger Publishing Company, Malabar, Florida.

Winkler, E and Guswa, S. (2002). Technology Assessment Report: Vortechs™ Treatment System. Vortechnics, Inc., Scarborough, ME. http://www.mass.gov/envir/lean_green/documents/techassessments/Vortechnics_Tech_Assessment.pdf

Wong, T.H.F. (1997). "Continuous deflective separation: Its mechanism and applications." *Proceedings of Water Environment Federation 70th Annual Conference and Exposition, Chicago, Illinois.*

Wong, T, S.W. and Li, Y. (1997). Importance of Urbanization Sequences on Assessment of Flood Peak Increase. *Hydrological Science and Technology* 13(1-4): 65-74.

Wong, T, S.W. and Li, Y. 1999. Theoretical Assessment of Changes in Design Flood Peak of an Overland Plane for Two Opposing Urbanization Sequences. *Hydrological Processes* 13: 1629-1647.

Yih, C.S. (1977). Fluid Mechanics. West River Press, Michigan, USA.

Yang, S.M. and Leal, L.G. (1991) "A note on memory-integral contributions to the force on a accelerating spherical drop at low Reynolds number." *Physics of Fluids A 3*, pp.1822.

Yih, C.H. (1977). Fluid Mechanics. West River Press, Michigan.

Ying, L. and Zhang P. 1997, Vortex Methods: Mathematics and Its Applications. Science Press/Kluwer Academic Publishers, Beijing/New York.

# VITA

**Yunjie Li**

## EDUCATION

Jan. 2009 Ph.D. in Civil & Environmental Engineering
Department of Civil & environmental Engineering
Rutgers, The State University of New Jersey
New Brunswick, New Jersey.

March 1998 Master of Engineering in Civil & Environmental Engineering
School of Civil and Environmental Engineering
Nanyang Technological University, Singapore

May 1990 Master of Engineering in Civil & Environmental Engineering
School of Civil Engineering, Tianjin University, PR China

Sept. 1987 Bachelor of Engineering in Civil Engineering
School of Civil Engineering, Tianjin University, PR China

## EXPERIENCE

2004 - 2008 Research / Teaching Assistant
Department of Civil & Environmental Engineering
Rutgers, The State University of New Jersey - New Brunswick, NJ

1999 – 2002 Civil Engineer
Shanghai Construction Group (S) Pte Ltd., Singapore

1997 – 1999 Civil Design Engineer
Econ Piling Pte Ltd., Singapore

1995 - 1997 Research Scholar
School of Civil and Environmental Engineering
Nanyang Technological University, Singapore

1994 – 1995 Civil Engineer
Lipsin Construction Pte Ltd, Singapore

1990 – 1994 Assistant Professor
School of Civil Engineering,
Shandong University of Technology, Jinan, China

1987 – 1990 Research Assistant
School of Civil engineering, Tianjin University, Tianjin, PR China

**PUBLICATIONS**

(1) Wong, T.S.W & Li, Y. (2000) "Determination of equilibrium detention storage for a serious of planes". Hydrological Science-Journal-des Science Hydrologiques, 45(50), 787-790.
(2) Wong, T.S.W & Li, Y. (1999) "Theoretical assessment of changes in design flood peak of an overland plane for two opposing urbanization sequences" Hydrological Process, Vol.13, No.11, 1629-1647
(3) Wong, T.S.W & Li, Y. (1998) "Assessment of changes in overland time of concentration for two opposing urbanization sequences". Hydrological Science-Journal-des Science Hydrologiques, 43(1), 115-130
(4) Wong, T.S.W & Li, Y. (1997) "Importance of Urbanization on assessment of flood peak increase". Hydrological Science and Technology, vol.13, No.1-4, American Institute of Hydrology, 65-74
(5) Li, Y. & Zhang, Y. (1994) "The critical discharge for groundwater recharge and its determination". Journal of Shandong University of Technology, Vol.24, No.4, 364-367
(6) Zhang, Y. & Li, Y. (1994) "Application of composite rainfall-runoff model in Zehe watershed". Journal of Shandong Hydraulic Technology and Science, vol.84, No.1, 42-51
(7) Zhang, Y., Li, Y. & Ding, S. (1994) "Study on an optimum model for flood control and groundwater recharge with reservoir and its application". Water Resources and Hydropower Engineering, vol. 250, No.8, 2-6
(8) Du, Z.& Li, Y. (1993) "Benefit analysis of groundwater recharge using floodwater in Tahe reservoir ". Journal of Shandong Hydraulic Technology and Science, vol.83, No.4, 60-63
(9) Li, T., Ji, Y. & Li, Y. (1991) "Study on the dynamic benefits of hydroelectric station in electric power system". Journal of Tianjin University, sup.1991, 48-54
(10) Ji, Y. & Li, Y. (1991) "Study on the benefits calculation approach of hydropower station". Hydroenergy Technique and Economy, Vol.42, No.3 15-20